FOI-R--1331--SE
September 2004
ISSN 1650-1942

Base data report

Anna Linderhed, Sten Nyberg, Stefan Sjökvist, Magnus Uppsäll

Optical Methods for Detection of Minefields

Sensor Technology
SE-581 11 Linköping

SWEDISH DEFENCE RESEARCH AGENCY

Sensor Technology
P.O. Box 1165
SE-581 11 Linköping

FOI-R--1331--SE

September 2004

ISSN 1650-1942

Base data report

Anna Linderhed, Sten Nyberg, Stefan Sjökvist, Magnus Uppsäll

Optical Methods for Detection of Minefields

Issuing organization	Report number, ISRN	Report type
FOI – Swedish Defence Research Agency Sensor Technology P.O. Box 1165 SE-581 11 Linköping	FOI-R--1331--SE	Base data report
	Research area code 5. Strike and protection	
	Month year September 2004	**Project no.** E 3022
	Sub area code 51 Weapons and Protection	
	Sub area code 2	

Author/s (editor/s)	Project manager
Anna Linderhed Sten Nyberg Stefan Sjökvist Magnus Uppsäll	Staffan Abrahamsson
	Approved by
	Sponsoring agency
	Scientifically and technically responsible

Report title

Optical Methods for Detection of Minefields

Abstract (not more than 200 words)

At FOI, former FOA, a research program has been running since 1994 with the purpose to use optical systems to detect buried as well as surface laid landmines. An optical system offers the possibility to scan a large area from an airborne or elevated platform. The work focuses on the possibilities to use infrared imaging systems. It is important not to limit the detection effort to mines only, but also to all kind of objects that can serve as indicator of presence, or absence, of mines and minefields. Signal/image processing, experiments, and modelling/simulations are research areas applied on the problem. FOI was one of seven partners in the EU project ARC, airborne minefield area reduction. The project was running from 2001 to 2003 and gave invaluable experience of development of a complex system, international cooperation and detection challenges in real minefields.

This report sums the work of the optical mine detection group at FOI so far and is written as an introduction to future work in the area. The aim is to report the multidisciplinary character of the research connected to the application, rather than presenting deep results.

Keywords

Landmine, optical, IR, infrared, detection, diurnal, modelling, signal, image, processing

Further bibliographic information	Language English
ISSN 1650-1942	**Pages** 110 p.
	Price acc. to pricelist

Utgivare	Rapportnummer, ISRN	Klassificering
Totalförsvarets Forskningsinstitut - FOI	FOI-R--1331--SE	Underlagsrapport
Sensorteknik	**Forskningsområde**	
Box 1165	5. Strike and protection	
581 11 Linköping	**Månad, år**	**Projektnummer**
	September 2004	E 3022
	Delområde	
	51 VVS med styrda vapen	
	Delområde 2	

Författare/redaktör	Projektledare
Anna Linderhed	Staffan Abrahamsson
Sten Nyberg	**Godkänd av**
Stefan Sjökvist	
Magnus Uppsäll	**Uppdragsgivare/kundbeteckning**
	Tekniskt och/eller vetenskapligt ansvarig

Rapportens titel (i översättning)

Optisk teknik för detektion av minfält

Sammanfattning (högst 200 ord)

Vid FOI, tidigare FOA, har ett forskningsprogram pågått sedan 1994 med syfte att använda optiska metoder för att detektera såväl nedgrävda som ytlagda landminor. Med ett optiskt system erbjuds möjligheten att avsöka ett stort område från en flygburen eller annan upphöjd plattform. Arbetet fokuserar på möjligheterna att använda bildalstrande IR-sensorer. Det är viktigt att inte bara minor, utan att även andra objekt som kan indikera närvaro eller frånvaro av minor och minfält detekteras. Signalanalys, experiment och modellering/simulering är olika forskningsområden som tillämpas. FOI var en av sju partners i EU-projektet ARC "Airborne Minefield area Reduction". Projektet pågick mellan åren 2001 och 2003 och gav ovärderlig erfarenhet av utveckling av ett komplext system, internationellt samarbete och detektionsutmaningar i verkliga minfält.

Denna rapport summerar arbetet som hittills utförts av gruppen för optisk mindetektion vid FOI och är skriven som en introduktion till efterföljande arbete inom området. Syftet är att ge en beskrivning av den multidisciplinära karaktären av forskningen inom tillämpningsområdet, snarare än att presentera djuplodande forskningsresultat.

Nyckelord

Landminor, optisk, IR, infraröd, detection, dygnsmässig, modellering, signal, bild, analys.

Övriga bibliografiska uppgifter	Språk Engelska
ISSN 1650-1942	**Antal sidor:** 110 s.
Distribution enligt missiv	**Pris: Enligt prislista**

CONTENTS

1 BACKGROUND

Landmines are a huge problem from a military point of view as well as a humanitarian. From a military perspective a critical issue is to move forces and materials with minimum delay and losses at maximum speed. After a conflict the mined areas have to be cleared in humanitarian demining campaigns.

Figure 1.1 Milekovici/Glinska Poljana, a mined valley in Croatia.

Antipersonnel (AP) mines remain a significant international threat to civilians despite recent intense efforts from developed countries and humanitarian aid organizations to clear the post conflict regions. Mines claim estimated 15,000–20,000 victims per year in some 90 countries [1]. They endanger the resumption of normal activities, from farming to commercial enterprise, long after periods of conflict have ceased. Although most of these mines were emplaced during wars now ended they continue to pose a serious risk to returning refugees and have placed vast tracts of farmland off limits. Despite the investment and the funding from many developed nations and nongovernmental organizations, at the current rate clearing all existing mines could take 450–500 years. The principles of mine detection have changed little since World War II. The typical deminer's tool kit today largely resembles those used more than 50 years ago. It consists of a metal detector, a prodding instrument (such as a stainless steel probe, pointed stick, or screwdriver), and a tripwire "feeler" made of a coat hanger or 14-gauge wire. The demining team typically divides a mined area into grids, commonly 100 m^2, splits the grids into lanes (usually 1 m wide), and then slowly advances down the lanes swinging the metal detector close to the ground. When the detector beeps, the deminer probes the suspected area to determine whether the detected object might be a mine. If the object is not a mine, then it is excavated and laid aside. If it is a mine, then it is detonated in place using a variety of methods

(shooting it with a gun, for example) [1]. Variations on this process occur depending on location. For example, in some cases mine-sniffing dogs supplement the metal detectors. In other places, mines are detonated with mechanical flails or rollers in advance of the detection. Mechanical mine clearing machines can be used, Figure 1.2 show a Swedish version. Figure 1.3 shows a mechanical vegetation cutter which only clears AP-mines.

Figure 1.2 SCANJACK mechanical mine clearance machine.

Figure 1.3 Remotely controlled mechanical vegetation cutter machine.

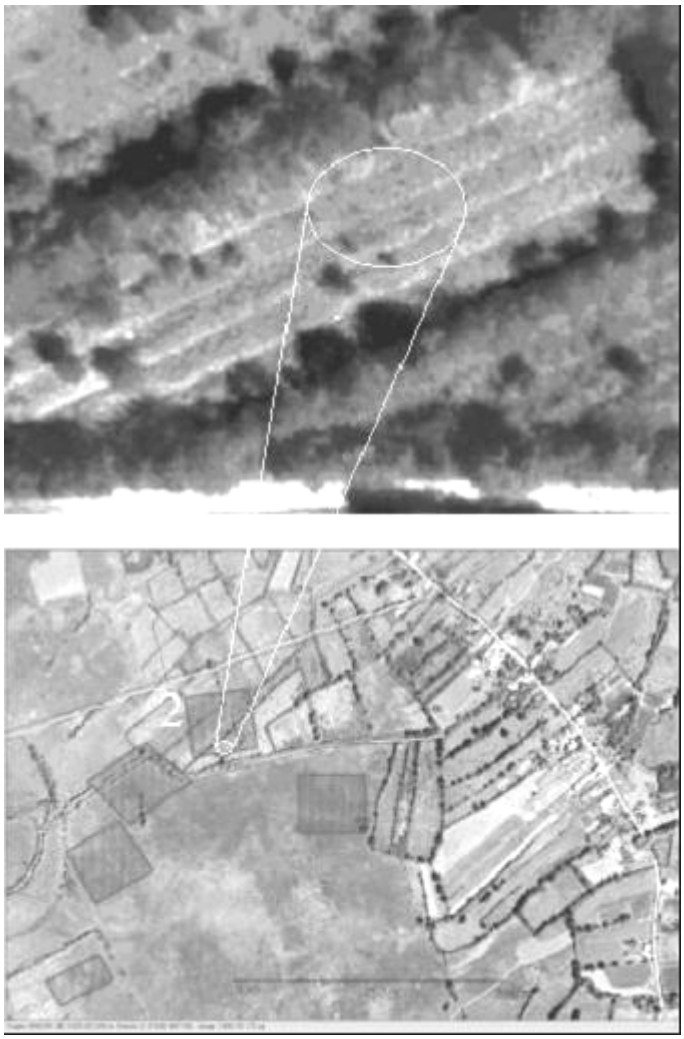

Figure 1.4 Lower: Area of Milekovici/Glinska Poljana and the identified minefields. Upper: IR image from 300m height of the selected area.

In Figure 1.4 an aerial photo of the valley in Figure 1.1 is presented. Although the whole valley was suspected minefields, some identified mine fields are marked in the photo. The close-up is an IR image taken at 300 m altitude. Figure 1.5 shows some results from the manual mine clearing procedure of the actual minefields described above. Each stick presents the position of one mine, and the right image shows some of the mines found.

Figure 1.5 The clearance of the minefield in Figure 1.4. Left: positions for the mines found. Right: some of the mines found.

Effective methods for mine detection as well as characterization of possible minefields and their borders are strongly needed for effectively facilitate the work carried out by survey and demining groups. No single technology available today seems to be sufficiently effective for detection of all types of mines in different conditions, combinations of sensors, algorithms, fundamental knowledge, data fusion etc. could raise the probability of detection [1].

Around the world there is a growing interest in reducing the usage of mines and to detect and clear existing mine fields. At FOI, former FOA, a research program has been running since 1994 with the purpose to use optical systems to detect buried as well as surface laid landmines [2]. In the demining process there are different phases: detection of minefields, detection of individual mines and mine clearance. Most of the detection techniques used today is focused on the single landmines, both the small anti-personnel- and the larger anti-tank mines. An optical system offers the possibility to scan a large area from an airborne or elevated platform. One aim of the work presented in this report, is first to detect the minefield then the single mine. In such an application, the optical system can be used to point out both contaminated areas and single mines. The present work focus on the possibilities of using infrared imaging systems, but the whole optical spectrum, with different systems from ultraviolet up to long wave infrared, is considered.

2 INTRODUCTION

One important issue, in addition to detect presence of minefields, is to avoid clearing mine free areas with expensive and time consuming methods. It is important not to limit the detection effort to mines only, but also to all kind of objects that can serve as indicator of presence, or absence, of mines or minefield. Combinations of sensors, algorithms, fundamental knowledge, data fusion etc. could raise the probability of detection. The conclusion in [1] is that, although the optical methods are feasible and promising, a great deal of research needs to be carried out under different conditions to achieve a high probability of detection. Efforts to clarify the thermal behaviour and IR signature of buried land mines through numerical modelling are presented in [3, 4]. At FOI research has been carried out for a long time on different mine and minefield detection methods, e.g. ground penetrating radar (GPR) [5], [6] and chemical detection [7]. Research on optical methods has been carried out for about ten years. The emphasis has been on understanding, describing, modelling and predicting prerequisites for infrared detection by means of thermal modelling [8]. However, the research has been carried out with an operational system in mind utilizing also multispectral and signal processing methods [9-11]. Research on signal processing aspects has been carried out in cooperation with Chalmers University of Technology. Researches on thermodynamical- and image processing aspects have been carried out with Linköping University.

An airborne optical system could be used to cover large areas in a short time in order to find minefields rather than single land mines, this is also mentioned as UN level 2 survey. Periodic pattern, unused roads, and suspicious objects like antennas and wooden sticks are features that can indicate minefields, Figure 2.6. The next step is to detect the single mine and also here the optical systems have advantages, as well as disadvantages. Surface laid mines could be detected because of different solar absorption properties compared with the surroundings. Buried mines could be detected due to secondary effects such as dig marks and disturbed vegetation, but also because of that the buried object will disturb the unitary heat and diffusion parameters in the actual soil.

The reality is that old minefields are often covered with vegetation. The mines are not always visible to the eye even if they are surface laid. In Figure 2.1 different examples of minefields are shown together with mines and minefield indicators in close-up pictures. Finding an optical method to detect these from the air is a challenge. Using sensors in different spectral bands we can see more, Figure 2.2 to Figure 2.4. Furthermore, by using the temporal domain, Figure 2.5, to track the typical changes of mines and minefields indicators over time gives opportunity to develop specific detection methods for the problem.

Figure 2.1 Left: Examples of minefields, Right: Close up on mine or minefield indicator.

Figure 2.2 A mosaic of a minefield in the visual band

Figure 2.3 A mosaic of a minefield in the NIR band

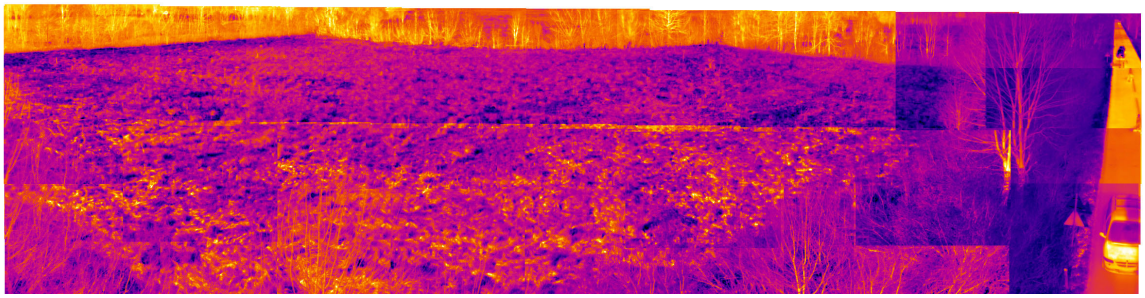

Figure 2.4 A mosaic of a minefield in the IR (8-9 micrometer) band

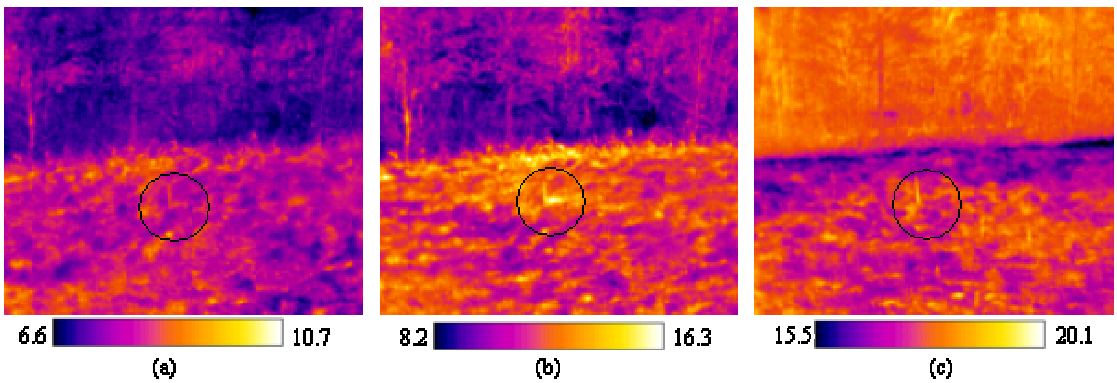

Figure 2.5 Mine indicator position in the IR band 8-9 μm at different times of the day: 08:14 (a), 08:22 (b) and 16:47 (c). The scale in each image represents apparent temperature in degrees Celsius.

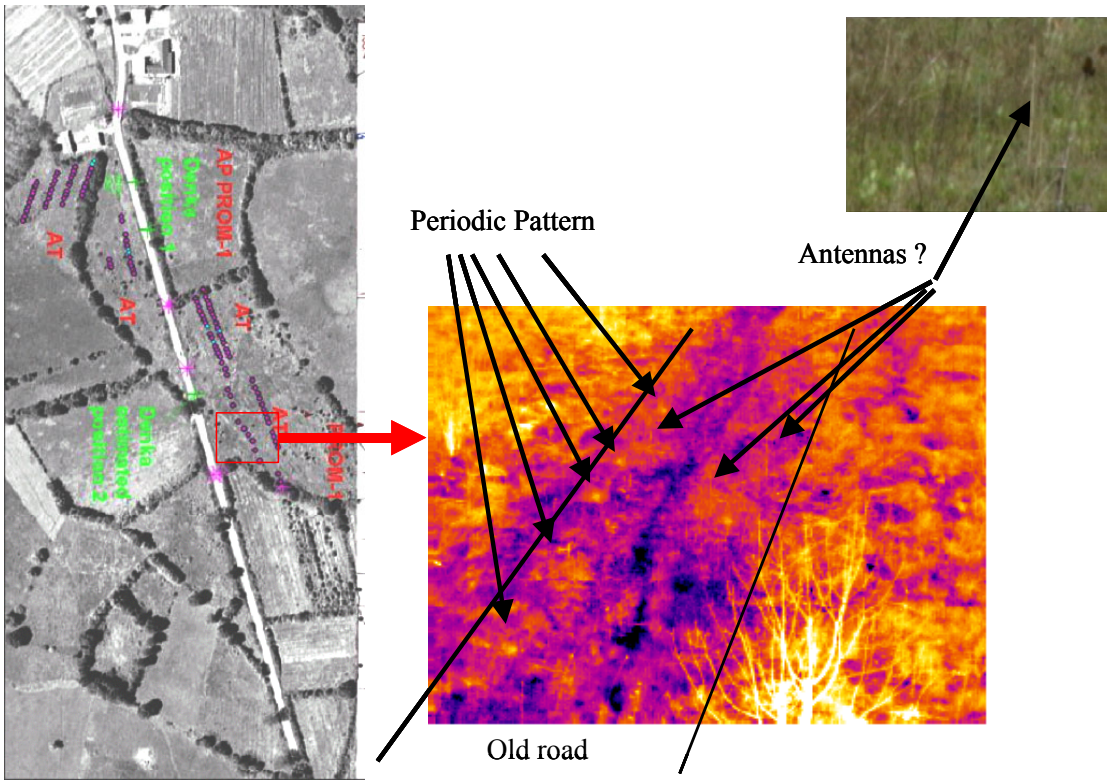

Figure 2.6 Example of images from a minefield in Marin Brod, Croatia, left: Arial photo of the area, middle: IR 8-9 µm, and top right: visual.

The overall concept for optical mine and minefield detection at FOI can be described according to Figure 2.7. Signal/Image processing, Experiments, and Modelling/Simulations are separate research areas here applied on the same problem which is a real world application. The development of methods in one research area takes results and methods from the other research areas into account.

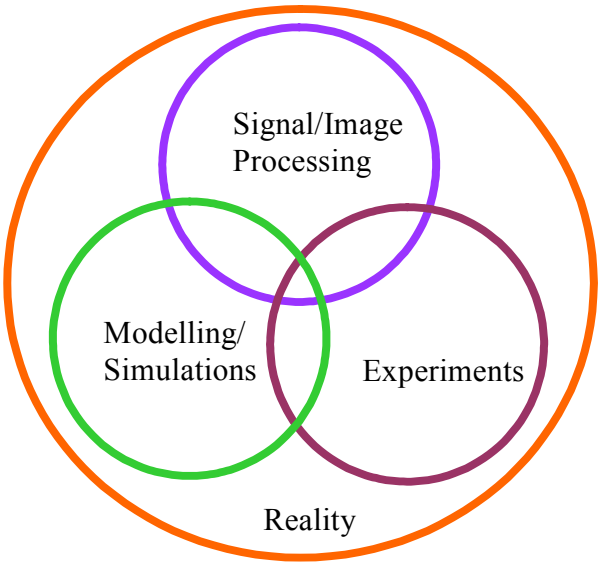

Figure 2.7 The research area includes experiments, modelling and simulations, and signal and image processing applied on real data.

Experiments are performed not only as a base for verifying the theoretical work on modelling and signal processing, but also as a source for the understanding of different phenomena that can be used for building the models and applying appropriate signal processing methods. Experiments are performed indoors under controlled conditions and outdoors in different test landscapes. Real minefields in Croatia have also been investigated. The equipment and test facilities are presented in chapter 3.

The modelling work deals much with thermodynamic modelling of heat and moisture transfer in soil with affecting objects, e.g. mines, under influence of boundary conditions such as energy exchange between the soil surface and the atmosphere. One of the main purposes of the modelling work is to understand and predict the mine induced thermal contrast on the surface that could be detected by an IR sensor. This is described in chapter 4.

The signal/image processing part deals much with the problem of detecting an object in a cluttered background. Different models for object and background features are used. The signal processing approach and methods are presented in chapter 5.

The general methodology is described in detail in Figure 2.8. Data capturing is performed by imaging sensors, the weather station and different loggers. A part of the data is fed into the numerical modelling algorithms and the images are pre-processed. The results from these two parts are merged in the signal processing.

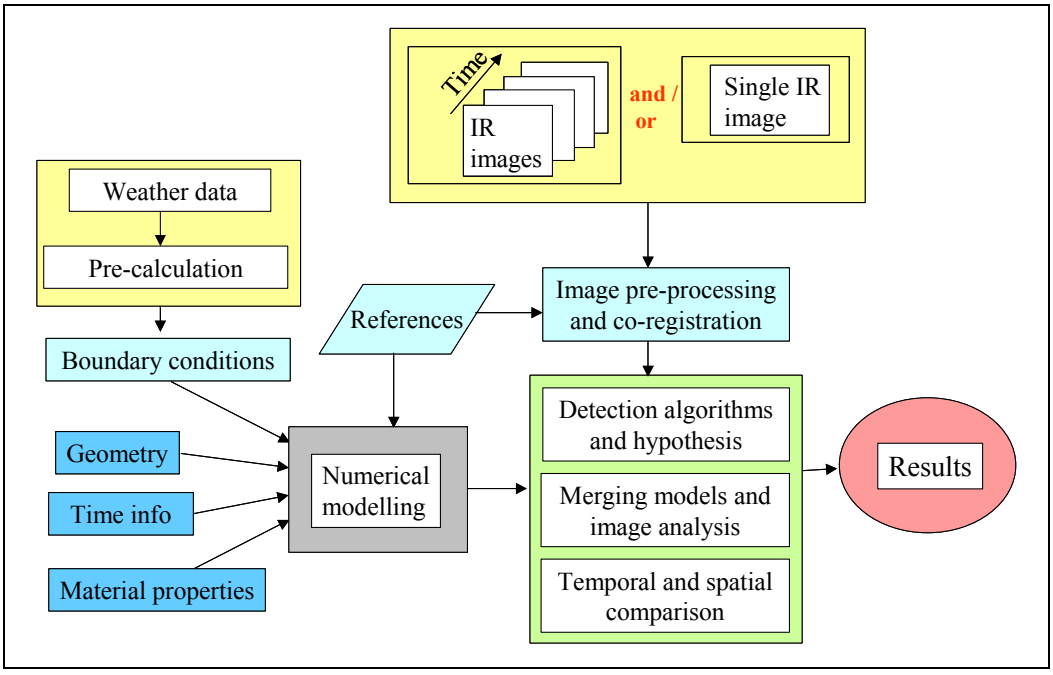

Figure 2.8 The schematically data flow of the presented method for temporal feature extraction.

This report sums the work of the optical mine detection group at FOI so far and is written as an introduction to following projects in the area. The aim is to report the evolutionary process and the wide range of research areas connected to the application rather than presenting deep research results.

3 MEASUREMENTS

Extensive measurements have been carried out, both full-scaled field measurements covering different environments as well as indoor laboratory measurements. The equipment used in the experiments have been summarized and explained in a special report [12]. This chapter deals with the data collection done by the optical mine detection group at FOI during the years 1997 to 2004. The chapter presents the sensors used and the different test facilities available, ranging from indoor sandboxes to minefields in Croatia. Different platforms have been used, from sky-lift to UAV. The data collection campaigns are summarized and the experience from the data collection and pre-processing are presented in this chapter.

3.1 SENSORS

Measurements have been carried out using different sensors. Imaging sensor in different spectral bands, sensors for collecting weather data and other reference sensors are presented here. Figure 3.1 show cameras mounted on a turntable on a lift.

Figure 3.1 Six different optical sensors mounted on the turntable. All useful wavelengths of the optical spectrum are covered.

An example of a sensor set-up for minefield measurements is presented in Table 3.1.

Sensor	Spectral range	Horizontal FOV (degrees)
AGEMA, Thermovision 900, SW AGEMA, Thermovision 900, LW FLIR Systems ThermaCAM SC3000	2-5.5 µm 7-14 µm 8-9 µm	20 or 5 20 or 5 20
XYBION IMC-201 Multispectral camera (6 bands)	320-390 nm 395-425 nm 490-510 nm 545-555 nm 675-685 nm 755-785 nm	28
SONY FCB-IX470P Video color camera	RGB	2.7 - 48
Camera for the near-IR Sony, SSC-M370CE	0.83 - 1.1 µm	14 or 3 - 96

Table 3.1. FOI sensors used in minefield measurements.

The most frequently used optronic sensors are ThermaCAM™ SC3000 from FLIR Systems for the thermal infrared, 8-9 µm. In the ARC project, TNO supplied a multispectral camera, Duncantech MS3100, for high resolution three bands visible and near infrared, see Figure 3.2.

Figure 3.2 Optronic sensors used on UAV in ARC project.

A number of weather and radiation parameters are measured with a weather station, Figure 3.3. It is a stand-alone system with an automated logging facility. Weather and radiation parameters that are measured are: visual sight, wind speed, wind direction, air temperature, soil temperature and moisture, relative humidity, air pressure, rain, net radiation, solar radiation (pyranometer), and sky radiation (pyrgeometer). The pyranometer measures hemispherical irradiance in the wavelength band 0.3-2.8 µm. The pyrgeometer measures hemispherical thermal irradiance in the wavelength band 3-50 µm and the net radiometer measures radiation in the wavelength band 0.3-60 µm.

Figure 3.3 Weather station.

The weather station is flexible in design in such a way that it is possible to use a subset of the most important sensors for situations when a complete weather station is too complex.

Reference markers have been designed and produced for the purpose of calibration of the IR camera on different operational heights, Figure 3.4 a. The markers are 50 cm by 50 cm each and are made of 3 mm aluminium plates and the backsides are thermally isolated with 70 mm thick Styrofoam with a very low conductivity. Four markers are painted with black colour and four with white colour with known reflectivity. Temperature sensors, Pt-100, are attached inside the aluminium in the centre of two of the black and two of the white markers. A 24-channel 16-bit logger system can be used to collect all data from the Pt-100 sensors, Figure 3.4 b. Since the parameters of the reference markers are known, we have a set of "true" temperatures from the sensor point of view. The calibration procedure when performing operational flights, is to make an IR registration of the reference marker once the operational altitude has been reached, and then set the focus. Later the influence from the atmosphere can be compensated, due to the actual transmission between surface and IR sensor, for each image.

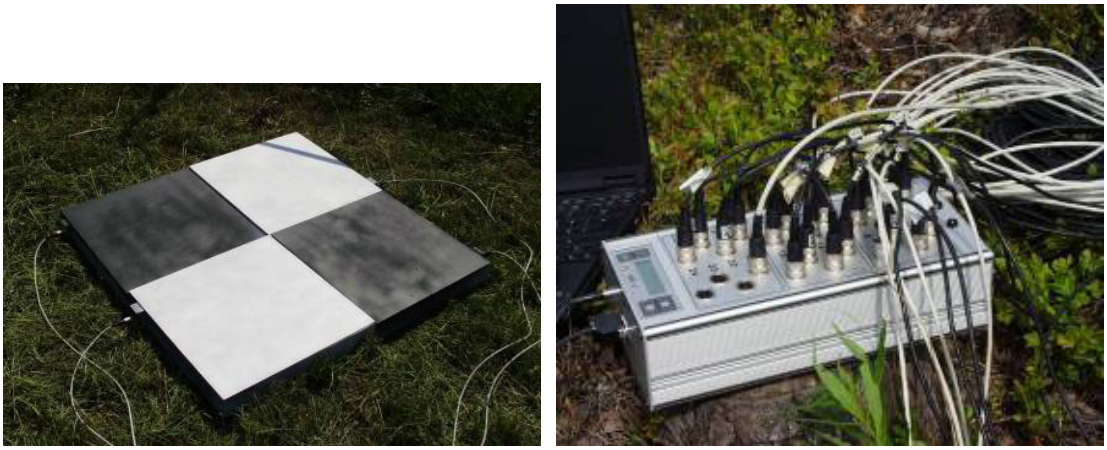

a b

Figure 3.4 a, Four, out of eight available, reference markers for temperature calibration. b, The 24-channel 16-bit logger system used to collect temperatures from references markers or soil at different depths.

3.2 TEST FACILITIES

Different kinds of test facilities have been used, e.g. indoor laboratory, outdoor laboratory with controlled environment except for weather, outdoor experimental test field and real minefields.

3.2.1 Indoors

An indoor test laboratory makes it possible to develop and test new equipment and algorithms under controlled conditions. The indoor laboratory environment is built up around two sandboxes. A small sandbox is equipped with a solar panel and a digital temperature recorder to carry out controlled laboratory experiments. The sandbox is shown in Figure 3.5 and consists of a square container, 1 m x 1 m x 0.4 m, insulated from the surroundings. The solar panel consists of 64 light sources which give a maximum irradiance of approximately 1000 W/m^2 at the surface of the sand and has a spectral distribution which corresponds well to that of the sun in the wavelength range 0.3-3 μm. The panel can be split into two parts, making it possible to mount IR cameras between the two parts. The irradiance can be varied either by adjusting the

height of the panel or by vary the radiance of the light sources. The digital temperature recorder and its accompanying logging program is PC-based and Pt-100 temperature probes are used.

Figure 3.5 Small sandbox and solar panel.

The other sandbox is larger, with the dimensions of 4.3x4.3x1.45 m, and equipped with a high precision XY positioner. This sandbox is designed primarily for controlled experiments with ground penetrating radar (GPR) but has also been used for experiments with optical sensors, Figure 3.6. The advantage is that a larger area can be repetitively scanned in order to detect non static features, like IR signature change for a large number of objects during heat up and cooling cycles. In this case it is not possible to use the solar panel as a direct heat radiator, other heat sources have to be used.

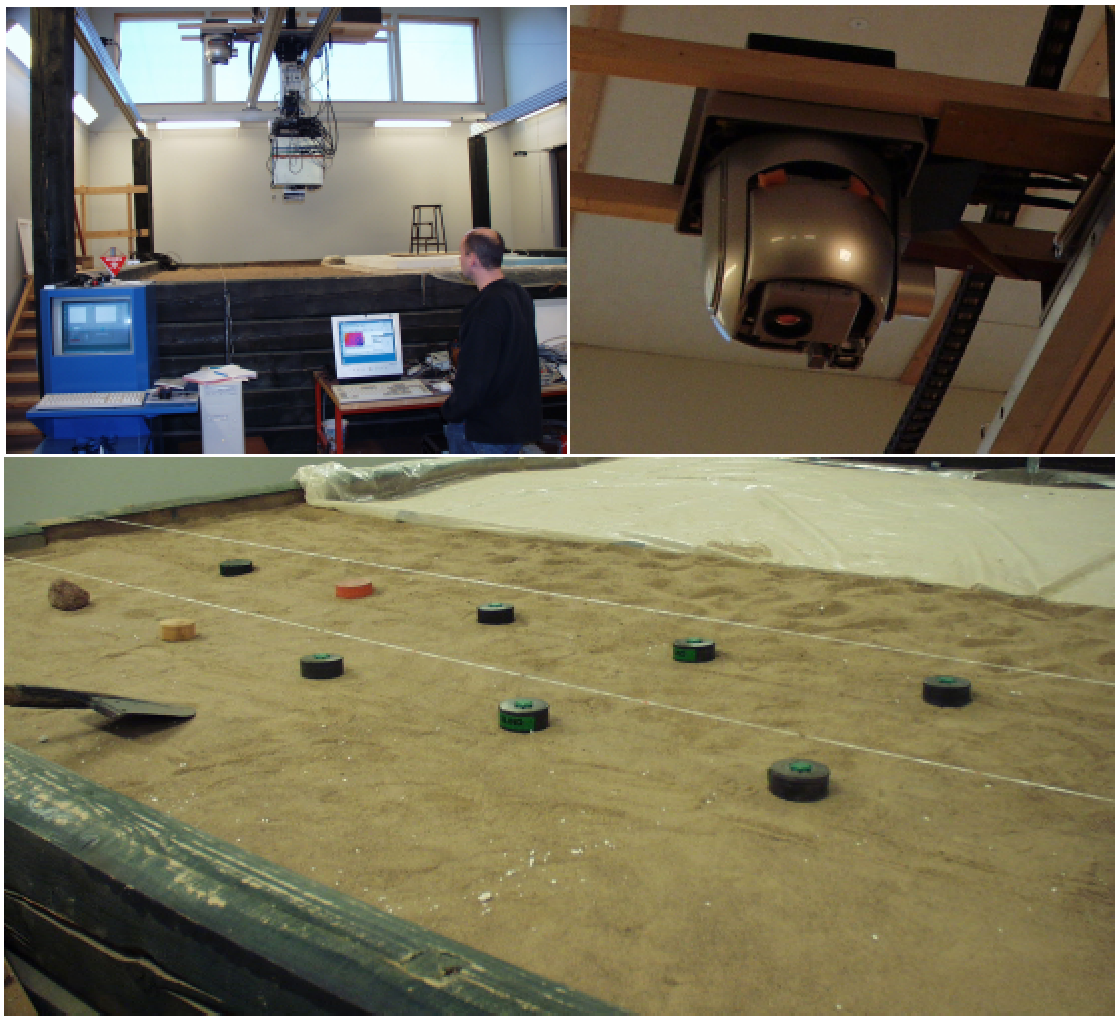

Figure 3.6 Upper left: Large sand box, 4.3x4.3x1.45 m, with high precision XY positioner. Upper right: An example of solution for sensor mounting. Bottom: Objects laid out before burial in sand.

3.2.2 Outdoors at FOI, Sandboxes

For the outdoor near laboratory experiments, eight boxes containing different soil qualities have been used, Figure 3.7. Box contents correspond to soil qualities in mine infected areas worldwide, e.g. the Balkans, Afghanistan, Kuwait, Mozambique, Angola, south-east Asia, Central America, and Africa besides Sweden. The wooden boxes are 3 m x 5 m and 0.7 m deep and are filled with clay, laterite, magnetite, coarse- and fine-grained sand, and moraine. The boxes can be protected with removable covers. Mines and other objects can be placed in the boxes for shorter or longer time periods.

Figure 3.7 To the left: one of eight experimental boxes containing sand in two different grain sizes. Sparse vegetation has been allowed to grove in one part. To the right: a close up.

3.2.3 Outdoors at FOI, Grass

A test landscape with mines buried in grass-covered soil is also available at FOI, Figure 3.8.

Figure 3.8 Outdoor test facility at FOI, winter and summer conditions.

3.2.4 Outdoors at FMV in Karlsborg

A fenced gravel road with buried mines has been available at FMV in Karlsborg, Figure 3.9. The road is now closed down, but was used for some diurnal measurements and analysis [9].

Figure 3.9 Gravel road with buried mines at FMV in Karlsborg, winter and summer conditions.

3.2.5 Outdoors at SWEDEC

At Swedish EOD and Demining Centre in Eksjö (SWEDEC), a new area for research and tests on explosives, including mines and UXO, has been established in cooperation with FOI, Figure 3.10. In the area there are various kinds of terrain represented, forest, low vegetation and gravel road. Measurements of different kind of real mines have been conducted in the area using optical sensors.

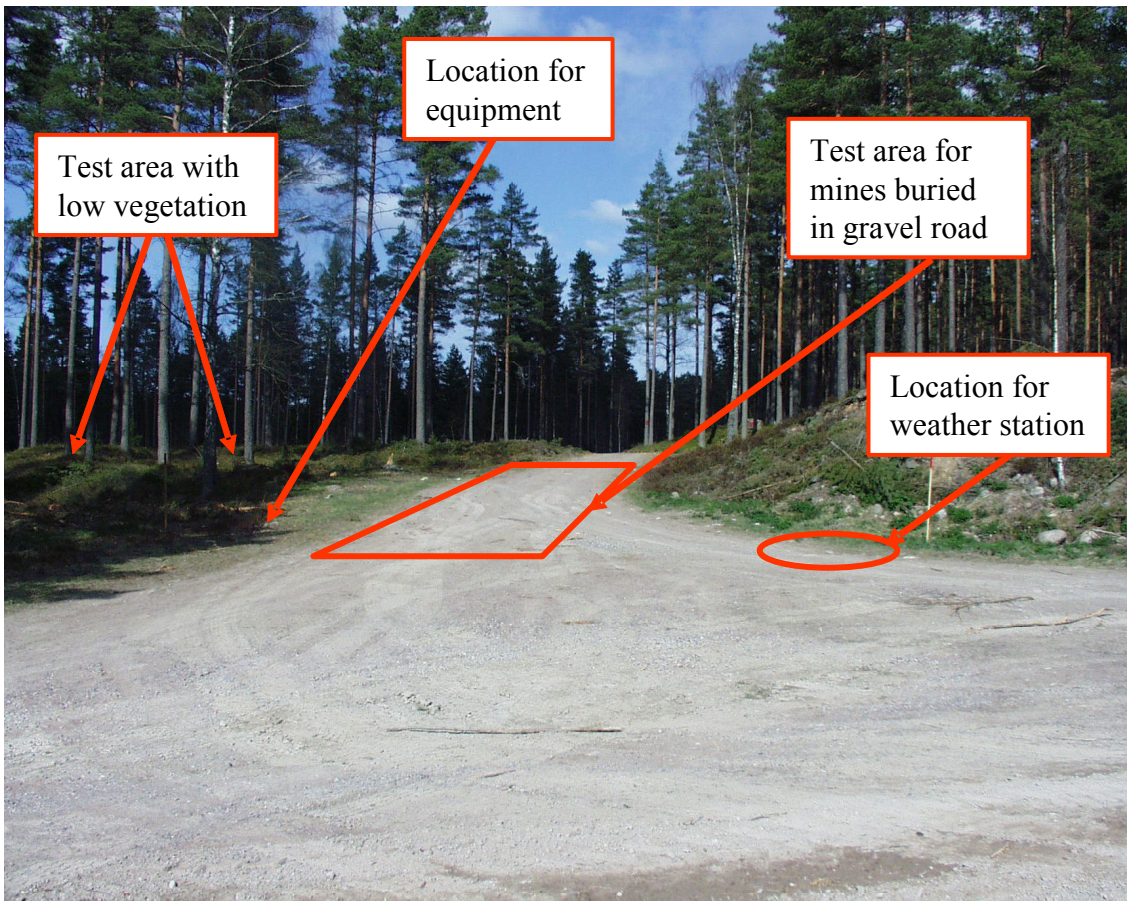

Figure 3.10 The gravel road part of area reserved for research and tests at SWEDEC test site, Eksjö.

3.2.6 Outdoors at TNO, Netherlands.

Measurements have been made on a grass field at TNO facility in Hague, Netherlands [13]. The purpose was to get information on spectral, spatial and temporal signatures of minefield indicator, Figure 3.11, and also diurnal infrared measurements were made on buried and surface laid mines at TNO test lanes [14], Figure 3.12.

Figure 3.11 Complete setup of the sky lift (left image), and test field with minefield indicators (right).

Figure 3.12. TNO test lanes (image from TNO web page)

3.2.7 Outdoors in Croatia

Ground based as well as airborne measurements have been made in Croatia on several occasions during the ARC project, reported in [11]. A mined area in village Marin Brod was used for combined ground and air based minefield registration, Figure 3.13. The minefield was covered with dense vegetation, grass and small bushes. This is typical for agriculture land that has been out of use for some years.

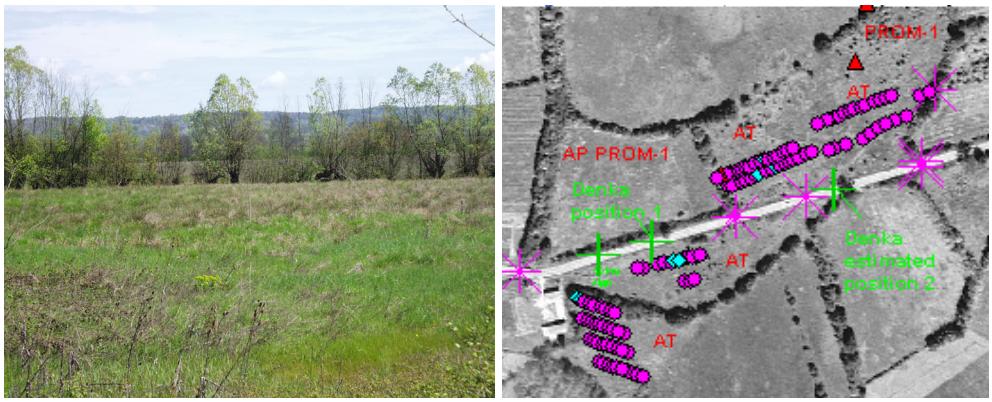

Figure 3.13 Area in Marin Brod, south of Zagreb, used for combined ground and air based minefield registration. Later, the area was demined and the results is shown to right.

Registrations have also been made of minefields in southern part of Croatia in Pristeg not far from Zadar city, Figure 3.14. The ground in this area consists of small rocks and pebbles and sparse vegetation.

Figure 3.14 Minefields in Pristeg.

Measurements were also made on minefield in a former agricultural area in Milecovici. This area is close to Marin Brod and has the same character with low dense vegetation and small bushes, Figure 3.15.

Figure 3.15 Minefield in Milekovici area.

3.2.8 Snow conditions in northern Sweden

A prestudy was conducted in northern part of Sweden in January 2003 on mines in 50-60 cm deep snow. An example of IR image is given in Figure 3.16. In the morning at 08:50 the background temperature is approximately -32 ^{o}C and the mine temperatures -19 ^{o}C. In the evening at 17:30 the background temperature is approximately -19 ^{o}C and the mine temperatures -18 ^{o}C.

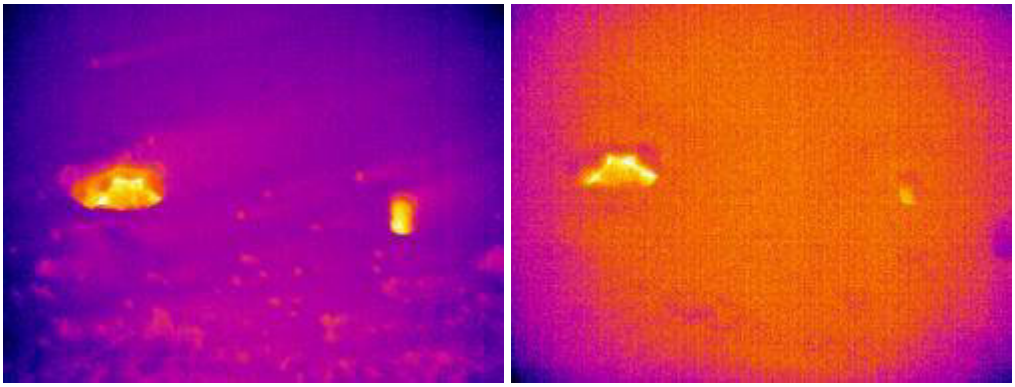

Figure 3.16 Mines in snow. AT mine 47/52 to the left, HB-876 to the right.

3.3 SENSOR PLATFORMS

Different sensor platforms have been used. In doors laboratory tests are performed with sensors mounted in a manual lift, Figure 3.5 or high precision x y positioner, Figure 3.6. Outdoors Mast/skylift is used for diurnal measurements. Different kind of airborne platforms are used for experiments on real or artificial minefields.

3.3.1 Mast/Skylift

One intended application of the research on optical methods for detecting landmines is the use of an airborne sensor platform. For that reason it is an advantage to be able to make diurnal measurements from an elevated position. In Figure 3.17 examples of an elevated mast is shown. Examples of sky lift based measurements are shown in Figure 3.8 and in Figure 3.11.

Figure 3.17 Elevated mast with sensors mounted on turntable.

3.3.2 Helicopters

Airborne measurements were made in the ARC project with sensors mounted in a MI-8 helicopter, Figure 3.18, and with selected sensors mounted on a Bell helicopter, Figure 3.19.

Figure 3.18 MI-8 Helicopter (left image) and sensor pack (right image).

Figure 3.19 Bell helicopter with sensors.

3.3.3 UAV

In the ARC concept, the CAMCOPTER® from Schiebel Corporation in Austria has been used as sensor platform, Figure 3.20. A data sheet for the platform is presented in Table 3.2.

Figure 3.20. CAMCOPTER® from Schiebel Corporation in Austria

Type:	CAMCOPTER® S.1 UAV System
Mission radius:	10 km (6 miles) standard up to 100 km (60 miles) with enhanced link
Standard sensor:	forward looking CCD Camera (pilot camera)
Data/video link:	C-band (data up- and down-link)
Control:	fully autonomous by waypoints, manually by joystick control
Navigation:	INS and DGPS-based

AERIAL VEHICLE

Power plant:	15 HP two-stroke, air cooled aviation engine
Tank volume:	13.5 liters (3.5 gal), expandable up to 30.5 liters (8.1 gal)
Rotor system:	two-blade main rotor with Bell-Hiller stabilizer and two-blade tail rotor
Cruise speed:	90 km/h (56 mph)
Climb rate:	180 m/min (600 ft/min)
Service ceiling:	3000 m (9900 ft) MSL
Maximum endurance:	6 hours
Length:	2500 mm (98.43")
Main rotor diameter:	3090 mm (121.65")
Empty weight:	43 kg (95 lbs)
Maximum payload:	25 kg (55 lbs)
Payload interface:	two switchable video inputs (PAL or NTSC), one RS-232C half duplex data interface power supply (3.5 A @ 5 to 28 VDC)
Ground interface:	diagnostic port, ground power-in

CONTROL STATION

Dimensions (storage):	508 mm (20.00") wide 580 mm (23.50") deep 273 mm (10.75") high
Monitor:	18" TFT color LCD 1280 x 1024 pixel flat screen
Processors:	Pentium III, 1 GHz, 512 MB RAM (expandable)
Storage media:	two removable 18.1 GB hard disk drives integrated CD ROM drive integrated read/write DVD drive 3.5" floppy disk drive
Interfaces:	RS-232C payload port PAL or NTSC video down-link
Power:	AC source, 85 - 132 V, 170 - 264 V, 47 - 440 Hz DC source, 20 - 32 V DC integrated UPS battery

Table 3.2 Data sheet for CAMCOPTER®.

The ARC payload system is mounted on the CAMCOPTER® payload pallet Figure 3.21. The payload system consists of two separated parts, the front part holds the cameras and the aft part the equipments e.g. computers and data storage devices.

Figure 3.21. ARC payload on CAMCOPTER®

The front part holds both the Thermacam and the Duncantech cameras in a common device. This device is connected with an outer arrangement with four wire dampers. This construction gives, with the four wire dampers, a centre of vibration reduction located at 8 Hz. The inner device could, for each flight mission, be turned in different viewing angles.

The aft vibration-isolated box, for the data acquisition equipments, consists of a two-stage dampening system. The upper dampers are made of rubber and the lower are four wire dampers.

3.3.4 MASP

In close collaboration with another project at FOI a Modular Airborne Sensor Platform (MASP) has been developed [15, 16] Figure 3.22. The sensors and supporting equipment such as data acquisition, navigation and gimbal is mounted in a pod carried by a full size helicopter in a single wire. The MASP system will be useful for research on detection of mines and minefields, especially because the sensor data is combined with high precision navigation data. This makes it possible to perform diurnal IR registrations with high position accuracy. It is very important when developing and testing detection algorithms based on temporal scene properties. One other major advantage of the system is that it doesn't require comprehensive helicopter installations.

Figure 3.22. Modular airborne sensor platform, MASP.

3.4 TURNTABLES

FOI has access to two turntable systems, one small Figure 3.23 (left) and one large Figure 3.23 (right), with the possibility to mount a number of sensors. With the turntables it is possible to perform high precision repetitive pan and tilt scans remotely controlled by computer. One purpose is to be able to capture diurnal sensor data from one position, but in a number of different orientations. The precision of the repetitive positioning is nearby pixel level. The small turntable supports payloads up to 15 kg, the big turntable supports payloads up to 150 kg.

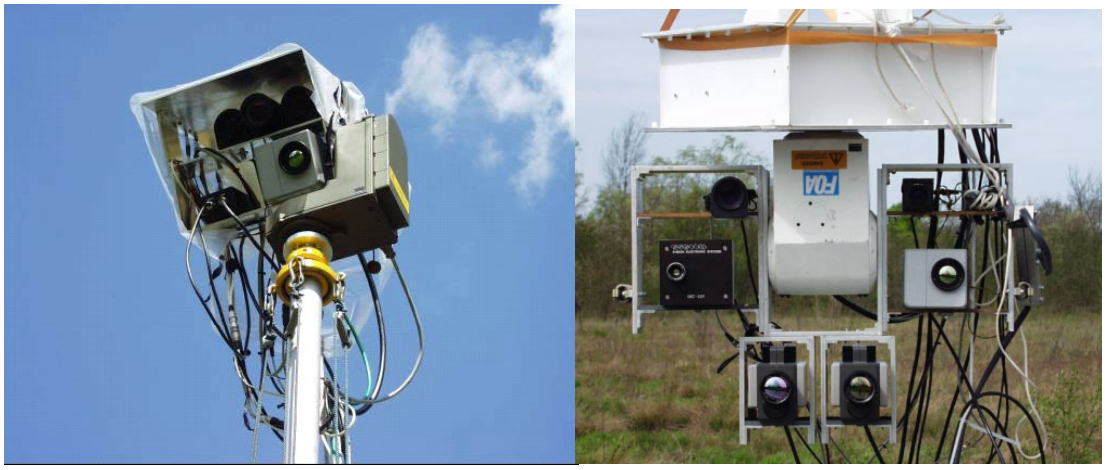

Figure 3.23. Small turntable (left) and big turntable (right).

3.5 DATA COLLECTION

In the planning phase of a measurement campaign there are a lot of things to consider. Depending on the varying nature of each campaign, it is of course impossible to make a complete list of all important factors, but in general, the list below reflects experience achieved during all years of experimental activities.

- Selection of location
  - Indoors for controllable conditions
  - Outdoors close to lab
  - Outdoors laid out mines
  - Outdoors real minefields

- Character of location
  - Homogenous e.g. sand
  - Gravel road
  - Grass and low vegetation
  - Partly vegetated
  - Forest
  - Sun orientation, consider diurnal shadow variation from surrounding trees and other obstacles (sensor platform)
  - Slopes in terrain will influence irradiation
  - Water content

- Type of object
  - AP-mines
  - AT-minor
  - Generic / real mines
  - False objects
  - Indicators of mines or minefield indicators
  - Indicators of activity often associated with mines
  - Directional fragmentation mines
  - Surface properties (not buried)
  - Heat capacity and heat conduction

- Time parameters
  - Time of year
  - Age of minefield, old and newly laid mines have different signatures
  - Repetitive measurements to study influence of minefield aging on signatures
  - Number of hours/days. Not necessary same for all sensors, it can be an advantage if measurement of weather parameters and temperature can start earlier.
  - Temporal sampling, how fast will studied phenomenon vary

- Sensor selection
  - Infrared
  - Visual
  - Ultraviolet
  - Spectral resolution (mono- multi- or hyperspectral)
  - Sensitivity
  - Polarisation
  - Spatial resolution, number of pixels on target
  - Weather station, complete or subset of sensors
  - Temperature measurements
  - Sensor position and orientation for each image

- Data acquisition and storage
  - Computers and memory size
  - Environmental influence e.g. water, temperature and vibrations
  - Data rate
  - Data handling and backup

- Platform selection
  - Tripod
  - Skylift/Mast
  - Moving flying, moving ground based or stationary
  - Turntable of fix mounte
  -
- Others
  - References for spatial and radiometric calibration
  - Working environment and working time
  - Data handling
  - Combat history (if applicable)
  - Permissions rules etc.
  - Logistics, transports, custom declarations (if applicable)
  - Weather protection of equipment
  - Access to electric power
  - Spare parts and mechanical
  - Insurance of personnel and equipment

3.5.1 Measurement campaigns

The measurements during the years have followed an evolutionary trend from having focus on laboratory measurements in the beginning to complete minefield measurements in later years. At all measurements at least one IR camera (long wave IR) has been used, often complemented with other cameras in the spectral range of middle and short wave IR, visual and ultra violet. Below is a list of measurement campaigns carried out between 1997 and June 2004.

- 1997, Mars and April, indoors, sand, FOI
- 1997, April and May, outdoors, gravel road, Karlsborg
- 1997, June, outdoors, clay, FOI
- 1997, June, outdoors, grass, Eksjö
- 1997, May, July and August, outdoors, sand, FOI
- 1997, August, outdoors, sand, clay, moraine, grass, FOI
- 1997, October, outdoors, grass, asphalt, FOI
- 1997, October, indoors, sand, FOI

- 1998, April, indoors, sand, FOI
- 1998, May, August, outdoors, sand, FOI
- 1998, November, outdoors, grass, FOI
- 1998, November, outdoors, gravel road, Karlsborg

- 1999, January, indoors, sand, FOI
- 1999, April, May, June, July, August, September, outdoors, sand, FOI (study of long term effects, duration 1999 to 2004, Pt-100 sensors)
- 1999, May, June, July, August, outdoors, grass, FOI
- 1999, May, outdoors, grass, FOI
- 1999, May, September, outdoors, gravel road, Karlsborg
- 1999, June, August outdoors, latherite, FOI

- 2000, January, April, indoors, sand, FOI
- 2000, May, September, outdoors, grass, FOI
- 2000, May, June, July, September, outdoors, sand, FOI
- 2000, July, outdoors, grass, FOI

- 2001, April, outdoors, grass, TNO Netherlands
- 2001, April, outdoors, minefields, Croatia (including airborne)
- 2001, July, outdoors, sand, TNO Netherlands
- 2001, October, outdoors, minefields, Croatia (including airborne)
- 2001, November, outdoors, test field, Vienna (including airborne)
- 2001, December, indoors, sand, FOI

- 2002, May, June, outdoors, test field, Vienna (including airborne)
- 2002, July, outdoors, minefields, Croatia (including airborne)
- 2002, August, outdoors, sand, FOI

- 2003, January, outdoors, snow, Boden
- 2003, April, outdoors, test field, Vienna (including airborne)
- 2003, April, outdoors, gravel road, Eksjö
- 2003, May, outdoors, minefields, Croatia (including airborne)
- 2003, November, test field, Vienna (including airborne)

- 2004, May, June, gravel road, vegetation, Eksjö
- 2004, June, outdoors, sand, FOI

The high performance 24-channel logger system with Pt-100 temperature probes is normally used to gather temperature data from different positions in the scene, e.g reference markers, different depths in the soil, vegetation layers, mines and mine like objects. In the outdoor measurement campaigns, the weather station has also usually been used. The logger system has been used to collect temperature data from different buried mines and their surroundings in long periods (4-5 months) 1999 to 2004.

3.6 IMAGE CO-REGISTRATION

For both mosaicing and temporal data analysis image co-registration is required. The implemented approaches are described below.

3.6.1 Co-registration , mosaicing

The images will have a different rotation, skew and possibly a different gain due to illumination changes. The image registration technique can estimate translation, zoom, rotation and skew of a high resolution image with respect to a overview low resolution image. The image registration will minimize the difference between the two transformed images. To account for illumination changes, the gain and offset difference between the two images can be estimated in an iterative procedure. A multi-stage approach has been developed for co-registration at FOI. A collection of images from a limited local area is chosen, typical 10-50 images from one flight. The pair wise co-registration of the overlap between all images from the area is computed using a phase based approach and the result forms a network. The alignment method is based on an 8-parametric plane/parallax displacement model implemented in an iterative framework, shown in Figure 3.24. The model is initiated by navigation data from the INS/GPS-module but, due to lack of precision in available navigation data, it needs support from the operator to initiate corresponding landmarks by visual inspection. A simple GUI has been developed for this purpose. Corresponding features are aligned using the phase value of Gabor filters that are tuned to all orientations and to typical spatial frequencies in the scene. Local regions with low contributions to the global solution are suppressed using robust statistics in the estimation of parameters. A global solution at a coarse spatial level is transferred to the next scale level. At the finest level, after the final global warping, a local displacement field is estimated at each pixel position. This parallax field can be used for further analysis since it corresponds to the 3D-structure of non-planar regions.

The pair wise match between images, estimated by the method described above, forms a network, see Figure 3.25. The final position of images is solved for the full network using a bundle adjustment method described as an information filter. The state vector consists of the ground position of each projected image corner from a flight, described by 8 corner parameters per image, and the initial navigation solution is used as an a priori estimate. For each link in the network, information is added to the information state iteratively. The information matrix is illustrated Figure 3.27. When all information from all linkages is added, the bundle adjustment is performed on the information state by solving the sparse linear equation, and a local mosaic is achieved. This position update is shown in Figure 3.26. The resulting three mosaics of a local area from noon, evening, and morning flights are shown in Figure 3.28 to Figure 3.30.

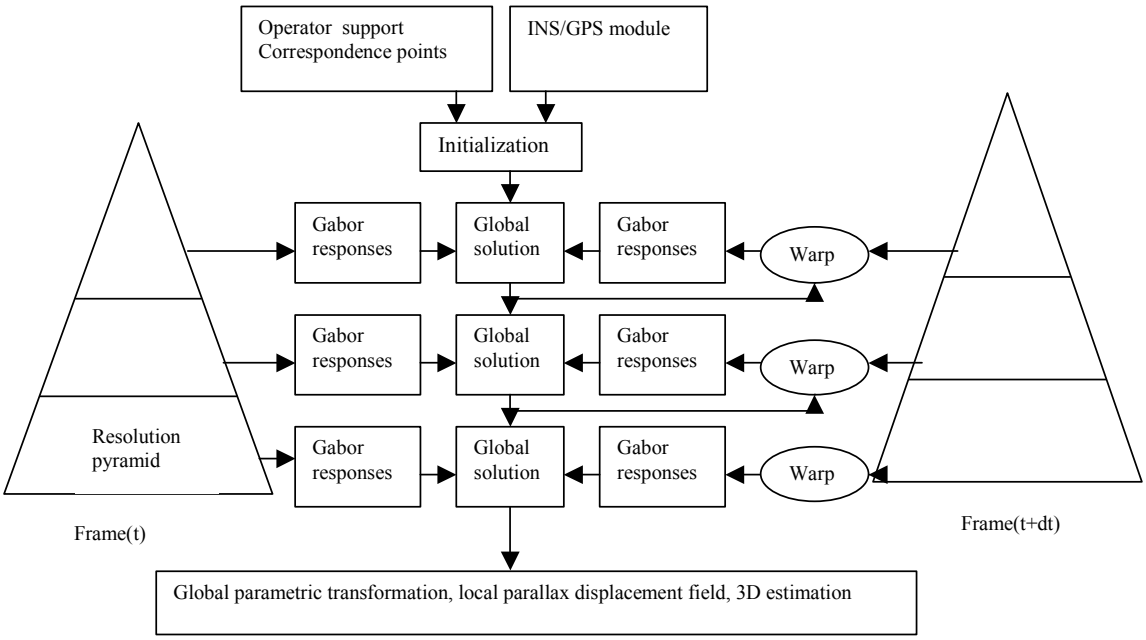

Figure 3.24 Co- registration of thermal imagery.

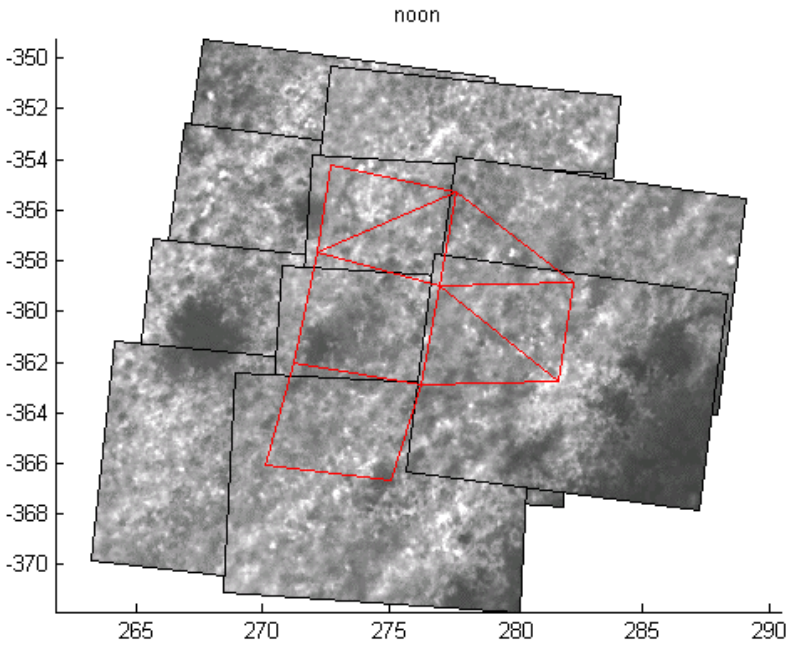

Figure 3.25 Typical network of co-registrated images before optimization.

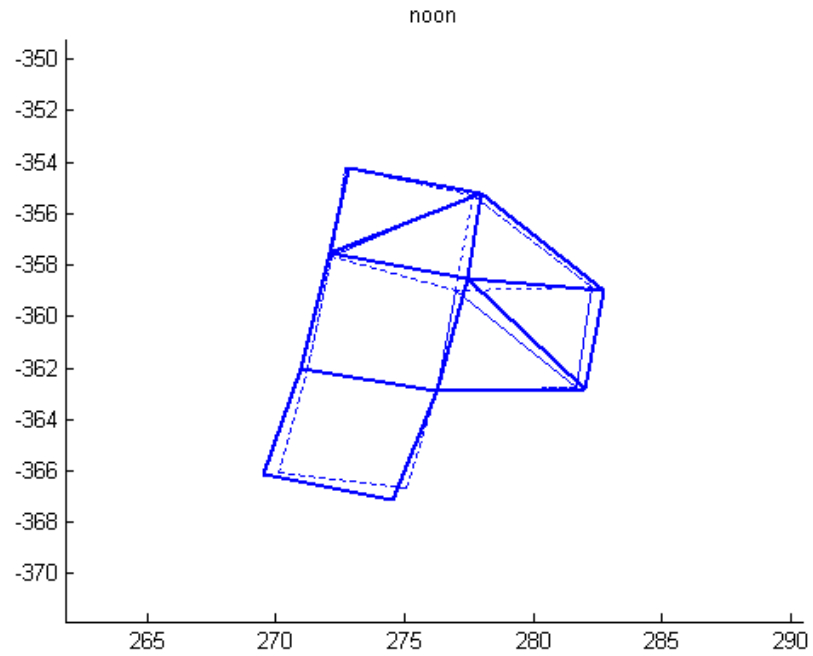

Figure 3.26 Corresponding network of coregistrated images during a update stage in the optimization. Thinner lines corresponds to links between initial position of all image centre.

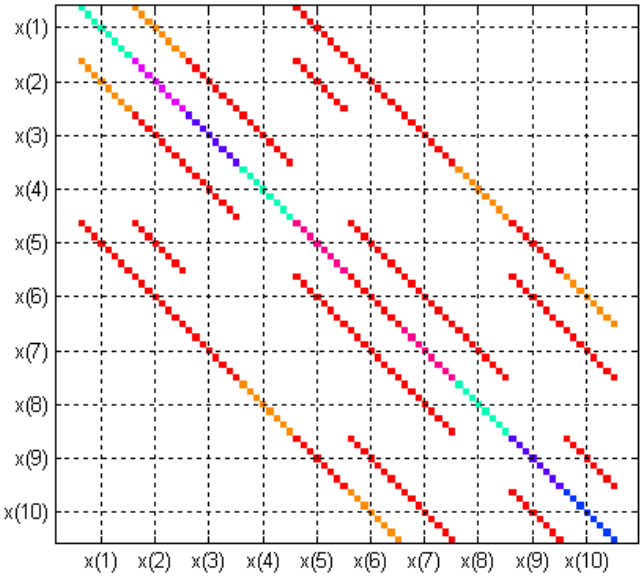

Figure 3.27 The sparse information matrix used for the local coregistration of flight pass 6. The position of images are represented by x(1) to x(10), each corresponding to eight corner coordinates.

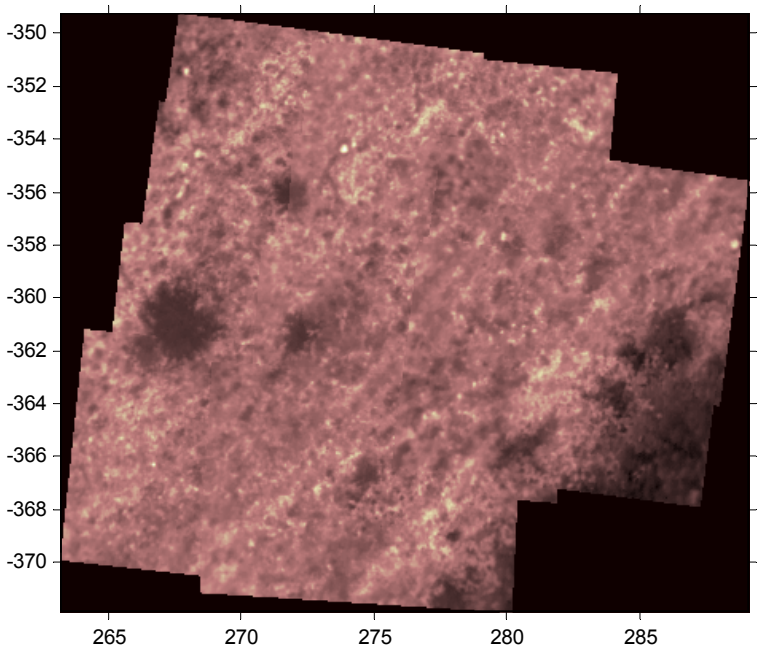

Figure 3.28 Local mosaic from flight pass noon.

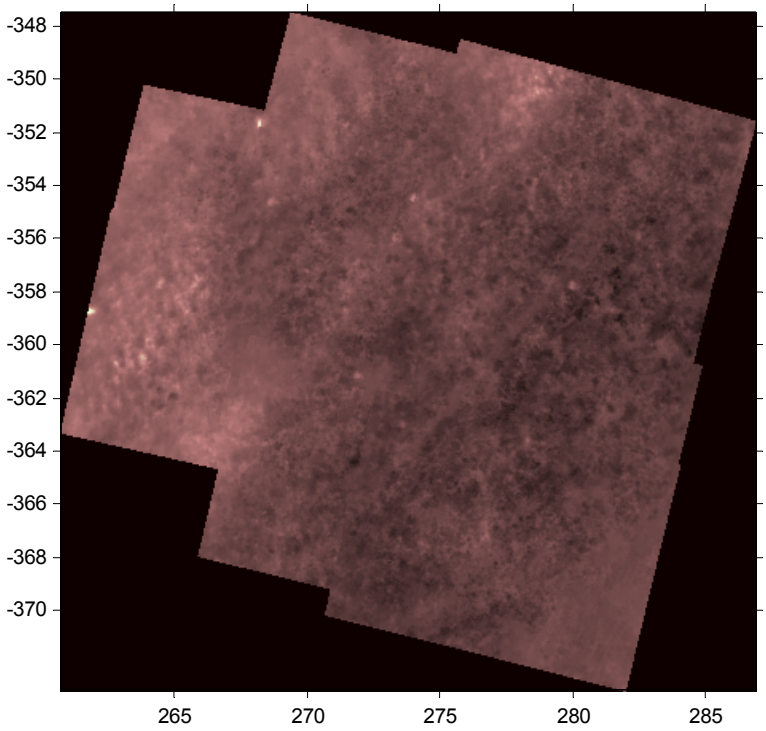

Figure 3.29 Corresponding local mosaic from flight pass evening.

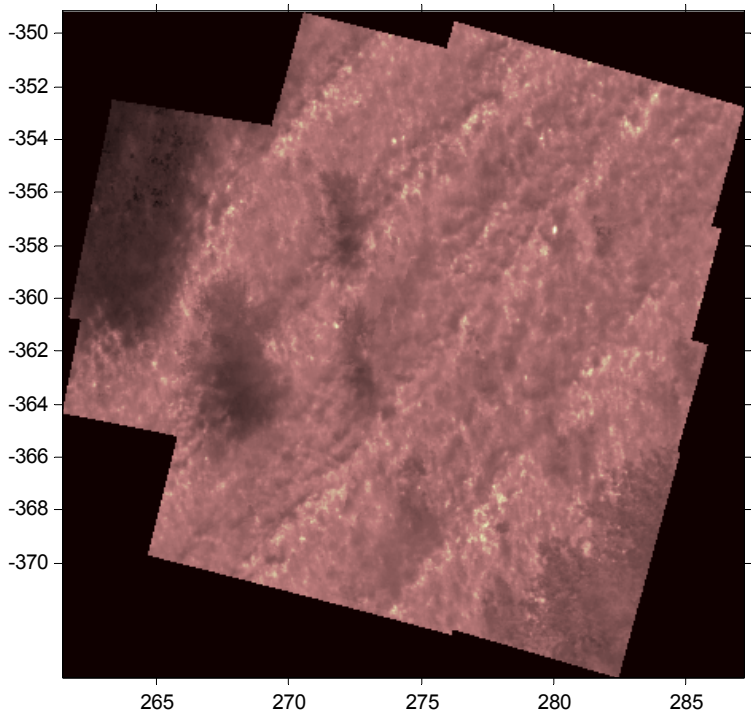

Figure 3.30 Corresponding local mosaic from flight pass morning.

3.6.2 Diurnal co-registration

To be able to apply temporal detection algorithms the images have to be co-registered pixel-to-pixel even when captured at different time. This is illustrated by Figure 3.31. Due to lack of good navigation data, manual inspection stage is needed to establish a number of correspondences between the mosaics from different flights. The final global solution for diurnal co-registration is created using the information matrices from all flights simultaneously.

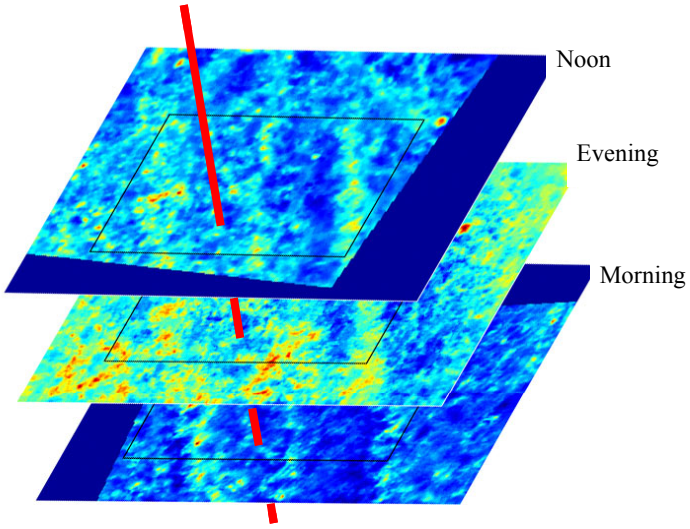

Figure 3.31 A schematic illustration of the co-registering of the analysed images collected at three different times during a diurnal cycle. The line shows the position correspondence for a specific pixel in the scene.

3.6.3 Image stabilization

Image stabilization is the image registration applied to a sequence from a single sensor. Contrary to the mosaicing purpose of image co-registration, the output is a new stabilized sequence. When the camera is mounted on an unsteady or moving platform and objects are far from the camera, the 3-D space motion of the camera will affect the images. Even small movements of the platform can result in large displacements of the images. This effect should be estimated and eliminated electronically by warping each image frame into precise alignment with a reference frame. The displacement between images has a predominantly global character. In most cases the distortion between two consecutive frames is a translation and rotation. The third dimension movement changes the distance between camera and object, resulting in a change of scale in the consecutive images. A survey of image registration methods is given in [17].

The main problem when stabilizing IR sequences collected during perhaps several days is the quite large lack of similarity between daytime and night time images. Normal direct cross correlation of the pixels fails often when most of the contrast almost disappears or even reverses, when the sun goes down. The method, used in most cases, has been to correlate a gradient image of the current frame with a frame chosen as reference. In this way we get a higher and more distinct correlation maximum. From the position of the correlation maximum the vertical and horizontal

displacement can then be computed. If needed the displacement estimation can be done with subpixel precision. To overcome the contrast problem in long time collection of data, a tracking approach has been tested. Each new frame is correlated with the previous frame and registered. However, a small error is accumulated for each frame and will at some moment be too big.

In a recent collection of data, rotation is an issue. To cope with rotation a method with translation, rotation, and scale-invariant registration has been used [18]. Here a logpolar transformation is applied to the Fourier transforms of the reference image and the image to be stabilized. This step is followed by a normal correlation. Again subpixel precision is available. This method has only been tested on a small number of frames.

4 MODELLING

The objective of this part of the work is to improve the understanding of the heat and mass transfer mechanisms around buried objects with the purpose to utilize the most favourable conditions for detection. The detectable contrast depends to a great extent on the history and the actual environmental properties interacting on the surface and the buried objects. Other issues are to support image analysis and feature extraction algorithms and as a decision support tool to predict when to carry out flights to achieve maximum contrasts.

Due to rapid variations in weather conditions a non-steady state thermal model is a relevant way to search a numerical solution for the temperature distribution in the mine and the local background. The measured weather parameters, registered normally every minute, are used as boundary conditions in the simulations. If no measured values are accessible the boundaries could be derived from models as well. The thermodynamic simulations are then carried out for different objects at different depths over the actual periods.

Here we give a limited discussion of the basic relations of the most important parameters, and some examples of them and their results. For more information see Sjökvist [8].

4.1 NUMERICAL MODELLING

Independent by the chosen method the governing partial differential equations have to be solved with respect to actual boundaries in order to solve the diurnal thermodynamic conditions between the surface of the soil, including mines and minelike objects, and the atmosphere. The actual numerical method chosen to solve the problem has mainly been the finite element method (FEM) but also some models have been implemented by the finite difference method (FDM).

From the beginning the chosen solver for the calculations was THAFEM, Thermal and Heat Analysis by Finite Element Method, see D. Loyd et al. [19]. THAFEM is based on a standard finite-element formulation. It is a medium-sized, special-purpose program, intended for two-dimensional plane and axi-symmetric problems, stationary as well as time-dependent. The equation system is solved by Crout's method and the Crank-Nicholson procedure [20] is used in time-dependent problems. Routines for phase transition, for internal heat generation and combustion are included in the program.

The diurnal temperature alteration occurs in a relatively thin layer, about 10-cm, near the surface. A buried object is normally located in this soil layer and will influence both the heat and mass transfer and, as a result of its presence, a temperature contrast can arise on the surface.

For numerical models, assumptions of the real environment and boundaries have to be made. The most important principle is that the energy interaction between the studied

object and the surrounding is balanced. In this case we are modelling the complex energy exchange between the surface of the soil, including mines and mine like objects, and the atmosphere.

All modelling work has been carried out very close to the experimental part of the project with the purpose to achieve high accordance between measured values and simulated.

The chosen numerical methods for solving the heat balance problem is the finite element method (FEM), in order to solve the diurnal thermodynamic conditions, see O. C. Zienkiewicz [21] This method is widely used and well suitable for solving parabolic partial differential equations such as heat transfer problems. In some models, finite difference methods (FDM) code have been written to solve specific tasks.

Later, a new model has been derived in the FEMLAB and MATLAB [22] environments. Also these sets of models are based upon physical laws implemented with FEM. One reason for using FEMLAB based models are the higher flexibility and the possibilities to couple different physical problems e.g. heat transfer, mass transfer and fluid mechanics in the same model. Also the possibilities to calculate in three dimensions and the collaboration with image processing algorithms are quite important factors. For a lecture in heat transfer the reader is supervised to Carslaw and Jaeger [23].

4.2 ENVIRONMENTAL MODELS

In a numerical model of the complex energy exchange between the surface of the soil, including mines and mine like objects, and the atmosphere, assumptions of the real environments have to be made, e.g. Deardorff [24], Miller [25] and Clement [26]. The basic equation for the principle of conservation of energy is given by:

$$\sum_{i=1}^{n} \dot{Q}(i) = 0$$

where $\dot{Q}(i)$ are n different energy transport processes between the studied objects and the local environment, and could in this case be derived from 7 different processes shown in Figure 4.1. The energy transport processes are:

$\dot{Q}(1)$ Heat and mass transfer in the soil and objects
$\dot{Q}(2)$ Convective heat transfer at the surface
$\dot{Q}(3)$ Absorbed radiation (< 3 μm)
$\dot{Q}(4)$ Longwave radiation exchange (> 3 μm)
$\dot{Q}(5)$ The surface emission
$\dot{Q}(6)$ Evaporation and condensation
$\dot{Q}(7)$ Sources and sinks

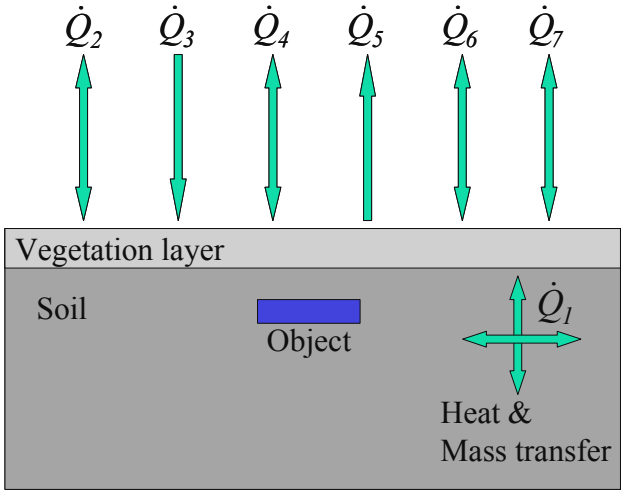

Figure 4.1 The energy transport processes between the studied object and the local environment. The arrows also shows the possible direction of the energy transports.

The overall problem could be formulated as a non-steady state equation where the energy balance over the surface exposed of natural energy exchanges. A lot of articles are presented on this topic and a good survey and overview can be found in J. S. Accetta and D. L.Shumaker [27]. The equation is written:

$$\frac{dT}{dt} = \frac{k_1}{\rho c}\left(\alpha_{sun} E_{sun} + \varepsilon_{sky} E_{sky} - \varepsilon\sigma T^4 - h(v)(T - T_a)\right) - k_2(T - T_0) + \dot{Q}$$

where E_{sun} and E_{sky} are the sun and sky irradiance on the surface, α_{sun} is the solar absorbtivity on ground, ε_{sky} is the sky emissivity, ε is the background emissivity, T is the surface temperature that we are solving for, T_a is the ambient air temperature, $h(v)$ is the convection coefficient as a function of the wind speed, T_0 is the diurnal temperature in the soil volume. This means a constant temperature at a specific depth where the diurnal temperature alteration will not occur. k_1 and k_2 are constants. Finally ρ and c are density and specific heat respectively. $\dot{Q}$ is a source or sink term that could be used for optional energy transports.

Normally some of the properties are known from literature or from measurements, e.g. density, ρ, and specific heat capacity, c. Some parameters are very hard to determine for the specific scenario that have to be modeled e.g. the absorbtivities, emissivities and wind coefficients.

For a more complete solution of a buried object, dependent of both heat transfer and the mass transfer in the soil, an approach with coupled differential equations need to be carried out , see e.g. Hartley [28], Kaviany [29] and Sjökvist [30, 31].

4.2.1 Soil parameters

The composition of the soil includes quite different materials with different thermophysical properties that also depend on the soil moisture contents. Field measurements of soil parameters for each of the soil components, like heat capacity, conductivity and moisture level, is a difficult task which can only be accomplished with indoor laboratory measurements. Therefore, it is common to measure bulk values for all these soil components together. It is also possible to use empirical developed models.

The heat conductivity, k, depends on the moisture content. As an example the moisture dependence for sand with a degree of quartz is shown in Figure 4.2.

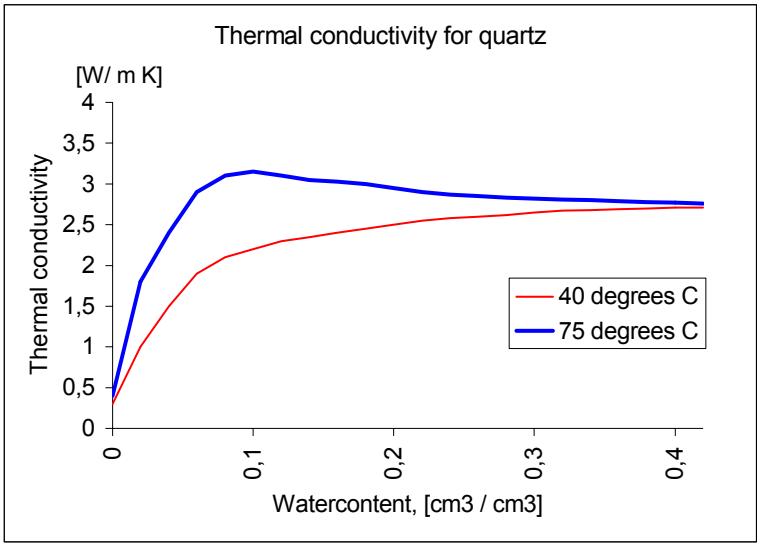

Figure 4.2. Thermal conductivity of sand with a high degree of quartz as a function of soil moisture content. From Jacobs [32].

Also the term with density, ρ, and specific heat capacity, c, depends on the moisture. A rough method is to summarize the soil content in the following way, see eg Miller [25] and De Vries [33, 34]:

$$\rho c = 1.9x_m + 2.5x_o + 4.2x_w \qquad (10^6\ \mathrm{Jm^{-3}\ K^{-1}})$$

where x_m, x_o and x_w are the volume fraction of minerals, organic matter and water. Air is neglected in this approach.

The moisture itself is a highly non-linear parameter that needs coupled differential equations to be solved. For porous materials, like soils, there are two governing, differential equations which depends on each other. From Philip & De Vries [35], De Vries [33] and Kaviany [29] we can obtain the general differential equations describing the heat conduction and the moisture movement in porous materials with combined temperature and moisture gradients.

The research area of soil characterization is old and well documented and there are a large amount of articles in this topic. For an extended insight in soil characterization recommends De Vries [33] and Jansson [36].

4.2.2 Surface absorbtivity

The absorbtivity, α_{sun}, of the energy from the sun radiation can be expressed $r = 1 - \alpha_{sun}$ where r is the wavelength dependent reflectivity of the actual surface. This reflectivity can be measured. As an example the reflectivity for dry and wet sand as a function of wavelength is shown in Figure 4.3. Two laboratory spectrophotometers were used. In the 0,2 - 2,5 micrometer-band a Cary 5G system was used, and in the 2,5 - 20 micrometer-band a Bruker IFS 55 FT-IR was used. The spectrophotometers measure a hemispherical integrated reflection coefficient.

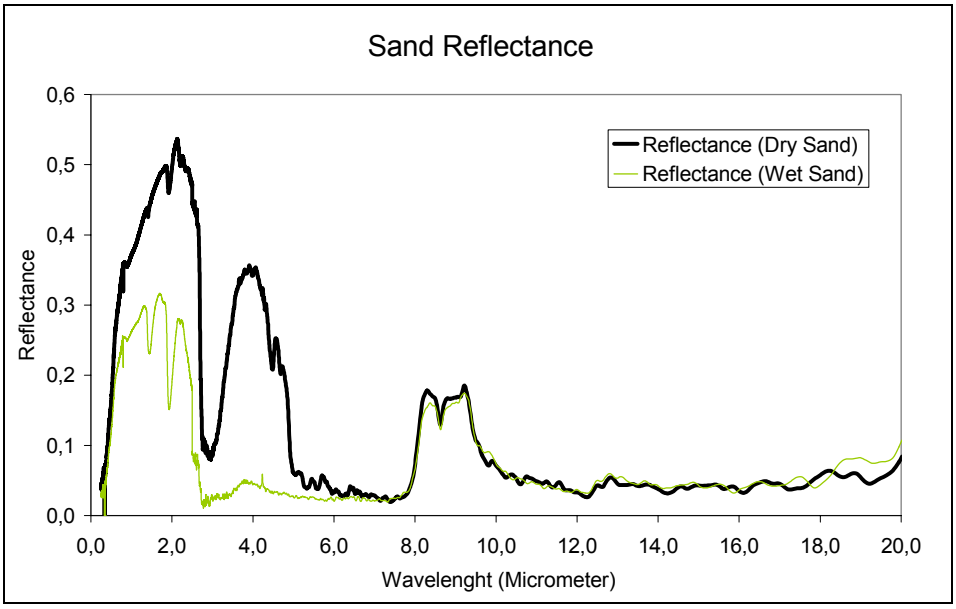

Figure 4.3. Measured reflectance of dry and wet sand.

4.2.3 Sky emissivity

Models for deriving the sky emissivity is proposed by Centeno [37] and Idso [38]. Both models are based on an semi empirical approach with inputs from only a few parameters. As an example, the Centeno model is written:

$$\varepsilon_{sky} = (1 - N) \cdot \left[0.0001 \cdot \left[5.7723 + 0.9555 \cdot (0.6017)^{Z}\right] \cdot H^{0.0665} \cdot T_a^{1.189}\right] + N \cdot \left[1 - \left(3000 + 1751 \cdot Z^{0.652}\right) \cdot H^{-1.5} \cdot T_a^{-1}\right]^4$$

Here Centeno defines N as the nebulosity of the sky and when N is equal to zero, the sky is clear with no disturbances from clouds, fogs or mist. When N =1 the sky is complete overcast. Z is the altitude above sea level in kilometers and H is the relative humidity. This sky emissivity model uses only T_a and H as measurable input parameters. Other models often use a number of more complex measurable

parameters as inputs. In Figure 4.4 the long wave sky irradiation at ground derived from the two models and from measurements, are shown.

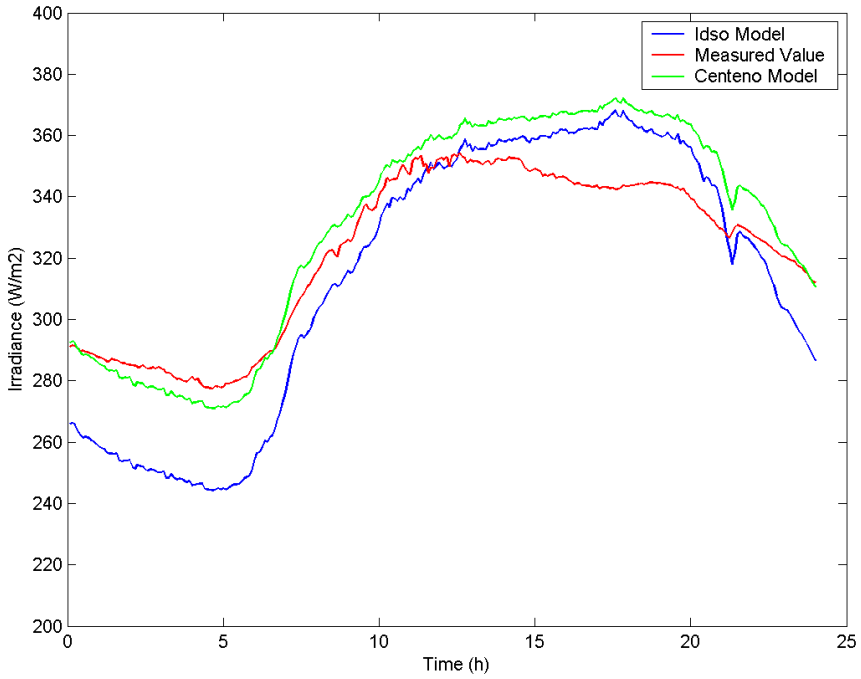

Figure 4.4. Sky irradiation at ground during a diurnal cycle 2003-06-03 Kvarn. Red; Measured values, Blue; Idso-modell, Green; Centeno-model. X-axi s is diurnal time (0 to 24h) and Y-axis is irradiance (W/m^2).

In some situations also a simple approach as $\dot{Q}_{sky} = \sigma \cdot \varepsilon \cdot (0.9 \cdot T_a)^4$ is good enough for an approximation of the sky irradiance.

4.2.4 Vegetation layer

Extensive measurements have been performed from a number of different research groups and a number of models with different levels of complexity have been developed in recent decades. The purpose has been to explain and predict different phenomena in the layer between the soil and the atmosphere, thereby enhancing the detection of hidden and buried objects. Some of the developed models build on statistical or empirical results, others on strictly physics-based equations. The easiest way to take the influence from the vegetation layer into consideration, for the energy transports, is to calculate its presence as a dampening layer/factor. A survey of different thermal background models can be found in F G Wollenweber [39], W R Reynolds [40], Deardorff [24] and Balick [41]. At present, there is no accessible universal thermal model for terrestrial surface background behaviour.

4.3 SIMULATION RESULTS

A simulation result gives the temperatures in all nodes in the FEM model, for every time step during the calculated period. We can choose to show the results in spatial or temporal dimension. A simulation can give the interesting answer on the question “Do we have favourable contrast for successful detection of landmines, and when?”

A normal 2-dimensional numerical model consists of approximately 300 up to 3000 elements and an example is shown in Figure 4.5. For a 3-dimensional model the number of elements is approximately 100000.

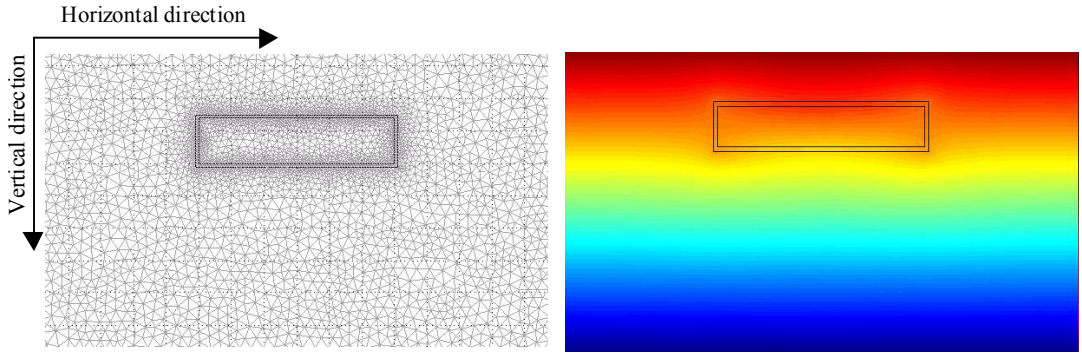

Figure 4.5. The discretesized model to left and an image from a simulation to right.

The model can also be studied in a 3 dimensional simulation shown in Figure 4.6. if it is necessary. 3-dimensional modelling and simulation needs a lot of computer power and is not recommended in a first approximation and implementation.

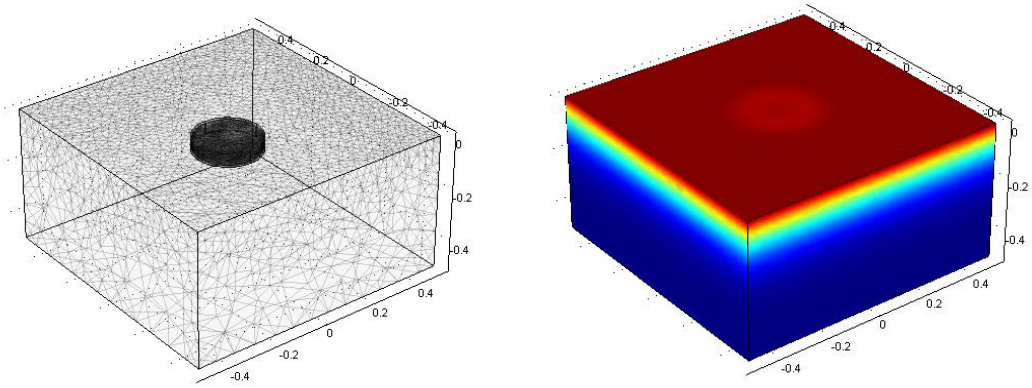

Figure 4.6. The discretesized model in 3 dimensions to left and a result image from a simulation to right.

As an example of material properties used in the simulations values from Table 4.1 could be used.

Material	Thermal Conductivity (W/m K)	Specific Heat (J/kg K)	Density (kg/m^3)	Global solar absorptivity
Soil, clay	2.7	1100	1900	0.76
Mine filling	0.24	334	950	
Mine shell: Aluminium	205	885	2780	0.85
Mine shell: Steel	54	465	7830	0.85
Mine shell: Polystyrene	1.54	1339	1038	0.85
Stone, Granite	2.9	890	2750	0.55
Wood, pine	0.20	2301	550	0.78
Air in Mine	0.026	1005	1.2	

Table 4.1 Example of material properties used in the calculations.

Results from field measurements and simulated results are shown in Figure 4.7 for a 36 hours period. The measured temperature is apparent temperature and the calculated is thermodynamic temperature.

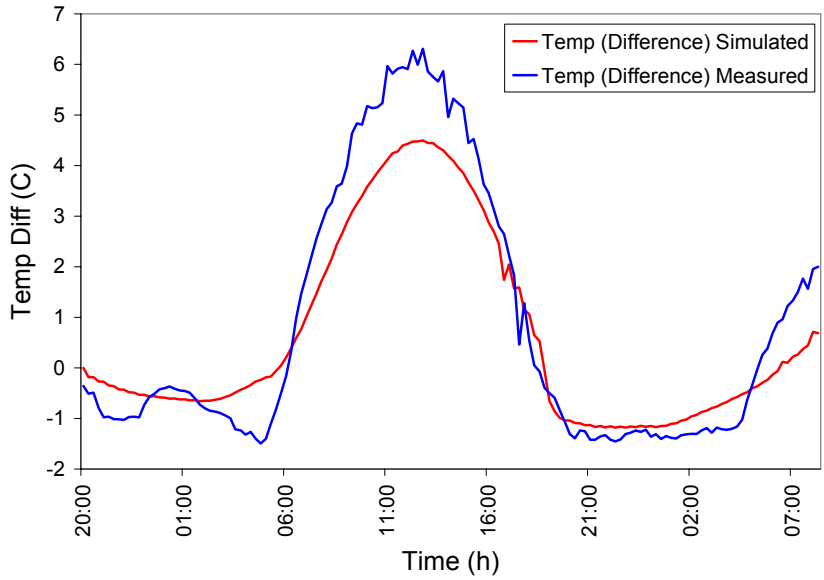

Figure 4.7 Simulated and measured temperature differences between the surface above the buried object and its neighboring surface, 30 cm from the objects center axis. Apparent temperature, measured with AGEMA 900 IR scanner 8-12µm, was used as measured temperature.

Another way to present the results is to study the isotherms in the soil volume. This result is shown in Figure 4.8 and in Sjökvist [30]. The isotherms are shown at four times 08:00, 13:00, 19:00 and 24:00. From the upper left picture the influence from the sun and the raising air temperature cause the isotherms to move downward, giving a detectable contrast. When the time is 13:00 (upper right picture) the isotherms are

closer to each other above the buried object than beside, this means that we have a great contrast. When the time has reached 19:00 the sun is down and the air temperature is also falling, this means that the isotherms start to move upward and now there is very little contrast. At midnight there is a little contrast above the buried object again. If the isotherms from Figure 4.8 are compared with the graph in Figure 4.7 we can see the relationship.

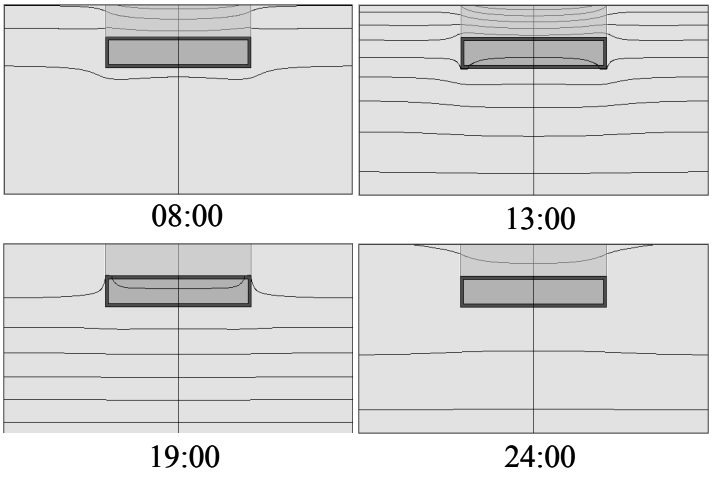

Figure 4.8 Simulated temperature isotherms in the soil volume at four different times, which are from upper left: 08:00, 13:00, 19:00, 24:00.

In Sjökvist [42] a minefield investigation was carried out from an airborne sensor platform on real minefields in Croatia. In the post process work a temporal analysis, see section 5.2, was carried out and the thermodynamically behaviour of a set of suspected objects were modelled and simulated with the actual conditions measured in situ. In Figure 4.9 the simulated temperatures of different relevant objects are shown. In the diagram also three vertical lines shows the times when the images were captured from the unmanned aerial vehicle during the campaign.

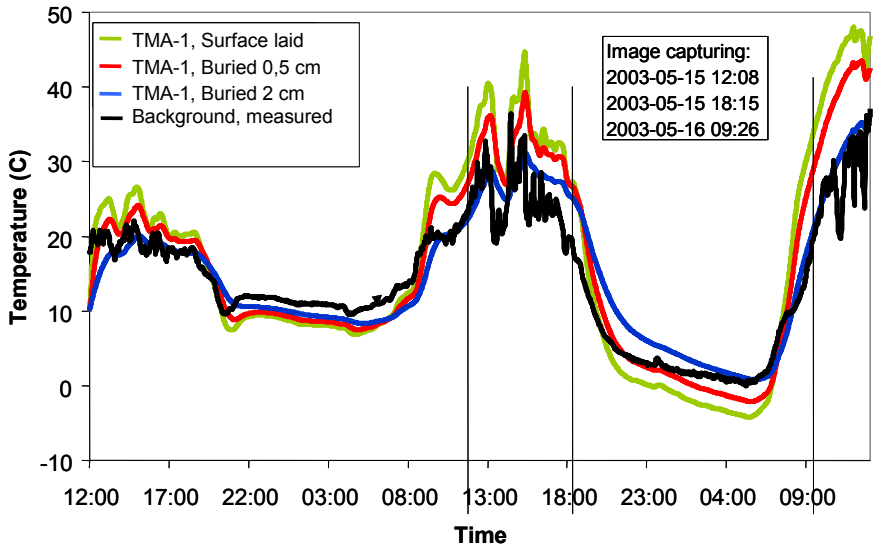

Figure 4.9 Surface temperature of the modelled, buried or shallow laid, TMA-1 mine and the measured, by Pt-100 sensors, background temperature.

The temperature differences between the modelled TMA-1 mine and the measured (by Pt-100 probes) background is shown in Figure 4.10.

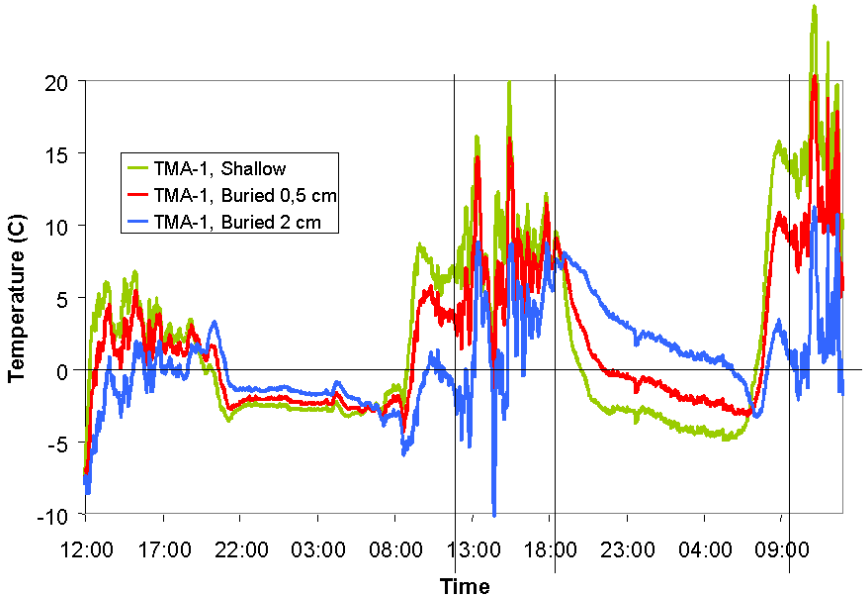

Figure 4.10 The temperature differences between the modelled TMA-1 mine and the measured (by Pt-100 probes) background. The vertical lines indicate the image capturing time.

5 ANALYSIS

Anomaly detection aims at finding objects or areas in an image having properties that, in some respect differs from the normal background. Given the very broad definition of minefield indicators, there is no possibility to find a set of typical samples to use as references for training a classifier. Instead there is a need to focus on properties that are common for at least some of the possible minefield indicators.

In this part different methods for mine detection is presented, ranging from spatial methods applied on one image to temporal methods using the sequence of images, or a few images, and a mix in between spatial and temporal methods.

5.1 SPATIAL PROCESSING

Spatial processing deals with the extraction of structural features, by combining texture, spectral and thermal information taking into account their spatial relationship in the image. General detection methods for spatial image processing can be found in [43] and [44].

5.1.1 Anomaly detection in IR images

In this approach we are focusing on IR thermal images and man-made objects. Two properties are appropriate in this context. Firstly, man made objects tend to have more straight boundaries than natural objects. Secondly, they are often made from a material different from the ground and vegetation. The result of this is that man-made objects have temperatures that differ from other parts in the scene depending on different material properties like emissivity, thermal conductivity and thermal capacity, amongst other things. Man made objects can be either colder than, warmer than, or have the same average temperature as the background. If an object has the same average apparent temperature as the background it might as well be detectable due to an internal temperature distribution that differs from the background. Anomaly detection can be used for the detection of objects with all kinds of average temperature contrast with respect to the background as long as the spatial variation of temperatures is different.

A feature image is extracted from the IR-image in order to find the so-called interesting areas. The current implementation uses a set of Gabor filters [45]. Three scales and four orientations are used. The outputs from these twelve filters are added into the feature image. The set of filters are applied to every pixel in the IR image forming an image activity image. Two layers are input to the segmentation, the thermal image and the summed output from a set of Gabor filters. The latter layer indicates areas of high contrast in the image. We model the two-dimensional density function of the layers with a mixture of Gaussian functions. For segmentation, each Gaussian is the centre of a class. The class with the highest average image activity generates the output. Selecting the pixels that correspond to the output class, results in a binary image.

In Figure 5.1 an example is shown from analysis of an IR mosaic of images taken from 300 m over a minefield in Croatia [13]. Yellow polygons represent hot regions and red points represent hot spots.

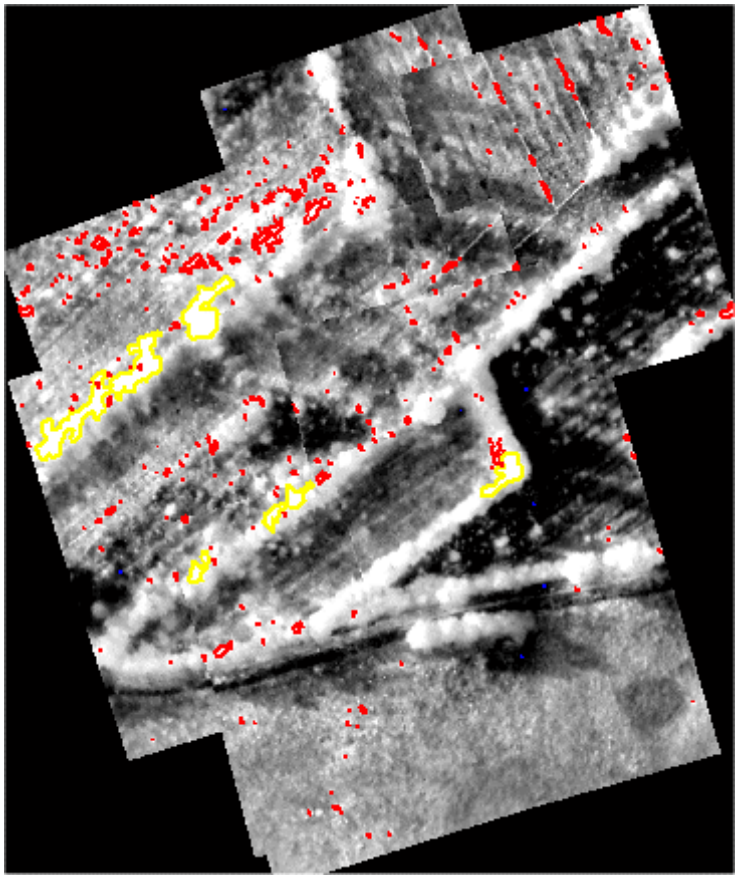

Figure 5.1 MFT_flight7_FLIR_Mosaic 300m. Detected anomalies. Yellow polygons: hot regions, Red points: hot spots.

5.1.2 Detection approach

It is difficult to obtain a complete knowledge regarding the properties of the mine signature. As a consequence, the spatio-temporal signature of the buried mines can not be assumed to be completely known by any detection algorithm. One approach is to circumvent this by modelling the uncertainty by means of a small number of parameters. These parameters might for instance be the contrast (mine signature amplitude), spatial smoothness, radius and temporal behaviour. For notation, let the parameter vector θ_s contain these, at detection instant, unknown parameters. Assuming an additive model, if we from an infrared image sequence, p(x,y,t), are to decide whether a mine is present at a specific location, the two competing hypotheses are:

H_0: $p(x,y,t)= n(x,y,t; \theta_n)$
H_1: $p(x,y,t)= s(x,y,t;\theta_s)+n(x,y,t;\theta_n)$.

Here $n(x,y,t;\theta_n)$ represents the background noise incorporating everything but the mine and $s(x,y,t;\theta_s)$ represents the mine signature. In order to model the image

statistics, we promote to use texture models to characterise the background noise. The parameters of such a model are incorporated into the noise parameter vector θ_n. We assume that these parameters can be trained using off-line data, thereby the noise distribution, $f_N(\ )$ can be assumed known during the detection procedure. A detector is formed by applying the Likelihood Ratio Test (LRT).

$$\frac{f(i(x,y,t)\,|\,H_1)}{f(i(x,y,t)\,|\,H_0)} \gtrless \eta .$$

5.2 TEMPORAL ANALYSIS

The temporal analysis relies on that the data is collected from the same area at different times. The collected image sequence is captured in a cube of dimension *X,Y, N,* where the image coordinates is *x,y* and the different images in the time sequence is represented by the third dimension *t=1...N* dimensions. The pixels are numbered *i=1,..,n* in a line scan manner and *n=X*Y* as shown in Figure 5.2. The arrow views position for the pixel temporal characteristics *i*.

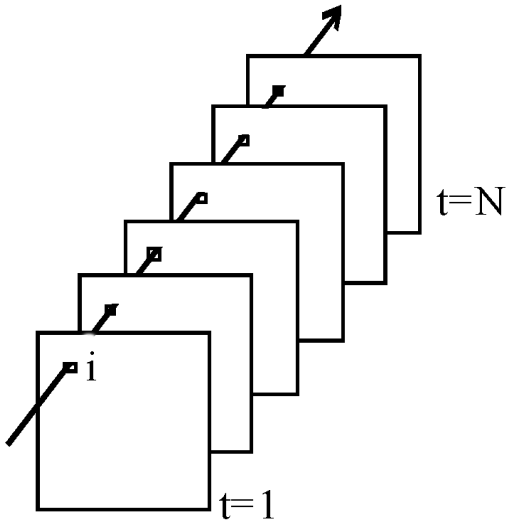

Figure 5.2 The image sequence cube with the position for the pixel temporal characteristics i viewed by the arrow.

The image sequence is represented by vector **p**
$\mathbf{p}(t,i)=[\ p_1(t),\ p_2(t),\ldots,\ p_n(t)]^T \qquad t=1...N$

The temporal analysis is performed on image sequences collected from the same scene over time. The time increment between consecutive images varies from seconds to days.

The main feature we use in detecting mines in thermal images is the contrast changes between the object and its surroundings. If we subtract from each image in the sequence its image mean the result is a zero mean image sequence. This has the effect that the global temperature change during the day is extracted and the data only contains the different temporal characteristics affected by locally acting parameters.

The remaining variances emanates from the different temporal characteristics we are interested in.

5.2.1 Temporal contrast analysis of suspect objects

The contrast variation of a know object in the scene can be used as signature reference and compared with the contrast variation of another areas in the scene. This makes it possible to analyse suspected objects.

In the minefield 1, there were lots of PROM-1 mines [13]. Before the measurements, a deminer had put out a reference wooden stick at the location of a mine. In the sequence of IR-images from the minefield there were several objects with features similar to the known wooden stick, Figure 5.3.

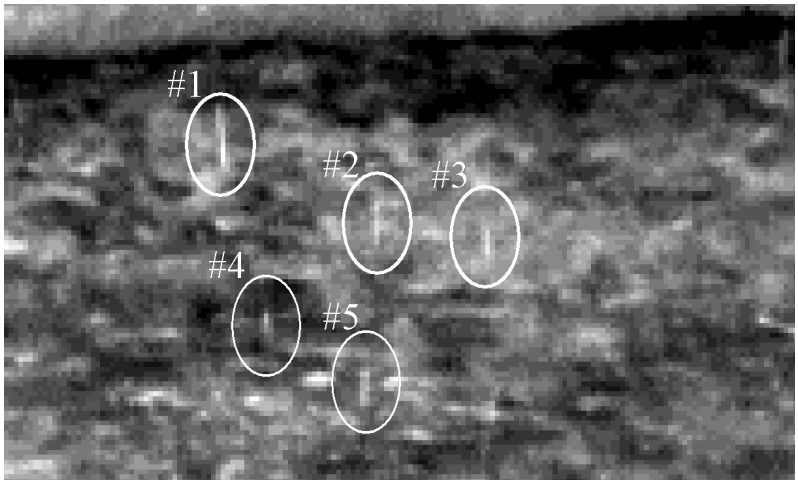

Figure 5.3 IR-image. Reference wooden stick, #1, and suspect objects, #2 - #5.

The location of the known wooden stick and the suspect objects were analysed with respect to apparent temperature in 40 IR-images, 8-9 µm, registered 2001-04-23 in the late afternoon and evening between 16:30 to 21:30. The values were calculated in an area one pixel wide and five pixels high. The values for the local backgrounds were calculated in a similar area, but shifted three pixels to the right of each object. The mean values and variances for each object m_o V_o and local background m_b V_b in all images were calculated and the dimensionless contrasts measure C was obtained by:

$$C = \sqrt{\frac{(m_o - m_b)^2}{(V_o + V_b)}}$$

For comparison the same analysis was made in exactly the same way, but with an offset of five pixels to the right for calculation of "object" and background. This is intended as a check for natural contrast variations in the scene. The results are presented in Figure 5.4. To the left are the contrasts and corresponding mean values for the known wooden stick, #1, and the suspect objects, #2 to #5 presented. To the right the contrasts and corresponding mean values for the offset areas, off #1 to off #5, are presented.

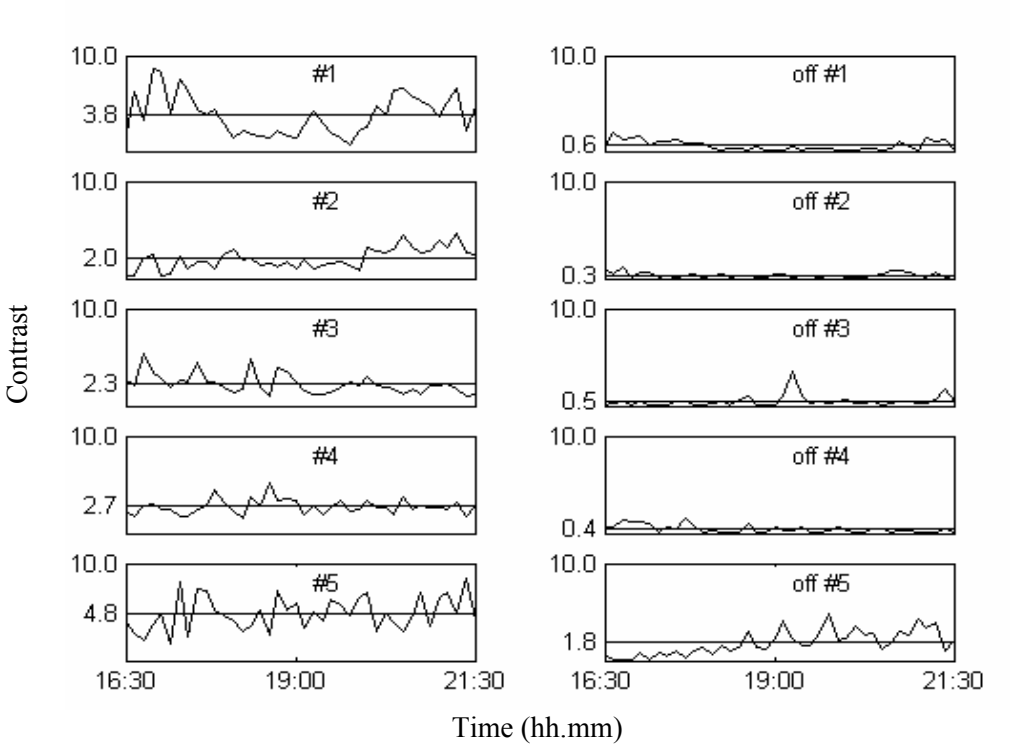

Figure 5.4 Contrasts. To the left are the contrasts and corresponding mean values for the known wooden stick, #1, and the suspect objects, #2 to #5 presented. To the right are the contrasts and corresponding mean values for the offset areas, off #1 to off #5, are presented.

The contrasts for the reference wooden stick and the suspect objects are, with one single exception, higher than random contrasts. Nothing at this stage of analysis contradicts the hypothesis that the suspected objects are made of wood [11].

5.2.2 Modelbased Temporal analysis of a sequence

In this approach we are focusing on IR images and predicted temperature behaviour of different possible mine and mine like objects [11]. The prediction is done by the use of heat transfer modelling described in chapter 3. The contrast measure is calculated as the difference between the temporal characteristics from two spatial locations. This is compared to the model result for different materials, and from this it is possible to detect these materials in the ground.

Detection is done by taking the difference of the contrast signal c_i of the pixels and the modelled contrast c_m, using the standard deviation of the difference signal

$$d_p = \sqrt{\frac{1}{n}\sum_{k=1}^{n}(c_k - c_m)^2}$$

for all pixels and threshold this. A resulting image is created where the simulated temperature differences fits the diurnal temperature differences measured by the sensor. In Figure 5.5 are shown the plots of a typical matching pixel contrast signal (blue) with the model (black) and the same for a typical non matching pixel.

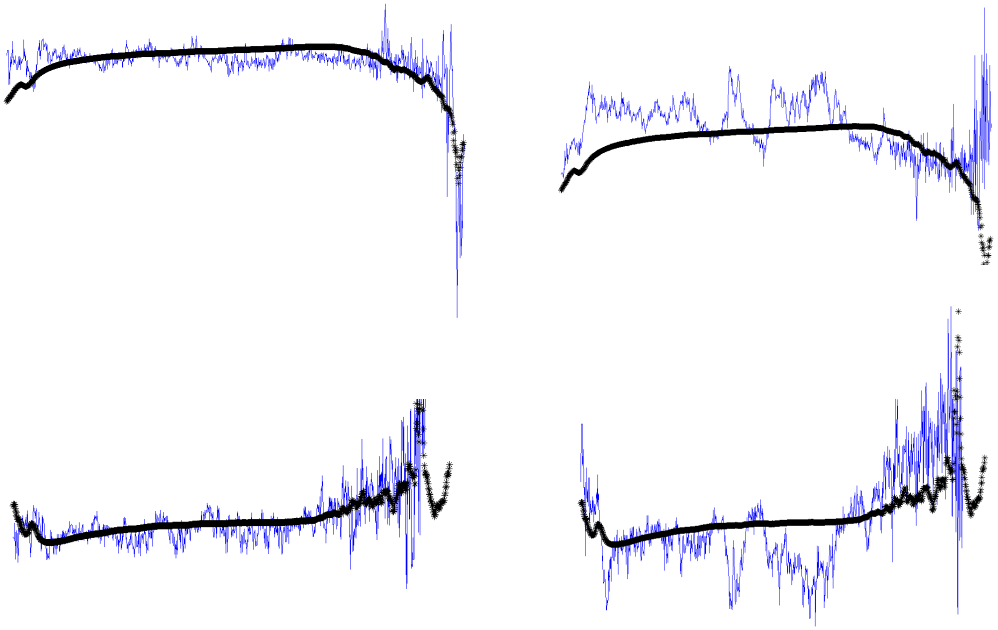

Figure 5.5 Example of temporal pixel contrast signal (blue) and model (black) for a matching pixel to the left and for a non matching pixel to the right, upper: aluminium mine and lower: steel mine.

5.2.3 Principal component analysis (PCA)

Principal component analysis (PCA) [46] finds the linear transformations of the data that produces uncorrelated components in such a way that the variance, or signal energy, is maximized. The uncorrelated components can be used for a more precise analysis of the data set. The temporal characteristics of each of the pixels can be represented by a linear combination of the temporal eigencharacteristics where the weights are the transform components.

The PCA uses the covariance matrix of the zero mean data. The covariance matrix of a random vector X is defined by

$C = E[(X – E[X]) (X – E[X])^T]$.

In practice we use the estimate

$$E[\mathbf{X}] \approx \mathbf{m}_x = \frac{1}{K}\sum_{k=1}^{K}\mathbf{x}_k$$ where K is the number of pixels in one image

and

$$\mathbf{C} \approx \frac{1}{K}\sum_{k=1}^{K}(\mathbf{x}_k - \mathbf{m}_x)(\mathbf{x}_k - \mathbf{m}_x)^{\mathrm{T}}$$

C is of dimension NxN where N is the size of our data cube in the time dimension, the number of images in the sequence.

Solving for
$\mathbf{C} - \lambda_i I = 0$ and
$\mathbf{C}W_i = \lambda_i W_i$
leaves us with the eigenvalues λi and the matrix W containing the corresponding eigenvectors as rows. The eigenvectors are our temporal eigencharacteristics.

Now we can transform our image sequence into a form that is easier to analyse by representing the data in the basis of the temporal eigencharacteristics.
$y = W(x - m_x)$ where x is the pixel temporal characteristics and m_x is the mean vector. The vectors y are uncorrelated. The transform is invertible, we can reconstruct x by transform vector y by $x = W^{-1}y = W^T y$ because W is symmetric.

Choosing the temporal eigencharacteristics of the k largest eigenvalues gives us the matrix Wk as the transform matrix. The approximation error from not using all of the eigenvectors is the sum of all the contribution from the neglected eigenvectors.

$$e = \sum_{i=k+1}^{N} \lambda_i$$

Normally the eigenvalues vary considerably in magnitude, and the smaller ones can be ignored without the introduction of significant error. This is a reduction of dimensions for representing the data and is a well known use of PCA. The 6 first temporal eigenvectors from the PCA of the image sequence used in section 4.2.1 is shown in Figure 5.6.

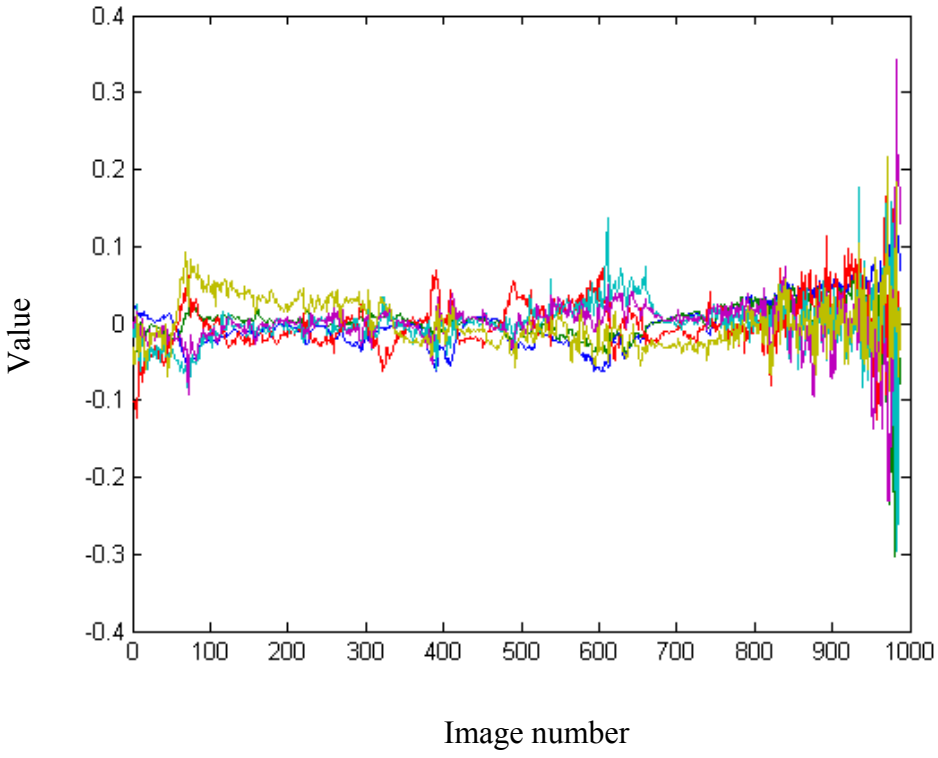

Figure 5.6 The 6 first temporal eigencharacteristics.

After transforming the data each pixel is represented by a vector containing the transform components, which are the weights in the linear combination of the temporal eigencharacteristics representing the temporal signature of this pixel. Viewing the transform components for each pixel in two-dimensional plots shows the pixel temporal characteristics represented in different bases. In Figure 5.7 the image sequence used in section 4.2.1 is presented with the first and third eigenvector as basis, first and second eigenvector as basis, first and fourth eigenvector as basis, first and fifth eigenvector as basis.

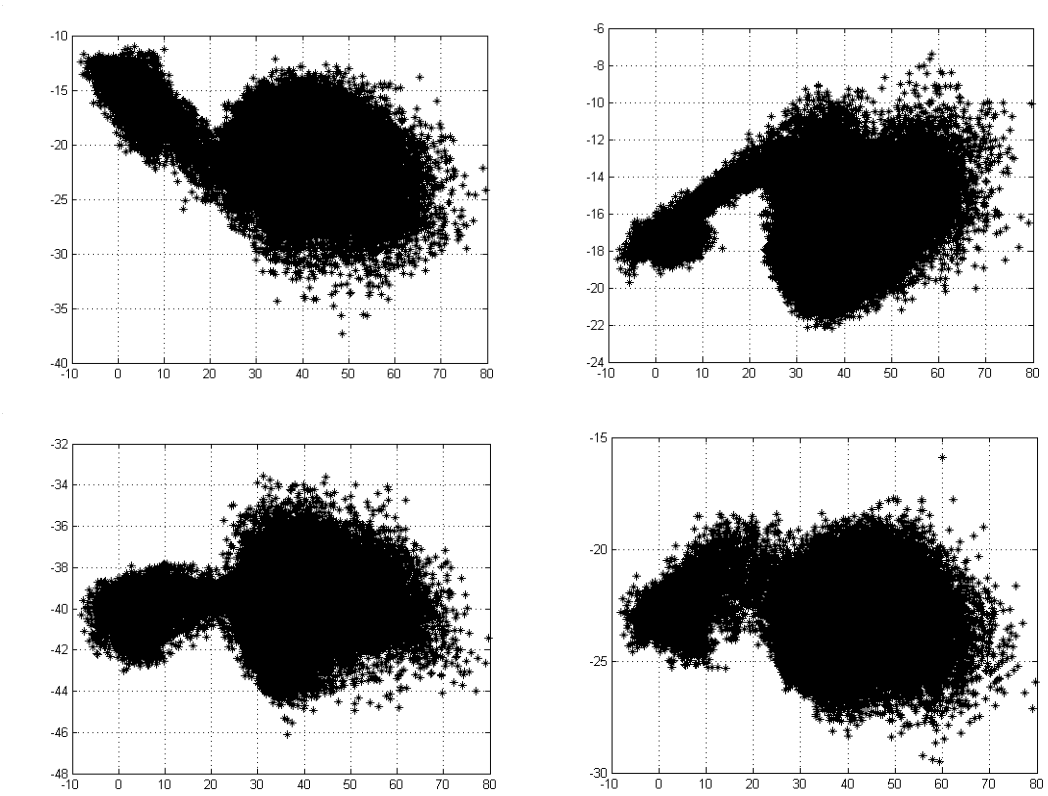

Figure 5.7 The image sequence used in section 4.2.1 is presented with the first and third eigenvector as basis, first and second eigenvector as basis, first and fourth eigenvector as basis, first and fifth eigenvector as basis.

Forming an image from the first component of each pixel gives us the first temporal eigenimage, forming an image from the second component of each pixel gives us the second temporal eigenimage, and so on. The temporal eigenimages corresponding to the six largest eigenvectors are shown in Figure 5.8, the first image containing the largest energy and the last containing the least energy. Every pixel's temporal characteristic can be represented by these images and the pixel's transform vector with minor error.

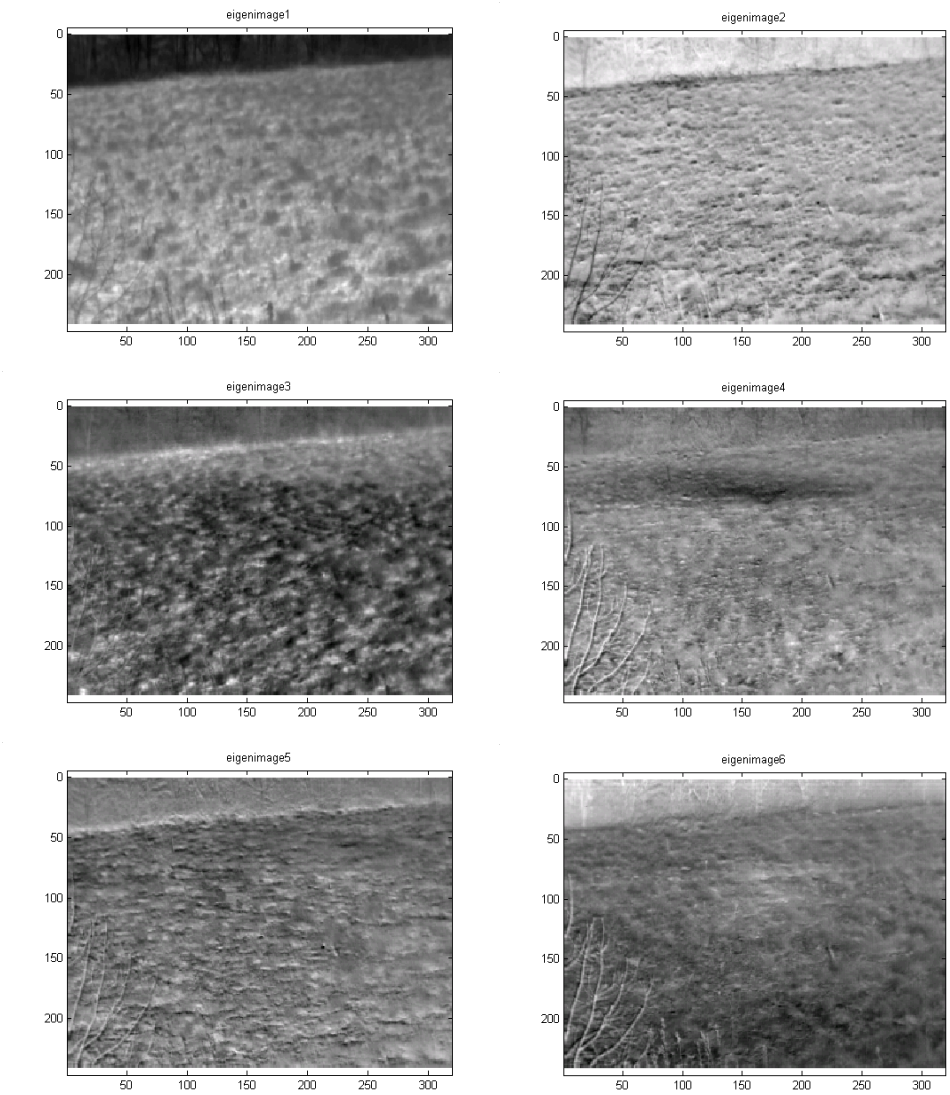

Figure 5.8 The first six temporal eigenimages corresponding to the six largest eigenvectors.

5.2.4 Detection of modelled objects in transform space

The pixels in the image sequence can be classified according to the temporal characteristics. By using a model from chapter 3 the pixels can be labelled “object” or “background”. In Figure 5.9 the models of five different objects are presented in the basis of the six eigenvectors presented above. In Figure 5.10 the same modelled objects are presented together with all the pixels in the basis of the first and third eigenvector. Figure 5.11 presents a zoom of Figure 5.10 in which we can see that the modelled objects are separated.

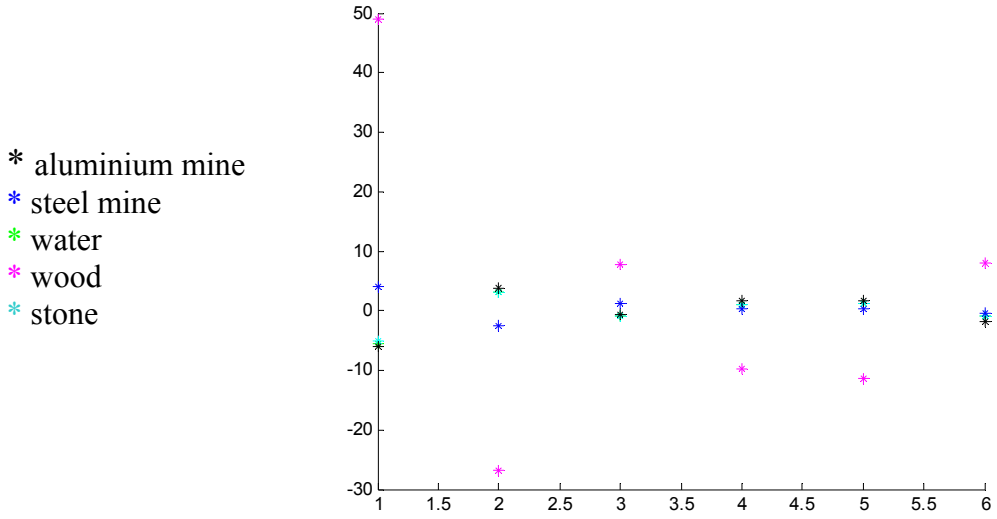

Figure 5.9 the models of five different objects are presented in the basis of the six eigencharacteristics

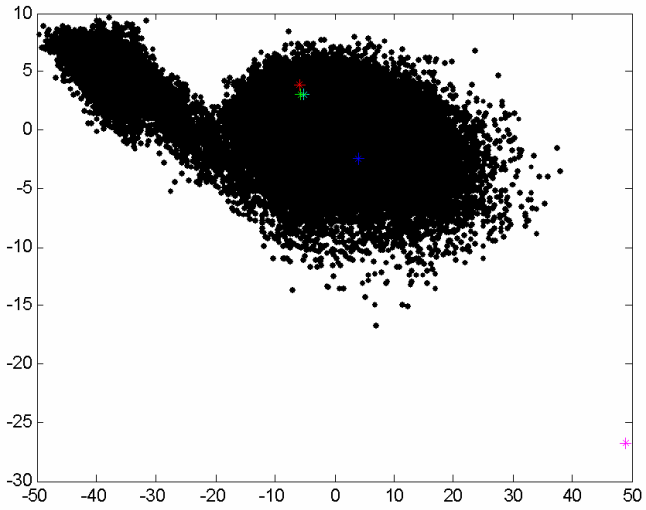

Figure 5.10 The modelled objects are presented together with all the pixels in the basis of the first and third eigenvector.

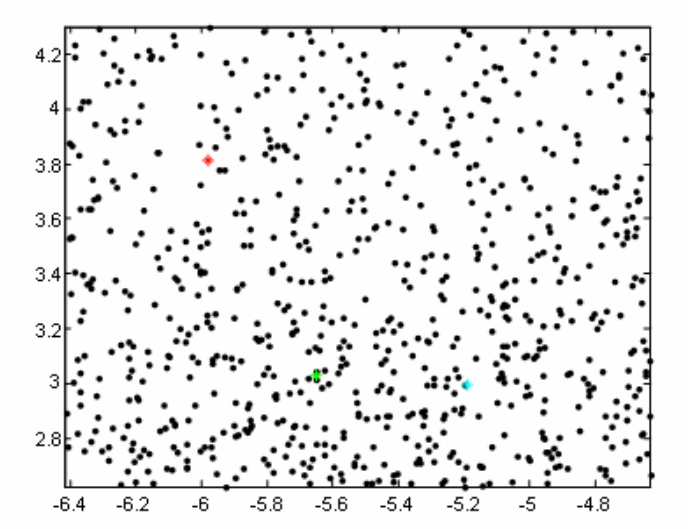

Figure 5.11 A zoom of Figure 5.10 in which we can see that the modelled objects are separated.

Normally detection is done with clusters exampled by Figure 5.7 that easily divides into separate classes. Basically, we measure the distance from a pixel characteristic to the target model and to the background model, and choose the smaller. A popular approach is the RX algorithm, which basically measures the Mahalanobis distance from the centre pixel the estimated background distribution [44].

In the case of mine detection the clusters are non-separated and we do not model the background. Classification of pixels into objects is done by measuring the distance to the modelled object characteristics. We use simple distance measures like the city-block distance

$$D_i = \sum_{n=1}^{N} |p_{ni} - q_n|$$

which is a square around the model in two dimensional space, or the Euclidian distance

$$D_i = \sqrt{\sum_{n=1}^{N} (p_{ni} - q_n)^2}$$

which is a circle around the model in two dimensional space [47].

In Figure 5.12 is an example from the detection of the pixels which has the same temporal characteristics as the modelled steel mine according to a specific threshold T. The Euclidian distance in six dimensions is plotted for each pixel and the pixels with distance values below T are defined to belong to the object and the rest is not object.

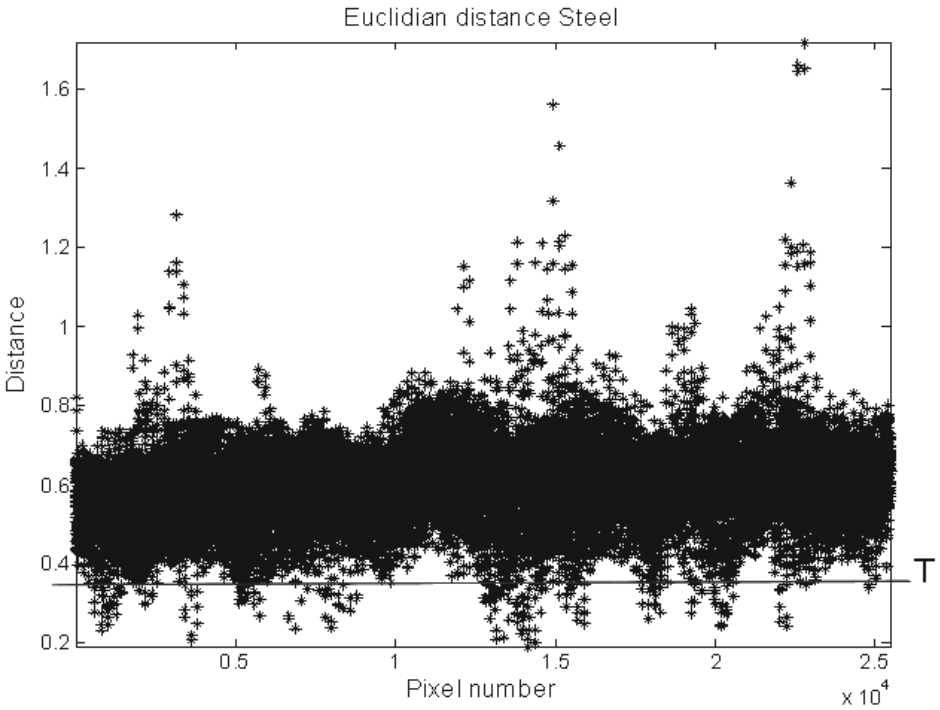

Figure 5.12 Euclidian distances for the data and simulated Steel mine object, the threshold T = 0.35 is marked with a line.

5.2.5 Model based Temporal analysis of a few images

The next approach is to analyse a few images from diurnal flights in the perspective of the modelled temporal signature [48]. This involves co-registration of the time separated images. Figure 5.13 shows the apparent temperature distribution for three images of the same area captured at three different times during the diurnal cycle. These images have been chosen to exemplify the presented method.

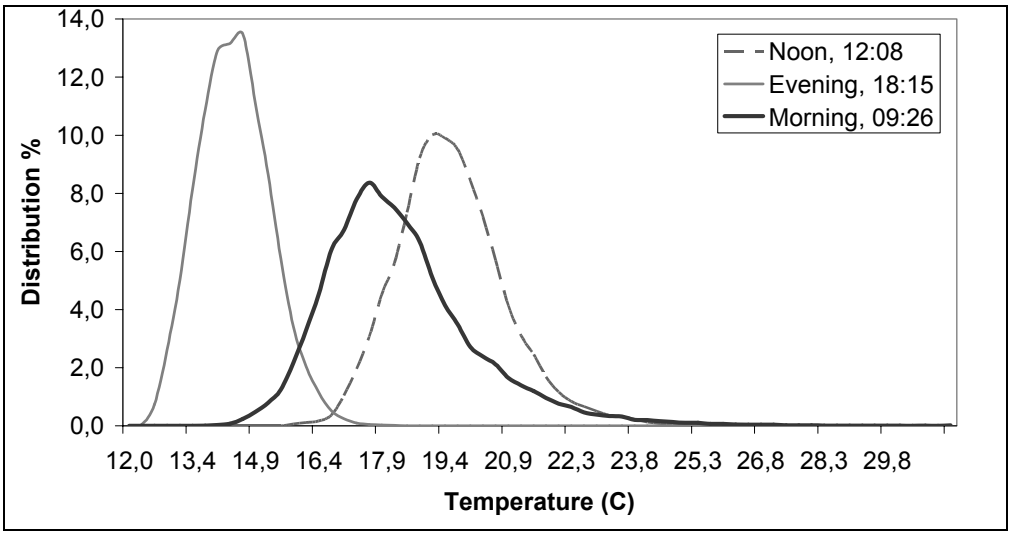

Figure 5.13 Temperature distribution for the three analysed images. From left: Evening flight, Morning flight and the noon flight.

Given the time for registration of the image, the model provides the expected temperature feature for the analysed object. The data is analysed using a contrast measure applied on each of the images in the sequence. The measured contrasts are compared to the estimated contrast from numerical modelling of different objects. From this it is possible to detect and classify objects, buried as well as surface laid using the detection methods presented in section 4.2.4. The data is analysed using the Principal Component Analysis (PCA) for transforming the data into an N-dimensional orthogonal feature space. The pixels are classified according to the Euclidian distance, in the N-dimensional feature space to the different modelled objects. Setting a threshold on the distance results in a classification of data in two classes, object or not object with respect to the threshold. The procedure is repeated for each object model.

5.2.6 Classifying anomaly positions according to the modelled objects

Another method is to extract interesting spatial features from the single images [48]. The use of the thermodynamic model is similar to the approach in section 5.2.5 but this time it is used directly to classify the anomalies at their respective positions, instead of analysing the whole image in the model perspective. The proposed detection method is a combination of anomaly detection and classification in the spatial and temporal domain.

Objects can be either colder than, warmer than or have the same average temperature as the background. The output from the spatial anomaly detection algorithm is shown in Figure 5.14. The algorithm has detected hot regions, cold regions, hot spot, and cold spot. Distances for the detected objects shown in Figure 5.14 are shown in Figure 5.15. There is no matching areas except for one spatial position, which have a distance to the aluminium cased mine lower than the chosen threshold in Figure 5.15. This position is marked with an arrow in Figure 5.14.

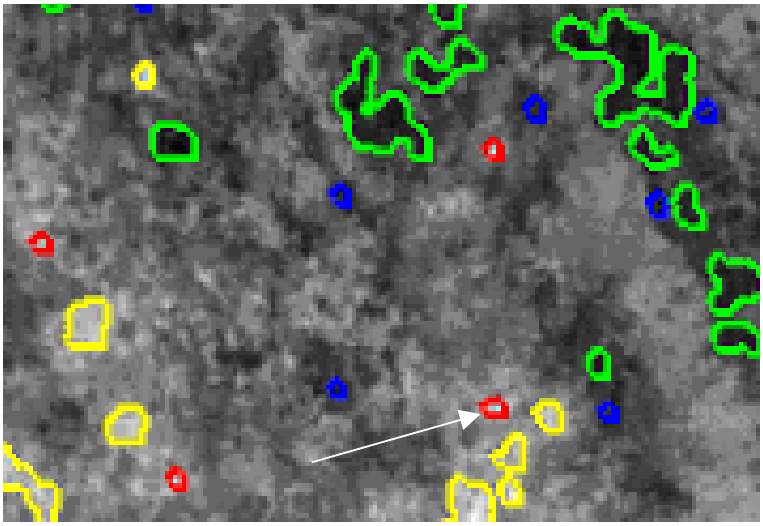

Figure 5.14 Result from spatial anomaly detection. Yellow polygons: hot regions, Green polygons: cold regions, Red points: hot spots, Blue points: cold spots. The arrow shows an area where spatial and temporal detection corresponds.

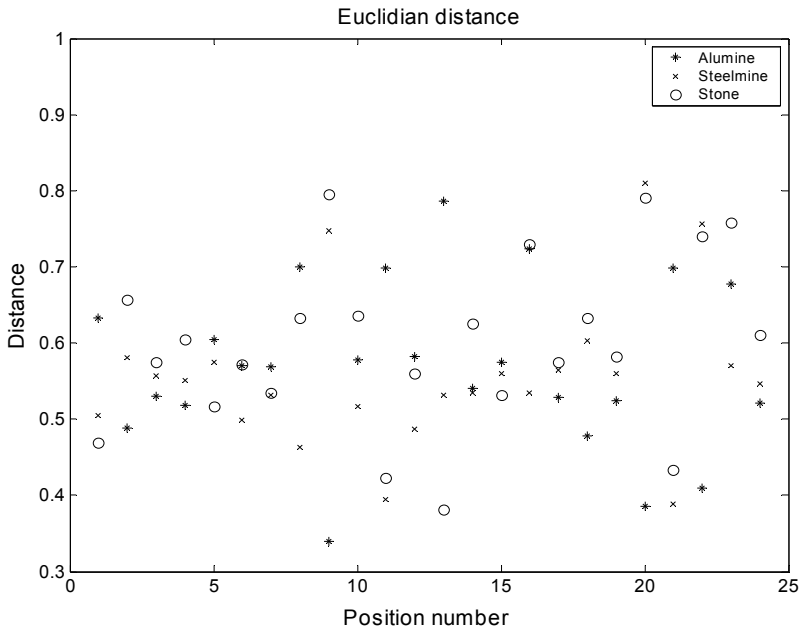

Figure 5.15 Distances for the detected objects shown in Figure 5.14. Circles for stone, stars for aluminium mine and plus for steel mine.

5.2.7 A difference method

The signal processing presented here is based on the theory of random processes and the principles of communicating a message over a disturbed channel [49]. The temperature of a position in a scene is represented by the random process x(ω,t). For each position, ω_i, we have a realisation of the process. The set of positions in the image Ω_i is a subset of the entire set of positions in the scene Ω. $\Omega_i \subset \Omega$. For an observation at time t_i, we have a random variable x(ω, t_i), which is an image and ω is the pixels in the i:th image. The diurnal measurements performed at three different times generate a random vector $\bar{x} = (x(\omega,t_1), x(\omega,t_2), x(\omega,t_3))$ also denoted as $\bar{x} = (x_1, x_2, x_3)$ in the basis of the measurements. The received vector $\bar{r}$ in the sensor is a corrupted version of the signal vector at the ground $\bar{x}$. $\bar{r} = \bar{x} + \bar{n}$ where $\bar{r}$ is the signal received by the sensor and $\bar{n}$ represent the disturbance and errors introduced by the assumptions of object emissivity, atmosphere, and the imaging device.

In this signal analysis approach we represent the measurements in the basis of the difference in time. First basis is the difference between noon and morning measurements, second basis is the difference between noon and evening, and the third basis is the difference between evening and morning. The basis images and their distribution by means of the histogram is shown in Figure 5.16 to Figure 5.18. Assuming that the disturbance vector is the same in the three measurements we have

$$\bar{r}_d = (r_{d1}, r_{d2}, r_{d3})$$
$$r_{d1} = (x_1 + n) - (x_2 + n) = x_1 - x_2$$
$$r_{d2} = (x_1 + n) - (x_3 + n) = x_1 - x_3$$
$$r_{d3} = (x_2 + n) - (x_3 + n) = x_2 - x_3$$

in the basis of the differences.

This way we do not consider the errors introduced by the atmosphere and imprecise calibration parameters.

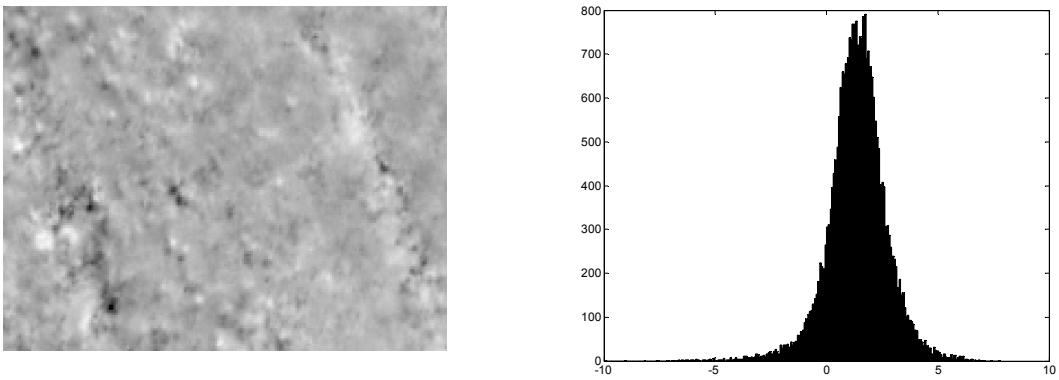

Figure 5.16 Temperature difference between noon and morning images. The basis image r_{d1} and the distribution by means of the histogram.

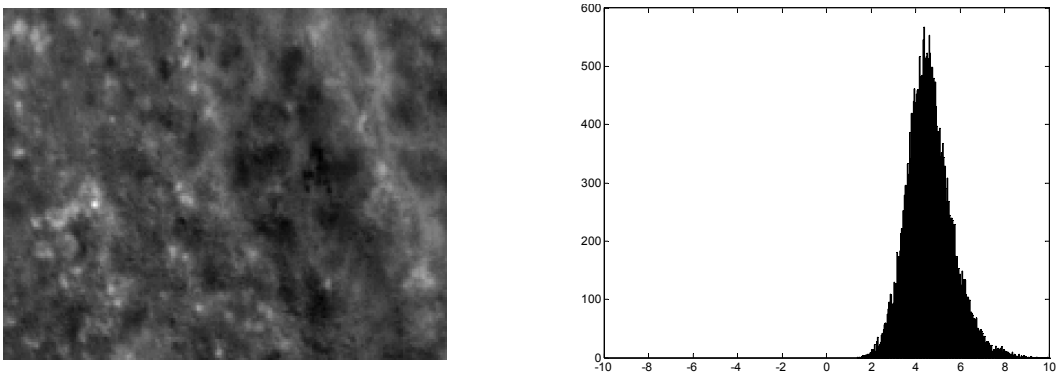

Figure 5.17 Temperature difference between noon and evening images. The basis image r_{d2} and the distribution by means of the histogram.

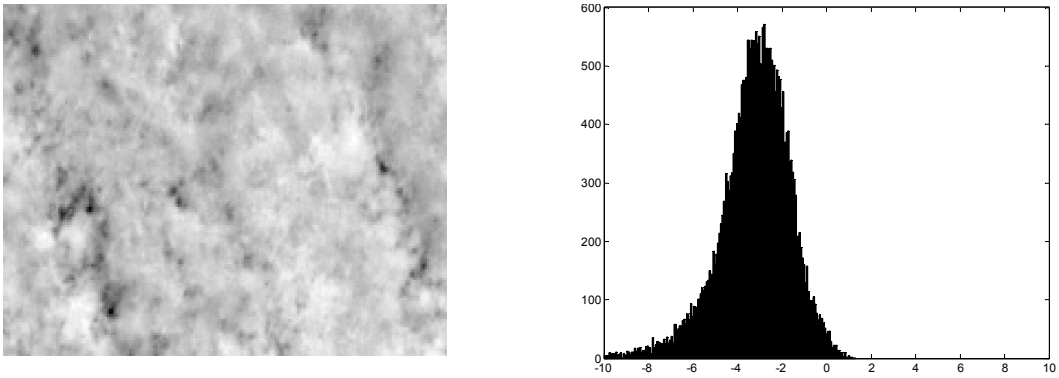

Figure 5.18 Temperature difference between evening and morning images. The basis image r_{d3} and the distribution by means of the histogram.

The influence on temperature distribution on ground from a number of different possible objects is modelled and simulated. Each object is represented by a vectors $\{\bar{s}_i\}$, i=1, …,N, where N is the number of objects. $\bar{s}_i$ is determined by $\bar{s}_i = (s_{i1}, s_{i2}, s_{i3})$ i= 1,… N, as defining N points in the three dimensional image space. The modelled objects can also be represented by N vectors $\{\bar{s}_{di}\}$, which are determined by $\bar{s}_{di} = (s_{di1}, s_{di2}, s_{di3})$ i=1,…, N, as defining N points in the difference space. The modelled objects values are shown in Figure 5.19, represented in the image basis to the left, and in the difference basis to the right.

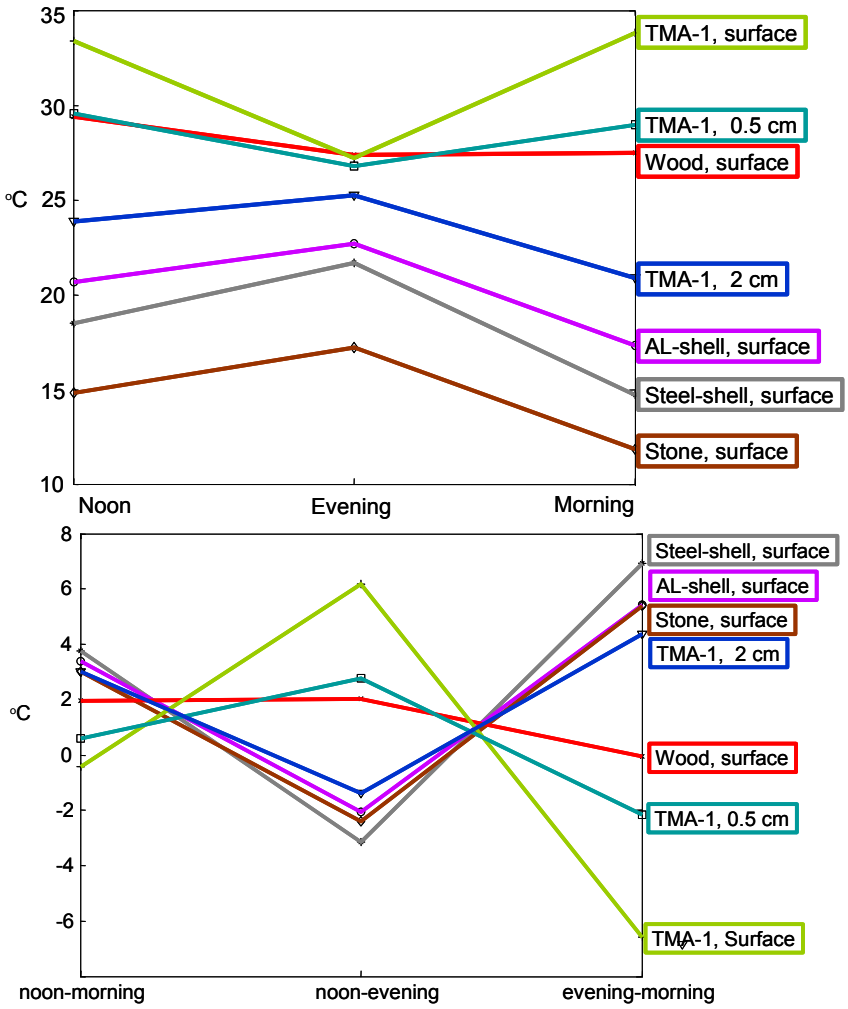

Figure 5.19 The simulated object temperature values corresponding to the time of image capture represented in the image basis, upper image. The corresponding temperature difference basis, lower image.

Detection of the different objects in the scene is done by the assumption that the apparent temperature of the pixel varies in the same manner as the modelled object. We can formulate this as a hypothesis test. We test on the difference between the temperature at different times of the day of the signal vector and the model vector.

The hypothesis is

$$H_0 : |\bar{r}_d - \bar{s}_{di}| > \Delta \quad \text{no object in the set of models is present}$$
$$H_1 : |\bar{r}_d - \bar{s}_{di}| \leq \Delta \quad \text{object of type i is present}$$

where $\bar{r}_d$ is the signal vector and $\bar{s}_d$ is the model vector in the three dimensional difference space.

The positions for the pixels that have the same level of temperature change as the modelled objects, when $\Delta = 0{,}1\,°C$ are shown in Figure 5.20.

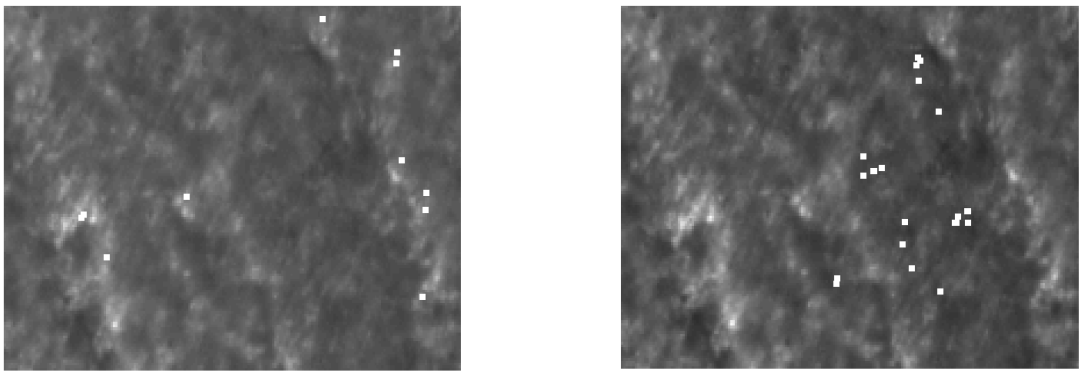

a b

Figure 5.20 Positions of detected objects. Marked pixels have a true correspondence due to the hypothesis test. a. The positions of the simulated surface laid TMA-1 mine. b. The positions of the simulated buried 0.5 cm TMA-1 mine.

5.3 TEMPORAL TIME CONSTANT DUE TO THERMAL INERTIA

The temporal variation of ground surface temperature reveals several properties of the ground. Here a simple experiment has been performed to see if it is possible to relate the temporal variation in apparent temperature to the heat capacity and heat exchange properties for different parts on the ground. The simple model used is that the current temperature depends on the sun radiation during some time interval before. Image (b) in Figure 5.21 is computed using an assumption that the temperature for each pixel in (a) is given by:

$$Out(m\Delta t) = \sum_{k=1}^{n} h(k - m\Delta t) * In(k - m\Delta t)\,, \quad m=1..40,$$

where *In* is the net radiation from the sun and the sky and *h(k)* is an impulse response. The value of n is equal to the number of time lags used. Here a small value of n=3 is used. For each pixel, 40 samples of the above equation is given, one for each frame in the sequence. Solving this over determined equation system gives an impulse response. It is assumed that h(k) is a decaying exponential function of the form

$$h(m\Delta t) = e^{-m\Delta t / tc}\,, \text{ where } tc \text{ is the time constant.}$$

The ratio between two consecutive terms is $e^{-\Delta t / tc}$ and this value is used as pixel value in the output image. A low time constant *tc*, gives a dark pixel. The speed of the temperature variation for a small region is supposed to be related to the heat capacity and heat exchange properties for that region. An example from a measurement recorded at TNO in Holland where conceivable garbage, which can be found in post-war fields, had been put out is shown in Figure 5.21. It shows to the left the first thermal image from a three-hour sequence. In the right part the time constant due to the heat capacity is shown. The time constant is estimated from around 40 frames, with a frame-to-frame time of five minutes. However, due to several simplifications the right image is only related to the time constant. As expected the heat time constant image has a great similarity with the original image.

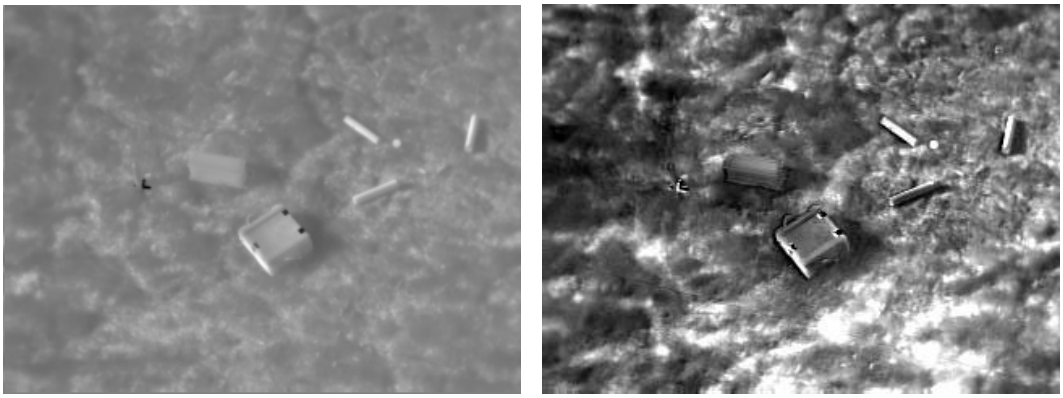

(a) (b)

Figure 5.21 Time constant from a sequence of IR frames. In (a), the first frame of a sequence is shown, and in (b), the time constant image is shown. In (a) bright parts correspond to a high apparent temperature and dark parts to low apparent temperature. In (b) bright parts correspond to high time constant and dark parts to low time constant.

5.4 COMMENTS

Different methods for data analysis are presented in this chapter, ranging from spatial methods applied on one image to temporal methods using the sequence of images, or a few images, and a mix in between spatial and temporal methods. These methods are presented with the application on the data set available at the time of development of the method. The aim of the presentation in this chapter is to show the different principal directions of the data analysis, rather than comparing the methods against each other. Evaluation of the methods is planned for the next year, including detection probability and false alarm rate.

6 ARC PROJECT ON HUMANITARIAN MINE ACTION

ARC was an applied EU funded project for the design and implementation of a demonstrator system for airborne assessment of minefields in humanitarian mine action. The project was running from beginning of 2001 and was finalised by the end of 2003. It was funded by 50% from EU and 50% from other sources. Partners were: FOI (Sweden), Geospace (Austria), GTD (Spain), Croatian Mine Action Center (Croatia), IMEC (Belgium), SCHIEBEL (Austria) and TNO (Netherlands).
The main responsibilities during demonstrator development were distributed among partners in the following way:

- FOI was sensor provider (IR camera) and responsible for temporal image analysis.
- Geospace was technical coordinator and responsible for mission planning interface, satellite data and the GIS.
- GTD was responsible for data fusion.
- Croatian Mine Action Center was end user and had the role of ensuring project relevance.
- IMEC was responsible for spatial image analysis.
- SCHIEBEL was administrative coordinator and platform (UAV) provider.
- TNO was sensor provider (multi spectral camera) and responsible for spectral analysis.

The ARC system consists of:

- An UAV with IR and multi spectral sensors, Figure 6.1.
- An UAV ground control station for the UAV, Figure 6.2.
- A ground station with database, GIS, mission planner, image processing and data fusion, Figure 6.3.

Data are stored on the UAV for later analysis in the ground station. The UAV can be pre programmed to a pattern of waypoints where image recording automatically can be started or stopped. ARC can be used for general survey (mapping), area reduction, minefield delineation and quality control.

Figure 6.1 UAV used in EU-project ARC as sensor platform for IR and multispectral sensors.

Figure 6.2. Ground control station for the UAV

Figure 6.3 Ground station with database, GIS, mission planner, image processing and data fusion

Sensor data are fused with satellite data and other GIS data. A pyramidal hierarchical approach is used to logically integrate the different information levels using available state-of-the-art remote sensing tools ranging from (coarser) satellite data to very high resolution (cm range) data acquired from the UAV, Figure 6.4.

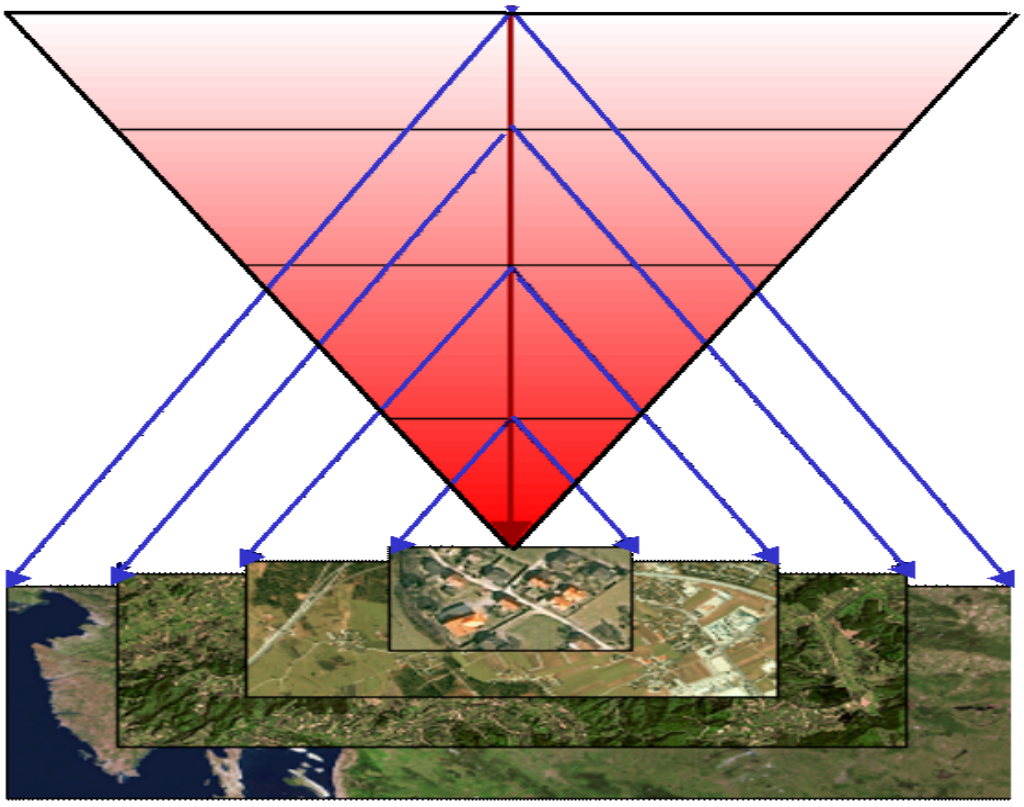

Figure 6.4 Schematic view of the pyramidal information structure applied in ARC.

The FOI method for temporal analysis is described in chapter 4. A more thorough description of the ARC system is given in: "ARC Final Public Report" [13].

In the evaluation chapter of the final report, some benefits of the ARC system are stated:

- Information gain compared to conventional method.
- Rapid surveying tool for the area of interest.
- Rapid identification of safe areas of special types.

For the conventional method the following benefits are stated:

- Operational for years, adapted to needs of humanitarian demining.
- Developed on the basis of IMAS, demining laws and sub laws.
- Technical feasibility known.

Some potential alternative applications for the ARC system are:

- Crisis Management - Disaster assessment and recovery e.g. for
  - mountain slides
  - river flooding
  - forest fires
  - avalanches
  - industrial (chemical or nuclear) disasters
- Planning support for peacekeeping operations
- Environmental monitoring

    - vegetation assessment and nature planning (e.g. forests or protected areas)
    - planning and assessment of the clearance of abandoned polluted areas
- General remote sensing
    - planning and assessment of archaeological field work (with the help of airborne survey/ground penetrating sensors)
    - planning of infrastructure projects
- Search for missing persons in forests or mountainous areas (e.g. using thermal information)
- Detect new marks of trespassing across e.g. a border
- Detect human activity, e.g. use or not use of houses
- Detect leakage in pipelines e.g. for water, gas and oil, by means of change in thermal properties.

For FOI the involvement in the project has had several advantages. Contacts, experiences and knowledge achieved by the ARC participation is very valuable for future FOI research on optical methods to support military and humanitarian mine related problems. It has been of special value to participate in an international project with industrial partners, other research organisations and last, but not least, an end user with access to real minefields and comprehensive experience of the problem. It has been very fruitful to participate in a project aiming at system development of an advanced tool for mine action. This experience can be of grate value for the future. Although the ARC partners didn't manage to fulfil all intended system objectives in the final minefield test, all functional blocks of the system, including mission planning, data analysis and data fusion, was proven to work.

Some concluding FOI remarks are:

- It is difficult to get flight accreditation for UAV!
- Another platform might be more appropriate.
- A hardware solution to achieve sensor orientation/position is preferable compared to software solutions utilizing image features.
- If size, power and weight restrictions are limiting factors it could be better to use one sensor at the time and not waive the demand for good position/orientation performance.
- Lots of efforts were spent on meetings, reports and administration with limited value for the final system.
- It was a good experience of a complex system development.
- Opportunity to treat a problem with real minefields instead of research environment.
- Ground truth is not easy to correlate to sensor data.
- There will easily be a large amount of data.
- It was a positive experience.
- Extraordinary qualitative and quantitative output of work was needed.

7 MARKET OPPORTUNITIES

Projects funded by European Union are expected for commercial exploitation. As FOI has decided to give more emphasis to exploitation of new market segments, the FOI work inside ARC on identification and assessment of different products and services is of general FOI interest. The business opportunities for FOI related subparts of ARC, can be divided into three main areas:

- Field measurements: Mast/skylift-, airborne based and environmental parameters measurements. The skylift based method can fill the gap between research and prototype. The airborne system is applicable for environmental monitoring and is very flexible regarding mission type.
- Payload: Sensor mounting and vibration damping applications where stable airborne image data acquisition and when high precision hardware navigation data are required. ThermaCam SC3000 can be used for environmental monitoring for detection of human activity and detection of heat losses.
- Post processing: Analysis in the mean of anomaly detection. Temporal infrared analysis could be used to detect a specific object with known characteristics.

One part of work inside ARC was to make a SWOT analysis of the different FOI products and services identified as exploitable. SWOT is an acronym for the four important factors: Strength, Weakness, Opportunities and Threat.

SWOT analysis was made on the following FOI services and products:

- Field Measurements, Mast/Skylift turntable based.
- Field Measurements, Airborne based
- Field Measurements, Environment/Weather
- Payload, Sensor mounting and vibration damping
- Payload, Sensors (ThermaCAM SC3000)
- Anomaly Detection Methods, Spatial, IR
- Anomaly Detection Methods, Temporal, IR

7.1 FIELD MEASUREMENTS, MAST/SKYLIFT TURNTABLE BASED

Components:

1. Elevated platform (pneumatic mast of skylift)
2. Pre-programmed turntable
3. Imaging sensors
4. Data acquisition unit

Result Outputs:

1. Diurnal registrations of images with dense time sampling
2. Temporal behaviour of different parts of the scene

Strengths	**Weaknesses**
• Diurnal measurements with dense time sampling • Cost effective • Robust and stable • Repetitive pre-programmed • Easy to program for defined scan pattern • Turntable is synchronised with IR-sensor • Easy to handle	• Limited height • Robustness against thunderstorms is not investigated • Only close area survey
Opportunities	**Threats**
• The method can fill the gap between research and prototype • Complement to airborne	• Anchored airship • Commercial systems for moving ground based cameras e.g. systems for broadcasting of events.

7.2 FIELD MEASUREMENTS, AIRBORNE BASED

Components:

1. Airborne platform with INS/GPS
2. IR sensor
3. Sensor mount and vibration damping
4. Data acquisition unit
5. Post processing on ground

Result Outputs:

1. Image mosaics
2. Spatial and temporal co-registered images
3. Spatial and temporal anomalies

Strengths	**Weaknesses**
• Wide area survey • Height is no practical limitation	• Weather sensitive • Limited operational time • Payload limitations in volume, weight and power consumption • Depending on supplier of airborne platform
Opportunities	**Threats**
• Environmental monitoring • Flexible regarding mission type • Crisis management	• Mature market • Large number of actors on the market

7.3 FIELD MEASUREMENTS, ENVIRONMENT/WEATHER

Components:

1. Weather station
2. Data logger
3. Temperature probes
4. Laptop for data storing

Result Outputs:

1. Local weather and temperature data

Strengths	**Weaknesses**
• Advanced portable weather station • High performance portable data logger for e.g. temperatures • Structured recording of important environmental and weather parameters • High time resolution in acquired data • Local weather data	• Complex hardware • Sensitive for disturbances
Opportunities	**Threats**
• Applications where weather boundary conditions are important for analysis	• Analysis of image data not depending of weather data • Sufficient with less advanced and/or lower number of sensors for weather data

7.4 PAYLOAD, SENSOR MOUNTING AND VIBRATION DAMPING

Components

1. Mounting frame for imaging sensors
2. Vibration dampers adapted to weight and vibration characteristics for cameras and rest of payload

Result Outputs:

1. Vibration damped environment for airborne equipment

Strengths	**Weaknesses**
• Robust construction • No image blur due to vibrations	• No exact data on camera position and orientation • Not weather protected • Not possible to control camera orientation while flying • limited span of weights due to construction
Opportunities	**Threats**
• Applications where stable airborne image data acquisition without high precision hardware navigation data are required.	• Small light weight gimbal systems with good navigation performance.

7.5 PAYLOAD, SENSORS (THERMACAM SC3000)

Components

1. ThermaCAM SC3000 IR camera
2. Memory stick

Result Outputs:

1. IR images with no blur and high thermal resolution

Strengths	**Weaknesses**
• Robust and reliable • High frame rate • Short integration time, no image blur • High thermal resolution • Images can be stored on memory card in camera	• Difficult to store images on custom made data acquisition unit • No auto focus • No optical zoom
Opportunities	**Threats**
• Environmental monitoring • Detection of human activity • Detection of heat losses	• New sensors with better performance • New sensors with lower price

7.6 ANOMALY DETECTION METHODS, SPATIAL, INFRARED

Components

1. IR images
2. Computer
3. Software

Result Outputs:

1. Regions in IR images with anomaly spatial properties
2.

Strengths	**Weaknesses**
• Indications of image regions with abnormal spatial properties e.g. manmade objects • Easy to adapt to different applications	• Approach not very application specific • No hypothesis on object class
Opportunities	**Threats**
• Detection of remains of human activity • Detection of manmade objects	• Other methods for image analysis

7.7 ANOMALY DETECTION METHODS, TEMPORAL, IR

Components

1. IR images
2. Computer
3. Software

Result Outputs:

1. Regions in IR images with anomaly temporal properties

Strengths	**Weaknesses**
• Specific objects has a predictable unique temporal behaviour • Possibilities to detect buried as well as surface laid objects • 24 hour usefulness	• Sensible for unfavourable weather interaction • Sensitive for wrong parameters for soil, surface and objects • Difficult to compare on a pixel by pixel level if small objects are of interest
Opportunities	**Threats**
• Wide area of usefulness • Could detect a specific object with known characteristics	• Better temporal analysis methods

8 SURVEY OF METHODS FROM OTHER GROUPS

Research is under way to develop new detection methods that search for characteristics other than metal content. No single mine detection technology can operate effectively against all mine types in all settings. For example, nuclear quadrupole resonance can find mines containing the explosive cyclotrimethylenenitramine (known as royal demolition explosive (RDX) relatively quickly, but it is slow in confirming the presence of trinitrotoluene (TNT). Acoustic mine detection systems have demonstrated very low false alarm rates, but they cannot find mines buried at depths greater than about one mine diameter. Chemical vapor sensors can find plastic mines in moist soils, but they have difficulty locating metal mines in dry environments. Given the limitations of individual sensor technologies, major breakthroughs in mine detection capability are likely to occur only with the development of a multisensor system. Numerous studies have compared and evaluated the performance of mine detection technologies, those currently fielded and those under development.

In this chapter we concentrate on Electro-Optical (EO) methods, reviewing some results from the RAND [1] report, the survey of methods by Bruschini [50], and the result form the latest proceedings from SPIE. Other organisations have investigated the area (Netherlands [51], Canada [52], NVESD [53]).

8.1 INFRARED/HYPERSPECTRAL SYSTEMS

Infrared/hyperspectral methods detect abnormal variations in electromagnetic radiation reflected or emitted by either surface mines or the soil and vegetation immediately above buried mines [1]. This category encompasses technologies of various modes of action, including active and passive irradiation using a broad range of electromagnetic wavelengths.

Thermal detection methods use diurnal variations in temperatures of areas near mines relative to surrounding areas. For example, mines or the soil above them tend to be warmer than surrounding areas during the day but lose heat more quickly at night. Non-thermal detection methods rely on the fact that areas near mines reflect light (either natural or artificial) differently than surrounding areas. Man made materials tend to preserve polarization because of their typically smooth surfaces, allowing discrimination of surface mines.

The EO methods are attractive because they do not involve physical contact and can be used from a safe distance. The systems are lightweight and are effective at scanning wide areas relatively quickly. When deployed from airborne platforms, they are particularly effective for detecting surface mines. Collecting and processing he signals temporally (as opposed to in “snapshots”) tends to improve performance by tracking diurnal cycles.

Electro-optical (EO) sensors can be used from a considerable standoff distance and they can rapidly survey large areas. Their ability to detect mines has been recognized since the 1950s [1]. Antipersonnel mines may be buried or surface-laid. Detection of surface mines is a trivial matter for a human observer, but of interest in wide-area search operations using airborne sensors. Little compelling performance data is

available for EO detection of antipersonnel mines. Much of the work to date comprises concept demonstrations and studies of specific phenomena. Minefield detection is typically much easier than detection of single mines because of the large number of mines involved and the additional spatial information (e.g., the presence of a spatial pattern. Significant European research in antipersonnel mine detection is under way [1]. Both thermal emissions and surface-scattering phenomena contribute to EO mine signatures, and the relative importance of these phenomena depends on whether the mine is deployed on the surface or is buried.

8.2 BURIED MINES

Detection of buried antipersonnel mines comprises a very challenging problem. A number of concepts have been examined for this problem.

8.2.1 Passive Thermal Detection

A large part of the solar energy incident on soil is absorbed, leading to heating. As a result of this heating, the soil emits thermal radiation detectable by a thermal infrared (IR) sensor. Natural solar heating and cooling over a diurnal cycle tend to affect a buried object and the surrounding soil differently, which leads to a detectable temperature difference. For a buried mine this difference arises because the mine is a better thermal insulator than the soil. During the day, the thin layer of soil over the mine tends to accumulate thermal energy because the mine impedes the transport of that heat deeper into the ground. As a result, soil over a mine will tend to be warmer than the surrounding soil. Conversely, in the evening hours, the soil layer over the mine gives up its thermal energy more rapidly than the surrounding soil and it appears cooler. Twice daily the soil over the mine and the background soil will assume the same temperature, making thermal detection impossible. The temperature difference and its temporal behaviour depend strongly on a variety of variable natural phenomena, including the time of day, prior solar illumination, wind speed, ground cover, and soil composition (e.g., moisture content). Most thermal detection concepts involve single looks (“snapshots”) of the region of interest. The soil over a mine has different thermal dynamics than homogeneous soil and, as a result, a time sequence of images can often produce better detection than a single image. Hence, staring sensors, which are impractical for many military scenarios, may be attractive for humanitarian demining.

Algorithms for mine detection are a critical part of any detection system. These are somewhat less mature, although a number of groups have reported progress in this area [1]. In the report we can find receiver operating characteristic (ROC) curves for thermal IR detection of a mixture of antipersonnel and antitank mines, data from the TNO (Netherlands Organisation for Applied Scientific Research) mine lanes in the Netherlands were examined and performance results are reported therein for 15 antipersonnel mines. Also limited results on thermal IR detection of buried antitank minefields from airborne sensors are summarized.

In one project (LAMBS, Littoral Assessment of Mine Burial Signatures) hyperspectral technique in the range 0.35 -14 μm is used to find robust spectral characteristics for detection of land mines in seaboards. Mines buried in sand and the

surroundings have been registered. Massive data collection and categorisation of mines have been performed, both surface laid and buried [54].

The surf zone is a challenging environment for conducting mine countermeasures operations. Breaking surf action causes bottom sediment resuspension and the formation of bubbles and foam. The environmental factors influencing the performance of airborne LIDAR sensors are examined by [55]. These factors can be highly dynamic.

A similar study was undertaken by [56] where lidar mine signature data collection to characterize electro-optic (EO) signatures of anti-invasion mines and environmental factors affecting their detection in the littorals. Two lidar sensors, one 3-D and one polarimetric, were used. The principle goal of this analysis is to characterize lidar signature features, especially 3 -D, of in-water mines and correlate those features to physical processes in the environments. Due to the constantly varying optical properties of the water, as well as dynamic wave activity, sensor data appears very noisy. Deeply submerged mines are difficult to detect due to the high turbidity and corresponding high attenuation levels of the water. Possible solutions to these issues include a concept of stare logic for the sensor, where the sensor images the same location periodically, or over a period of time. A staring approach would provide spans of image data which could be exploited to identify the optimal images from which to perform detection.

Soil parameters relevant to the operation of IR systems such as texture, water content, and soil-water salinity also include thermal resistivity, thermal diffusivity and specific heat capacity, all of which are expected to depend on soil moisture content. There is a general need for an information database devoted specifically to relevant soil properties, their geographic distribution and climate-driven variability. A knowledge of these soil properties in diverse landmine-affected areas will thus be of significant importance to landmine detection efforts both in the development, testing and selection of equipment as well as in predicting their performance in a given region [57, 58] .

Analytical calculation for temperature propagation through homogeneous and layered soils is compared with a numerical model (HYDRUS-2D) shows that the relatively simple analytical solution proposed here is reasonably accurate. The results show that an increase in soil water content has a significant effect on the thermal signature, as well as on the phase shift of the maximum temperature difference. Different soil textures have relatively little effect on the temperature at the surface [59].

Signature variations with time and environmental conditions are a persistent problem for thermal IR mine detection. The optimum time for detection and the expected contrast on factors noted above that are often unknown to a remote observer. Surface clutter from reflected light and inhomogeneous soil properties is also problematic. In many cases the size of these clutter artefacts is comparable to that of antipersonnel mines, which leads to false alarms. Thermal emission from foliage (at the temperature of living, respiring vegetation) tends to mask the temperature of the underlying soil (and the thermal mine signature). The processes that produce thermal IR target signatures and clutter are poorly understood. In some cases, good detection performance has been demonstrated, but when such systems fail, the reasons for

failure are often not evident. A better understanding of target and clutter signatures could substantially improve their effectiveness by allowing them to be deployed appropriately. Staring sensors should also be considered, which take data over an extended period in time, waiting for favourable conditions to arise. Time-history information will also help to compensate for the variability of thermal signatures with time and environmental conditions [1].

Autonomous detection of tripwires using optical systems is of great interest. A video camera with sensitivity in the near infrared (IR) is used together with coherence enhancing diffusion filtering can recover broken edges and smooth background without smoothing coherent structures [60].

8.3 SURFACE MINES

Surface mine detection is primarily of interest for airborne or other platforms with a significant standoff distance. At large distances, the number of pixels on the mine decreases, but some compensating factors exist. The surface scattering properties of the mine are detectable in addition to thermal phenomena. Also the thermal signatures of buried mines often have vague shapes, and when the light arrives at low elevation angles, shadows may also be exploited in detection [1].

8.3.1 Passive Thermal Detection

Because a mine's thermal properties are considerably different than those of vegetation, a solar-heated mine viewed with a thermal IR sensor typically has a high contrast. This contrast often exists even when the mine is painted to camouflage its presence. Differences in paints or coloration on different parts of the mine may lead to complex, distinctive thermal signatures because of different solar absorptions [1].

The ability to detect landmines using normal infrared cameras, only measuring intensity, is limited by the presence of clutter (stones, soil variations). Using a polarimetric infrared camera allows for not only the measurement of intensity but also of two additional polarimetric signals.

One project gives a comparison of two vehicle-mounted infrared systems for landmine detection. The first system is a downward looking standard infrared camera, and the second system is using a forward-looking polarimetric infrared camera. On the training set the polarimetric infrared system performs better especially for low false alarm rates. On the independent evaluation set the differences are much smaller. On the ferruginous soil test lane the down-ward looking system performs better at certain points whereas on the grass test lane the forward-looking system performs better at certain points [61].

Polarization measurements in the IR region, especially in the 8-12 μm wavelength region (LW), are useful to detect man-made object in a natural environment [62]. It has been shown that polarization measurements have improved the possibility to detect partly covered objects. This makes reconnaissance and surveillance sensors and warners more efficient. Further, the emissivity as a function of emission angle has been measured for different coverage of the mine.

8.3.2 Passive Nonthermal Detection

The surface scattering properties of mines are distinct from those of soil and vegetation, particularly when measured in the spectral domain, and that spectral dependence can be a powerful discriminator. In addition to their spectral properties, many mines are relatively flat and covered with the same material over much of their top surface. This leads to the appearance of a uniform region in the imagery, which tends to be useful in image processing. The polarization properties of surface-laid mines can also be exploited by a passive sensor. The polarimetric signature of unstructured random surfaces such as grass tends to be random itself, which leads to an unpolarized return. In contrast, the smooth surfaces of man-made materials tend to produce a polarized signature when viewed at low elevation angles. Polarimetric signatures can exist even where there is no detectable thermal signature. [1]

Spatial-spectral anomaly detection (the "RX Algorithm") has been exploited on the USMC's Coastal Battlefield Reconnaissance and Analysis (COBRA) Advanced Technology Demonstration (ATD) and several associated technology base studies, and has been found to be a useful method for the automated detection of surface-emplaced antitank land mines in airborne multispectral imagery. RX is a reference image processing algorithm often cited in literature. The RX throughput on the ATD was about 38 times real time using a single Sun UltraSparc system. A goal was to demonstrate RX in real-time. Implementation of the RX algorithm in a single Field Programmable Gate Array (FPGA) is a major first step toward achieving real-time land mine detection, a solution that achieves a real-time implementation of the RX algorithm at video rates using COBRA ATD data [63].

An airborne active sensor system for mine and obstacle detection in very shallow water, through the surf-zone and onto the beach is presented in [64]. The system uses an integrated scanner, detector, and telescope receiver architecture. The system couples all receiver components and LIDAR electronics to achieve the system compaction required for tactical UAV integration while providing a large aperture. It also includes an advanced compact multifunction laser transmitter, and a compact 3-D camera. Additionally, the laser will provide time multiplexed multi-colour output to perform day/night multispectral imaging for beach surveillance.

Another project studies systems that are developed to identify objects of interest on the ocean bottom. Both LIDAR technology and the Laser Line Scan technology is studied. Both of these sensors produce high fidelity imagery. The LIDAR produce two-dimensional (2-D) contrast images only while Laser produces three-dimensional (3-D) data that can be rendered into 2-D contrast images and range maps. Although still an emerging technology, recent advances have begun to point to significant advantages with the supplementary range information (3-D information) in identifying objects of interest on the sea floor [65].

One project has demonstrated a night time operational minefield detection capability using commercial off-the-shelf high-power Laser Diode Arrays (LDAs). LDAs promise compact and efficient lighting to allow for extended reconnaissance operations for future mine detection systems. When combined with high-resolution intensified imaging systems, LDAs can illuminate otherwise unseen areas. Future wavelength options will open the way for active multispectral imaging with LDAs [66].

Research has shown that naturally occurring light outdoors and underwater is partially linearly polarized. With a three-channel sensor, naturally occurring polarization signatures have been measured. Performance results from the field-testing of targets in the Very Shallow Water and Surf Zone regions are presented. These results show that partial polarization provides a quantifiable signature that can be exploited by employing the right algorithms [67].

Airborne multispectral imagery was collected over various targets on the beach and in the water in an attempt to characterize the surf zone environment with respect to electro-optical system capabilities. The MANTIS (Mission Adaptable Narrowband Tunable Imaging Sensor) systems were flown in an IR – red - green – blue (700, 600, 550, 480 nm) configuration from altitudes ranging from 200 to 700 meters. Data collected has been lightly analyzed and a surf zone index (SZI) defined and calculated. This index allows mine hunting system performance measurements in the surf zone to be normalized by environmental conditions. The SZI takes into account water clarity, wave energy, and foam persistence [68].

A specular polarimetric model does not give insight why certain man-made objects like landmines give a higher polarimetric signature than natural background. By introducing a polarimetric bidirectional reflectance distribution function (BRDF) the specular model is extended. This model gives a better prediction of the polarimetric signature and gives a close match to the measurements of landmines with different casings as well as the sand background. These values explain why the polarimetric signal of the background is very low compared to the landmines. As a consequence the landmines are distinguishable from the background even when the intensity (or blackbody temperature) is the same. [69].

Hyperspectral imaging is an important technology for the passive optical detection of surface and buried land mines from an airborne platform. The primary surface mine observable is a spectral difference between the mine body and the background. Algorithms developed for the military surveillance application can be directly applied to the surface mine problem [70].

Detection of tripwires is an active area of investigation. The utilization of robotic vehicles capable of performing this task is one of the goals of this project. The current detection algorithm that has been pruned down to run in real-time on the robotic platform consists of a Hough transform to find candidate lines followed by post-processing to score the candidate lines for the likelihood that they correspond to a trip wire [71].

Whereas multispectral imagery is sensed over multiple narrowband wavelengths, sensing over two broadband spectrums has the advantage of increased signal resulting from integrated energy over larger spectrums. Preliminary results presented in [72] show that very basic image fusion processing applied to visible and SWIR imagery produces reasonable illumination invariant segmentation of objects against background. This suggests the use of a simplified compact camera architecture using visible and SWIR sensing focal plane arrays for performing detection of mines and other important objects of interest.

8.3.3 Active Sensing for Surface Mines

Only active sensors of non-thermal phenomena are of interest because actively provoking a thermal signature from a significant distance requires impractical amounts of power. The use of active sensors is appealing for polarimetric sensors in which a fixed polarization can be transmitted. The basis for an active polarimetric sensor is quite different from the passive polarimetric sensors noted above, in which low elevation angles are preferred to detect the polarized signature of the mine. Active sensors tend to operate at near-nadir viewing angles, where a smooth mine surface will not depolarize the (polarized) illumination, while scattering from randomly oriented foliage will be depolarized

8.4 SIGNAL PROCESSING AND MODELLING

In the landmine detection scenario, a particular sensor, or set of sensors, is used to interrogate one or several spatial locations for which a mine/no-mine decision is to be made. The sensing process may be automated, as is the case for vehicular or autonomous systems, or may involve a human manually operating the sensor. A sensor may record all of the response defined by the phenomenology associated with that sensor, or it may only record a portion of the response. Signal-processing algorithms for landmine detection are necessarily constrained by the available sensor data. Algorithms are also constrained by the system configuration as well as their impact on operator training requirements [1].

Signal processing for landmine detection seeks to exploit discrimination information in measured signals from a variety of sensors. This information can be of many types, including frequency, shape, and size. Signal processing is used to mitigate system effects, characterize and discard sensor responses to the environment, compute discriminating features for classification of sets of measurements as either mines or non-mines, and provide feedback to operators.

Signal-processing algorithms for landmine detection must detect the presence of an object in the geological background and discriminate signals associated with landmines from signals associated with discrete clutter objects. In general, signal-processing algorithms perform best when the physics that define the problem are integrated within the mathematical constructs underlying the theory of signal processing and pattern recognition. The utilization of computational models describing sensor phenomenology, physics based feature selection, statistical models of mines and clutter, and spatial information have all led to dramatic reductions in the false alarm rates of landmine detection systems. Because the physics that governs each sensor modality differs, feature sets extracted from data collected by different sensors usually are not consistent across sensors. However, several common approaches to processing the raw signals or the extracted features have been applied across sensor modalities.

A “traditional” approach to the problem of mine detection in the context of using multilayer perceptron (MLP) neural networks for classification consists first in the use of feature selection techniques, followed by some cross validation based training algorithm. The contrast results obtained using a “traditional” approach, with those

obtained from using the Support Vector Machine (SVM) based framework for classifier design is described in [73]. The SVM approach is regarded as more attractive for large feature sets due to the optimization of a criterion in training, which is closely related to theoretical bounds on classifier generalization ability.

The utility of Constant False Alarm Rate (CFAR) algorithms is that the selection of a detection threshold may be made independently of image intensity. However, wide application of the algorithms shows that detection values are highly dependent on scene characteristics. Fitting the output of the detection algorithm with a model of a portion of the theoretical results allows for background independent threshold selection [74].

8.5 MULTISENSORSYSTEM

The use of near, mid wavelength and long wavelength infrared imagery for the detection of mines and concealed weapons is demonstrated using several techniques. The fusion algorithms used are wavelet based fusion and Fuzzy Logic Approach (FLA) fusion. The FLA is presented as one of several possible methods for combining images from different sensors for achieving an image that displays more information than either image separately. Metrics are suggested that could rate the fidelity of the fused images, such as, an entropy metric [75].

With the purpose of investigate issues of dynamically detection of land mines a demonstration vehicle is presented in [76]. Three sensors are mounted on a vehicle, a passive sensor sensible in visual and IR bands and a GPR as the active sensor. The data fusion is done in a following vehicle. Early results show the ability to detect surface laid AP mines and also larger mines. Buried mines can also be detected.

LOTUS is a project to develop, integrate and demonstrate the proof-of-concept of a multi-sensor landmine detection system for humanitarian de-mining. The idea is to combine three sensors into a vehicle-mounted system. The system includes a metal detector, an infrared (IR) camera system, and ground-penetrating radar (GPR). The idea of using three sensors is to reduce the problems caused by false alarms of individual sensors due to "background clutter" [77].

The primary mission for the system presented in [78] is route clearance, automatically detecting and marking metallic and nonmetallic Anti-Tank (AT) mines. The system consists of a mine detection and marking system mounted on a teleoperated mine detection vehicle providing a three-meter detection swath and include nine Ground Penetrating Radars (GPR), nine Pulsed Magnetic Induction (PMI) metal detectors, and (as an option) two long-wave infrared (LWIR) cameras and a main computer system mounted in a mine protected clearance vehicle Both vehicles have overpass capability for AT mines, as well as armor anti-mine blast protection. The navigation system in combination with the sensors has been shown to locate targets to within the desired 0.25 m (0.5m specified) mine halo at speeds up to 8 kph. Mines have been marked electronically to within 0.25m at speeds ranging from 2 to 12 kph.

8.6 TRENDS FOR THE FUTURE

A miniature UAV is capable of flying a pre-programmed route autonomously, with manual override as an option. At the conclusion of the mission, the vehicle returns for landing, after which it can be quickly disassembled and stored until its next use. Thermal imaging extends the utility of miniature UAVs to operations in complete darkness and limited visibility, but historically thermal imagers have been too large and heavy for this application. That changed in 1999 with the introduction of Indigo System's Alpha™ camera, which established a new class of thermal imaging product termed the infrared "microsensor". Substantially smaller and lighter than any other infrared imaging product available at the time, Alpha™ was the first camera that could be readily packaged into the nose of a miniature UAV. Its low power consumption was also a key enabling feature. Building upon the success of Alpha™, Indigo then took the microsensor class a step further with its Omega™ camera, which broke all the records established by Alpha™ for small size, weight, and power.[79]

8.7 CONCLUSIONS

The methods, particularly thermal imaging, have been used in several prototype multisensor systems, but extreme variability in performance as a function of dynamic environmental characteristics has precluded their use for close-in detection and accurate identification of mine locations. Despite maturity of the sensor, the algorithms to process the signals in an informative way are relatively undeveloped and are not linked to physical phenomena. Thermal signatures currently are not well understood, and a comprehensive predictive model does not exist. Moreover, waves at the frequencies used by the methods cannot penetrate soil surfaces, and the localized hyperspectral anomalies produced by mine emplacement are temporary and are quickly eliminated by weathering. Thus, the technologies are able to detect buried mines under only limited transient conditions.

With the possible exception of methods that would simulate solar heating as a means to enhance the thermal signatures of buried targets, infrared/hyperspectral methods are not particularly suitable for close-in buried mine detection. The underlying phenomena are not sufficiently characterized, and natural processes quickly erase the detectable surface anomalies. The technology has demonstrated ability and expected future promise for airborne minefield detection, especially for surface mines, but it is not expected to be useful for close-in detection of buried mines.

Greater use of hyperspectral and polarimetric methods will permit more information per pixel, which aids detection. More extensive tests should be conducted on antipersonnel mines to determine the true performance of these sensors. In such work, improved spatial resolution will be required. Finally improvements in image processing techniques are likely to offer significant gains.

9 AREA MUNITION AND DIRECTIONAL FRAGMENTATION MINES

A prestudy has been conducted on optical methods for detecting wide area munition and directional fragmentation. Regarding wide area munition the Hornet mine from USA serves as an illustration, see Figure 9.1. From [80], the following information is achieved: it operates on targets within100 m range and consists of a ground launcher and a sublet. The ground launcher has seismic and acoustic sensors to detect targets and the sublet has an infrared sensor to search for target and fires a high-velocity heavy-metal slug. The mine is knee tall and 20 cm in diameter. It is visually detectable in most field conditions. The conclusion is that the size and characteristic signature makes the mine detectable with optical sensors from airborne platforms.

Figure 9.1 Hornet antitank mine (image from [80]).

From the same source, [80], the data in Table 9.1 has been put together regarding characteristics for some different types of directional fragmentation mines. In addition, the maximum detection distances for an IR camera, ThermaCAM SC300, have been calculated for each mine. A standard Criterion for detection has been used, Johnson [81]. According to this criterion, one line pair is needed across the minimum dimension of the object. For a CCD camera this criterion is converted to a demand of two pixels across the minimum dimension of the object. Given the instantaneous field of view of 1.1 milliradian and dimensions of the mine, the maximum detection distances in the last column in Figure 9.1 are calculated. The shapes of the mines are of three different types, claymore, rectangular and circular. The front area of a claymore shaped mine is horizontally convex and vertically concave. In Figure 9.2, example images are shown of the mine types.

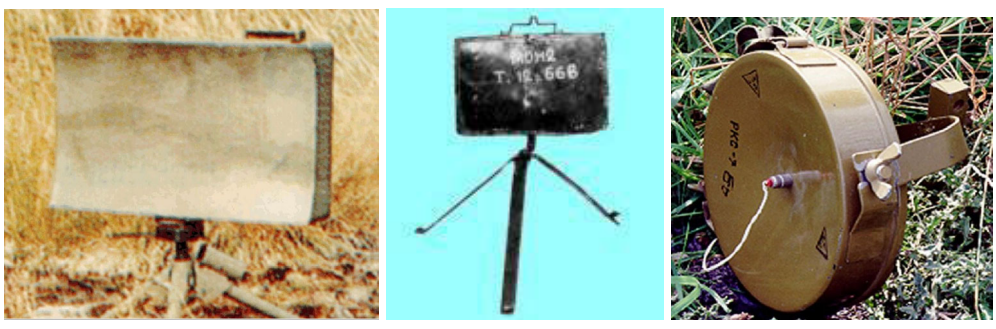

Figure 9.2 Examples of claymore, rectangular and circular shaped mines (images from [80])

Name	Origin	Type	Casing (pl= plastic, met=metal)	Shape (cl=claymore, re=rectangular, ci=circular)	Colors	Weight, [kg]	Explosive [kg]	Length [mm]	Width [mm]	Height [mm]	Lethal max range [m]	Hazard range [m]	**Max detection distance [m**
APM-1	AUS	AP	pl	cl	Green Olive Sand	1,0	0,4	140	40	80	60	300	**36**
APM-2	AUS	AP	pl	cl	Green Olive Sand	3,0	1,3	315	N/A	155	60	300	**70**
Directional Apers	Chile	AP	pl	cl	Green Olive	1,6	0,5	220	60	140	100	300	**64**
FFV 013	SE	AP	pl	cl	Green Olive	20,0	?	420	N/A	250	150	300	**114**
HM 1000	AUS	AP	pl	cl	Green Olive	2,4	?	290	30	130	60	300	**59**
K440	S Korea	AP	pl	cl	Green Olive	1,6	0,7	178	40	104	60	300	**47**
M18A1	USA	AP	pl	cl	Green Olive Sand	1,6	0,7	216	35	83	60	300	**38**
M89	AUS	AP	pl	cl	Green Olive	4,0	2,3	315	55	155	60	300	**70**
MAI GA4	Romania	AP	pl	cl	Green Olive	22,8	12,0	400	100	260	100	300	**118**
MAPED F1	France	AP	pl	cl	Green Olive	1,0	?	180	60	120	60	300	**55**
MDH-2	Vietnam	AP	met	re	Green Olive	?	1,4	190	54	120	125	160	**55**
Mini-MS 803	S Africa	AP	pl	cl	Green Olive Sand	1,0	0,5	220	35	70	60	300	**32**
Model 123	Thailand	AP	pl	cl	Green Olive Sand	1,5	0,3	115	60	90	60	300	**41**
MON 50	Russia	AP	pl	cl	Green, Olive, Grey	2,0	0,7	226	35	155	60	300	70
MON 90	Russia	AP	pl	cl	Green Olive	12,1	6,2	345	153	202	90	300	**92**
MRUD	Serbia	AP	pl	cl	Light green, Olive	1,5	0,9	230	50	89	90	300	**40**
No 2	S Africa	AP	pl	cl	Green Olive Sand	1,6	0,7	216	35	83	60	300	**38**
P5 Mk 1	Pakistan	AP	pl	cl	Green Olive Brown Sand	1,6	0,9	230	50	90	60	300	**41**
SMI 20/1C	Austria	AP	pl	cl	Green Olive Sand	1,9	0,9	N/A	260	110	100	300	**50**
SMI 21/11C	Austria	AP	pl	cl	Green Olive Sand	20,0	11,5	N/A	560	235	150	300	**107**
SMI 21/3C	Austria	AP	pl	cl	Green Olive Sand	8,2	4,2	N/A	240	180	150	300	**82**
VS-DAFM1	Italy	AP	pl	cl	Green Olive Sand	3,6	?	342	38	168	60	300	**76**
VS-DAFM6	Italy	AP	pl	cl	Green Olive Sand	18,2	?	N/A	530	270	100	300	**123**
VS-DAFM7	Italy	AP	pl	cl	Green Olive Sand	10,7	?	N/A	190	170	100	300	**77**
MDH-10	Vietnam	AP	met	ci	Green Olive	5,0	2,0	N/A	N/A	80	125	160	**100**
MDH-5	Vietnam	AP	met	ci	Green Olive	0,8	0,3	N/A	49	N/A	125	160	**52**
MDH-7	Vietnam	AP	met	ci	Green Olive	3,8	1,6	N/A	51	N/A	125	160	**90**
MON 100	Russia	AP	met	ci	Green Olive	5,0	2,0	N/A	83	N/A	125	160	**107**
MON 200	Russia	AP	met	ci	Green Olive	25,0	12,0	N/A	130	N/A	200	240	**197**
ZAPS	Zimbabwe	AP	pl	ci	Green Olive	1,7	0,5	N/A	N/A	75	30	250	**91**

Table 9.1 A list of properties for directional fragmentation mines and maximum expected detection distance for IR camera ThermaCAM™ SC 3000.

The maximum expected detection distance only reflect needed spatial resolutions and are probably an overestimation of performance for the following reasons:

- Only geometrical properties are taken into account, not radiometric.
- The contrast between object and background is not considered.
- If background clutter has spatial variations similar to the dimensions of the mine, the probability of detection will decrease.
- The projection angle can vary. The calculation is made under assumption of a front view perspective of the object towards the sensor. If the minimum

projected dimension of the mine, seen from the sensor, decreases, then the expected detection distance decreases as well.
- Influence from the atmosphere and particles in the air can decrease sensor performance.
- Visual obstacles between sensor and object can also decrease detection performance.

As an example of diurnal variations, infrared measurements were made of three different objects similar to directional fragmentation mines: large claymore shaped, small claymore shaped and circular mine like object.

For the IR registrations, the camera ThermaCAM™ SC 3000 from FLIR Systems was used and measurements were carried out automatically for about three and a half day, from 2004-05-28 to 2004-06-01. The weather was clear with high temperature differences between day and night. An IR image, containing the large claymore shaped mine like object and areas for calculating average and standard deviation, is shown in Figure 9.3.

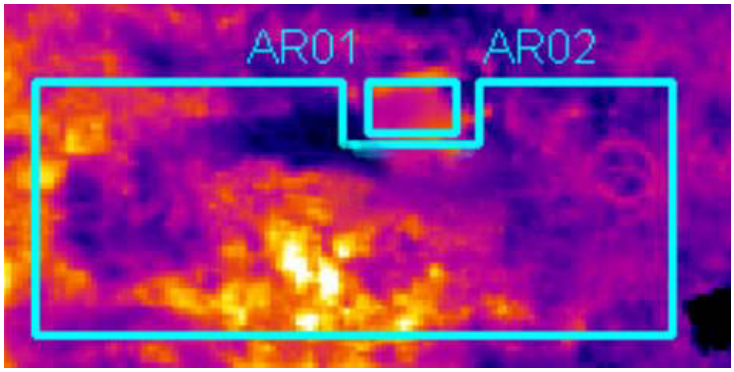

Figure 9.3 An IR image of the large claymore shaped mine like object and areas that were used for calculating average and standard deviation for object (AR01) and local background (AR02).

Software from FLIR systems, Thermacam Researcher 2001, was used for analysis. Values were extracted once an hour for the period, except for the time between approximately midnight and noon when no data are available due to temperature depending sensor platform change in position and orientation, which made the mine to disappear from the field of view of the camera. In Figure 9.4, the temperatures and in Figure 9.5, the temperature differences are shown. It should be pointed out that temperatures in this section are apparent temperatures and they correspond well to object temperatures if the objects radiates like blackbodies.

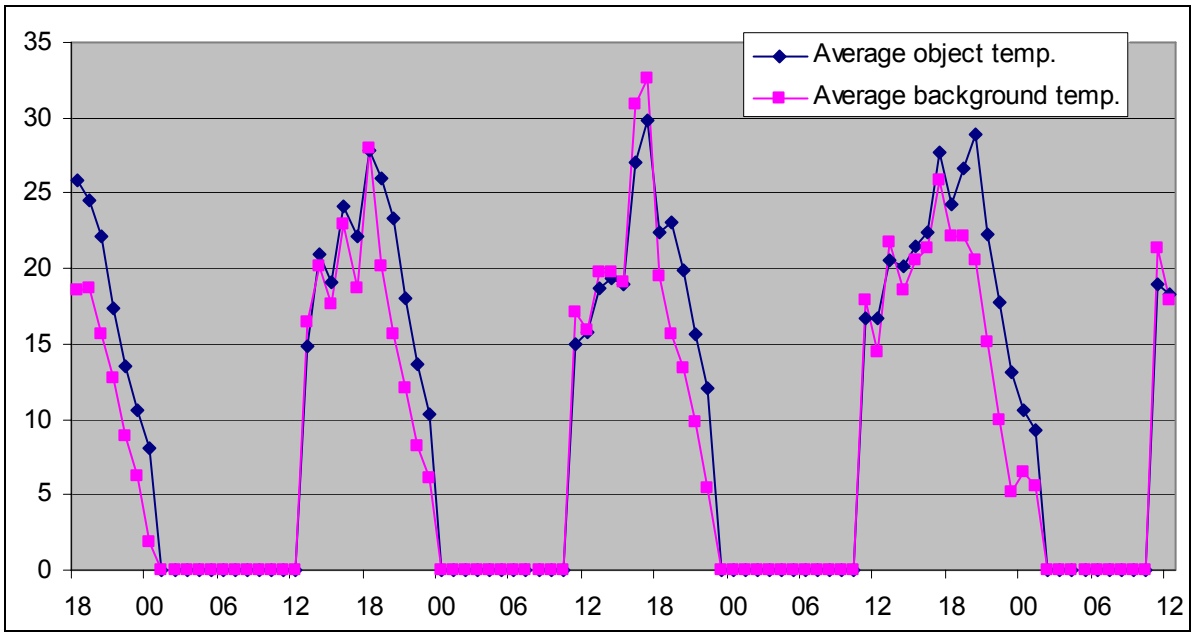

Figure 9.4 Average temperatures in analysed areas for the large claymore shaped mine like object and local background at different times of the day. No data are available from approximately midnight to noon.

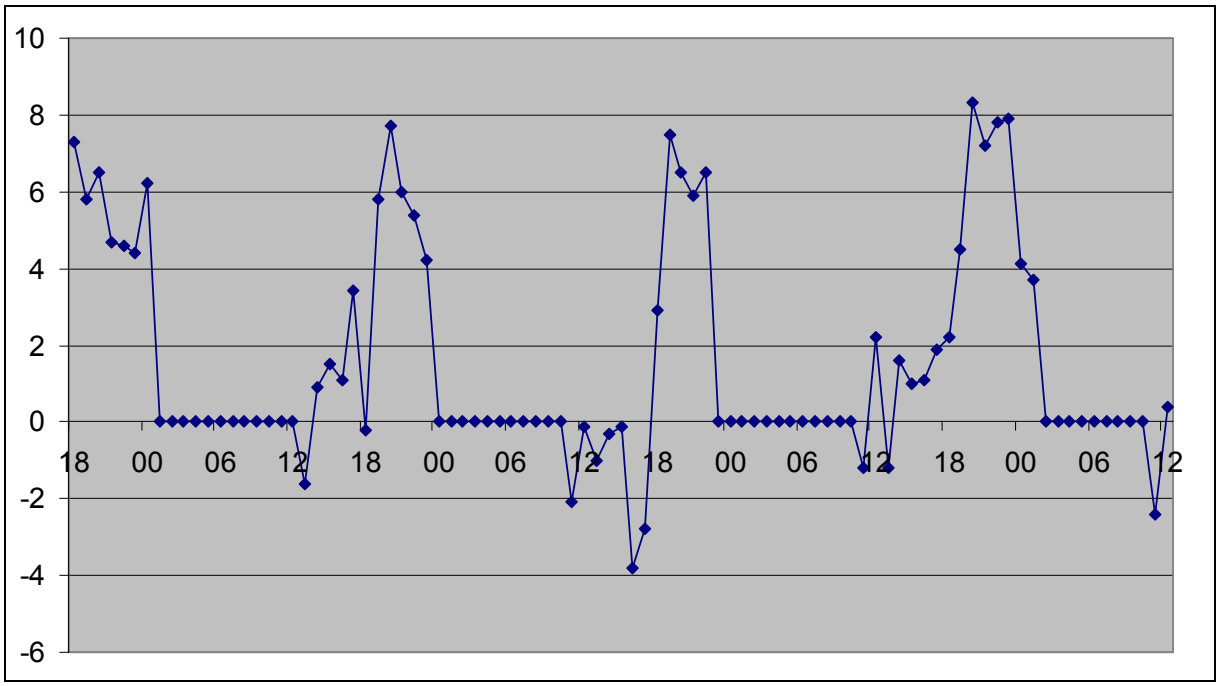

Figure 9.5 Temperature differences between the large claymore shaped mine like object and local background at different times of the day. No data are available from approximately midnight to noon.

The perceived contrast does not only depend on the average temperature difference, but also on the temperature variation of object and background. For this purpose a more realistic contrast measure was extracted according to the following formula:

$$C = \sqrt{\frac{(m_o - m_b)^2}{(V_o + V_b)}}$$

Where:

C=contrast (no dimension)
m_o = object mean (average) temperature
m_b = background mean (average) temperature
V_o = object temperature variance
V_b = background temperature variance

Note that the contrast with this definition has no dimension and can be zero or positive, never negative. In Figure 9.6, the IR contrast is presented for the large claymore shaped object.

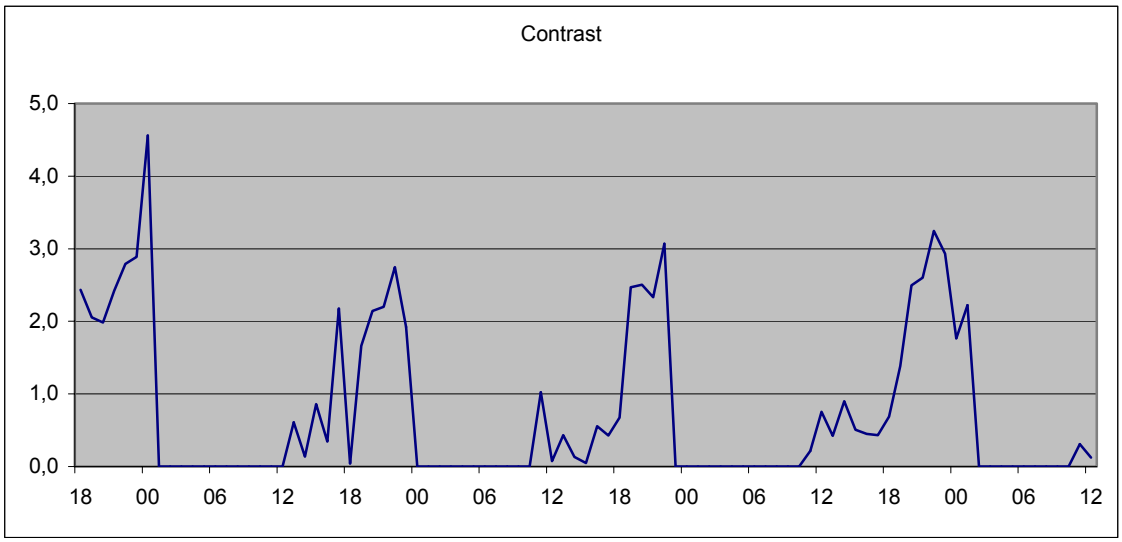

Figure 9.6 Diurnal IR contrast variation for the large claymore shaped object. No data available from approximately midnight to noon.

A tendency in the figures is that the maximum temperatures occurs around 6 pm, but depending on a slower night time decrease of the object temperature compared to the background temperature, the temperature difference, as well as the contrast, are at maximum later in the evening. Nothing can be said from this material on how the values are in the time span between midnight and noon. The corresponding analyse were made for small claymore shaped mine like object and circular shaped mine like object. The areas used for analysis are presented in Figure 9.7, temperatures in Figure 9.8, temperature differences in Figure 9.9 and contrasts in Figure 9.10.

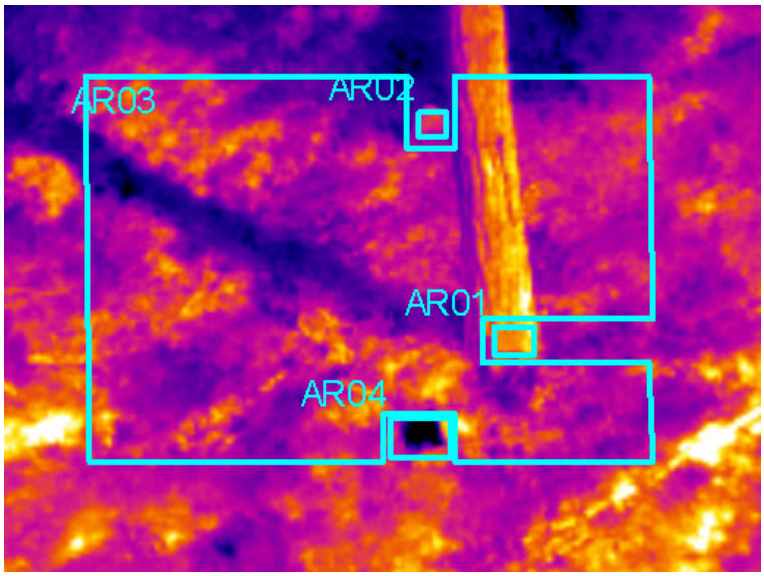

Figure 9.7 An IR image of the objects: small claymore mine like object (AR01), circular mine like object (AR02) and local background (AR03). A reference plate (AR04) was used for localisation reference and was not used for analysis of apparent temperatures.

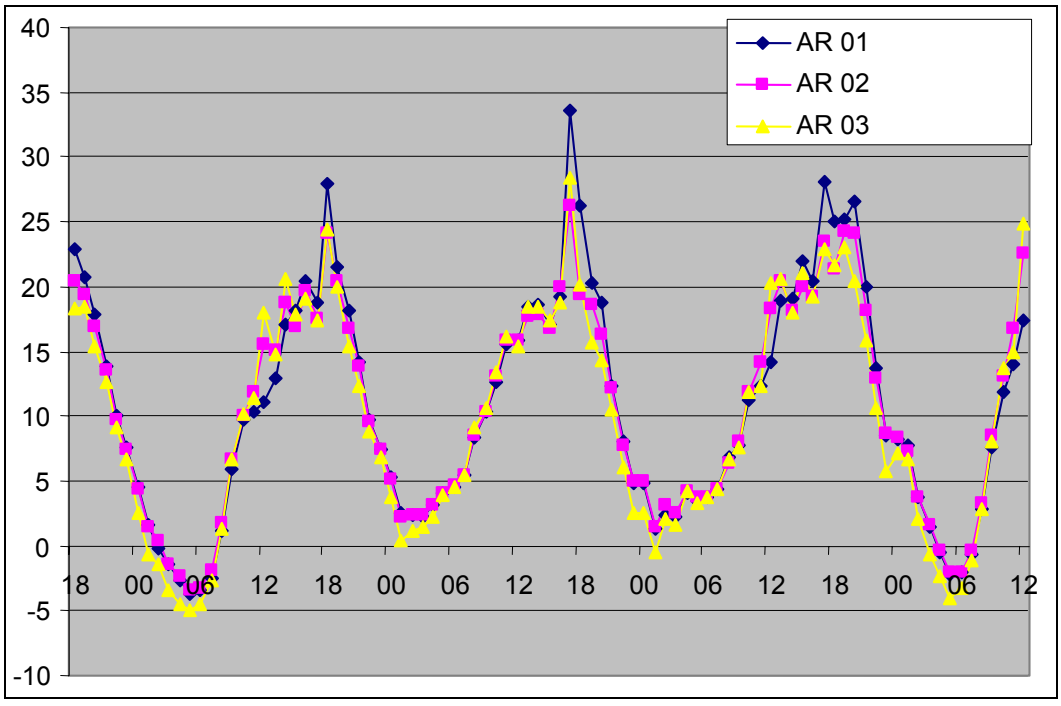

Figure 9.8. Average temperatures in analysed areas for the small claymore shaped mine like object (AR 01), for circular shaped mine like object (AR 02) and for local background (AR 03) at different times of the day.

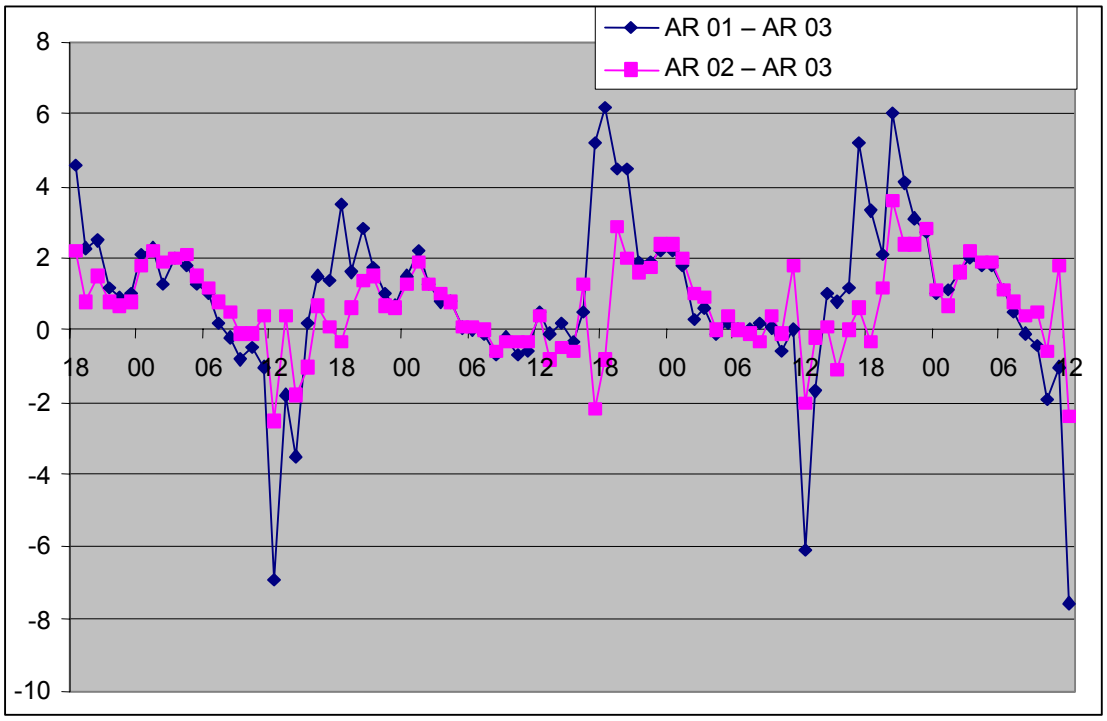

Figure 9.9. Temperature difference between the small claymore shaped mine like object and local background (AR 01 - AR 03) and difference between circular shaped mine like object and background (AR 02 - AR 03) at different times of the day.

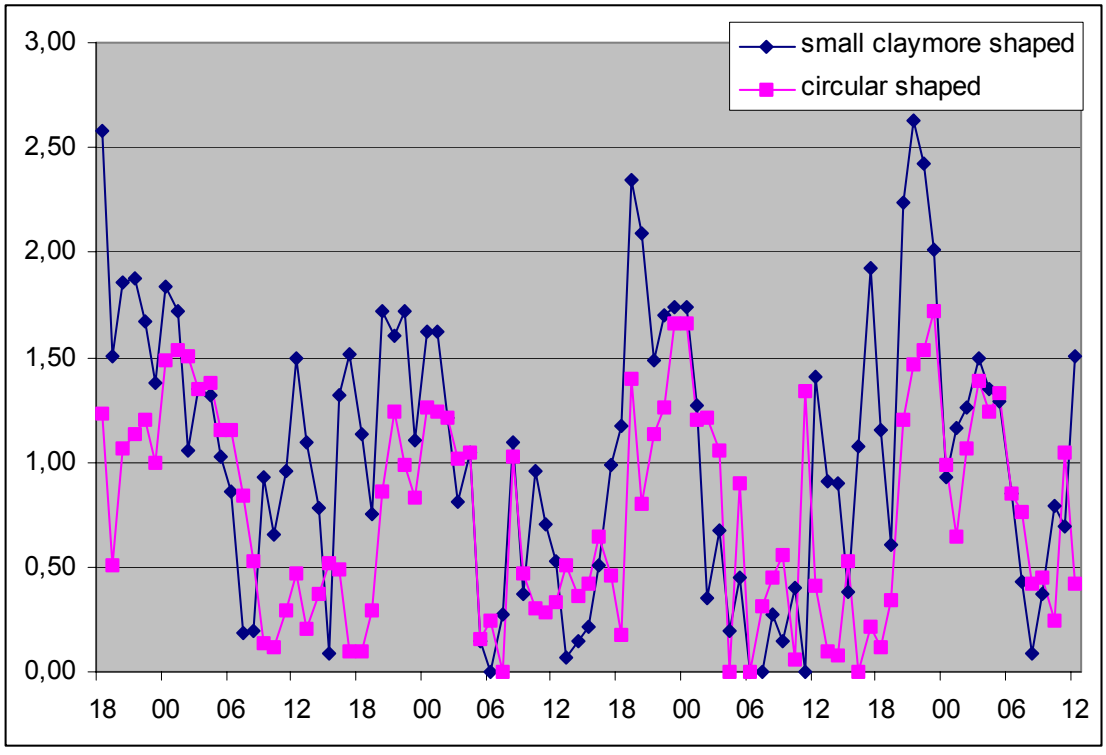

Figure 9.10. Diurnal IR contrast variation for the small claymore shaped mine like object and for the circular shaped mine like object.

Under present conditions, it seems to be a tendency for the infrared contrast to be more pronounced during nighttimes.

10 SELECTED PUBLICATIONS FROM THE OPTICAL MINE DETECTION GROUP AT FOI

The start of the optical mine detection work of this group was in 1993. Radar, multispectral and biosensor techniques for mine detection was presented 1993 at Symposium on Anti-personnel mines at the International Committee of the Red Cross in Montreux, Larsson [82].

After a couple of years of work the results of measurements of buried land mines in indoor and outdoor sand boxes, modelling and detection was presented in 1997 Sjökvist [83], 1998 Sjökvist [84], Georgson [85] and Sjökvist [30] at both national and international conferences.

In 1999 a report on the work in the first years was presented, Georgson [2]. Result was presented at international mine specific conference, Georgson[86] and national image processing conference, Sjökvist [87] and at a conference on advanced numerical methods in Poland, Sjökvist [31]. In 1999 the first thesis out of the group was presented, Sjökvist [8].

In 2000 the work of the group was reported at Nordic Demining Research Forum Georgson [88]and Lundberg [89], and to the national public, Sjökvist [90] as well as international at Detection and Remediation Technologies for Mines and Minelike Targets V, Lundberg [91] and Uppsäll [9].

The next year the EU project ARC started and some work was reported in Georgson [92] and results from the group were presented at Statistical Signal Processing workshop, Svensson [93], International Conference on Acoustics Speech and Signal Processing, Lundberg[94], Detection and Remediation Technologies for Mines and Minelike Targets VI, Lundberg [95], and Subsurface and surface sensing technologies and applications III, Sjökvist [10]. Also the second thesis from this group was presented, Lundberg [96]. The work in the EU-funded ARC project was reported at Fifth International Airborne Remote Sensing Conference, Schutte [97].

In 2002 a journal paper, Garci-Padron [98], and two signal processing conference papers were presented, Linderhed [99] and Linderhed [100], by members of this group. At Detection and Remediation Technologies for Mines and Minelike Targets VII, the work on minefield data was presented, Linderhed [11].

In 2003 the work of this group in the EU-funded ARC project was presented in Uppsäll [101], the results was presented at International Conference on Requirements and Technology for the Detection, Removal and Neutralization of Landmines and UXO, Sjökvist [48], and the third thesis of this group was presented, Lundberg [102].

Finally in 2004 results were presented at Detection and Remediation Technologies for Mines and Minelike Targets VIII, Sjökvist [42]. The ARC project was reported in [13, 103, 104] and presented at Nordic Demining Research Forum, Uppsäll [105].

During the years 2001-2004 the group has contributed substantially to the following deliverables in the EU-funded ARC project shown in Table 10.1

Del	Deliverable name	Security	Year
D1	Kickoff Meeting Report	Rest	2001
D2	Project Webpage	Pub	2001
D3	Trial-I Specification	Int	2001
D4	End User Requirements Report	Rest	2001/2002
D5	Quarterly Management report No 1	Rest	2001
D6	Dissemination and Use Plan	Rest	2001
D7	Trial-I Evaluation Report	Rest	2001
D8	Trial-II Specification	Int	2001
D9	System Requirements Report	Rest	2002
D10	Data Fusion Concept	Rest	2001/2002
D11	Operational Requirements Report	Rest	2002
D12	UAV Trial-II Preparation	Int	2001
D13	System Concept	Rest	2001
D14	Quarterly Management report No 2	Rest	2001
D15	Trial-II Evaluation Report	Pub	2002
D16	Quarterly Management Report No 3	Rest	2001
D17	Control Station Design		=>D22
D18	Airborne Platform Design		=> D22
D19	Optronic Sensors Design		=> D22
D20	Data Fusion Design		=> D22
D21	Assessment Report	Rest	2002
D22	Demonstrator Design	Rest	2002
D23	Quarterly Management Report No 4	Rest	2002
D24	Annual Report No. 1	Pub	2002
D25	Cost Statement year 1	Int	2002
D26	Trial-III Specification	Pub	2002
D27	Trial-III UAV and payload	Int	2002
D28	Trial-III Evaluation Report	Rest	2003
D29	Quarterly Management Report No. 5	Rest	2002
D30	Quarterly Management Report No. 6	Rest	2002
D31	Exploitation Intermediate Report	Rest	2002
D36	Demonstrator Implementation	Rest	2003

Del	Deliverable name	Security	Year
	Report		
D37	Trial-IV Specification	Rest	2003
D38	Quarterly Management Report No. 7	Rest	2002
D39	ARC system 0.1	Int	2003
D40	Trial-IV Evaluation Report	Rest	2003
D41	Annual Report No. 2	Pub	2003
D42	Quarterly management report No. 8	Rest	2003
D43	Minefield Test Specification	Rest	2003
D44	Cost statement year 2	Int	2003
D45	Minefield Demonstration Specification	Rest	2003
D46	Integration Report	Rest	2003
D47	Quarterly Management Report No. 9	Rest	2003
D47a	Quarterly Management Report No. 10	Rest	2003
D47b	Quarterly Management Report No. 11	Rest	2003
D48	Airborne Platform Integration Report		=> D46
D49	Minefield Test Evaluation Report	Rest	2003
D50	Demonstrator System 1.0	Rest	2003
D51	Demonstration Report		=> D53
D52	System Performance Report		=> D53
D53	ARC System Report	Rest	2003
D54	Project Information CD-ROM	Pub	2004
D55	Exploitation Perspective	Rest	2003/2004
D56	Final Project Report	Pub	2004
D57	Technology Implementation Plan	Rest	2004

Table 10.1 Deliverables in the EU-funded ARC project. Security classes: Int: Internal circulation within project (and Commission Project Officer if requested) Rest: Restricted circulation list and Commission PO only. Pub: Public document.

11 CONCLUSIONS AND RECOMMENDATIONS

This report contains examples and descriptions of measurements and following analysis of a numerous optical mine detection experiments. It is a complex problem and needs a multidisciplinary approach and demands performance of high quality in all steps included. Detectable contrasts between mines and their local background have a strong diurnal variation. Due to the rapid altering of the weather conditions, a non-steady state thermal model based on physical properties is needed and is a relevant way to estimate when favourable contrast will occur. Weather conditions have to be taken into consideration in modelling as well as in image processing. A well-balanced approach between spatial, spectral and temporal signal and image processing has to be conducted to obtain high detection performance. In order to fuse images from several sensors as well as for building mosaics, positions and directions of the sensors have to be well known. Detection algorithms should use as much a priori information as possible. Scene understanding is needed for an increased number of situations in order to support national and international operations.

Future work should emphasis on combinations of sensors and detection algorithms. A prerequisite for this is that physical based numerical modelling is combined with signal and image detection methods.

- We can expect detectable contrasts under specific and well-known conditions for both surface and buried land mines, especially with IR systems.
- Weather parameters should be collected not only during the measurements but also many hours in advance to allow a realistic modelling and phenomena interpretation.
- The approach of using temporal information together with more traditional processing of images shows a high potential of the possibilities to detect and classify single objects as well as minefields from an IR sensor.
- In order co-register images with images, or maps, it is essential to use a high precision navigation system and also use markers in the scene.
- A system approach has to be used when designing a sensor system for mine detection. No part can be left out.
- Have both military and humanitarian requirements in mind when designing a sensor system.
- Do not forget the end-user who will operate the system and use its output.
- Use of polarization properties together with laser illumination may enhance the detection result.
- Multi- and hyper- spectral imaging may be beneficial.

12 REFERENCES

[1] J. MacDonald, J. R. Lockwood, and others, *Alternatives for landmine detection*, RAND Science and Technology Policy Institute, 2003, ISBN 0-8330-3301-8.

[2] M. Georgson, S. Sjökvist, M. Uppsäll, L. Pettersson, A.-L. Christiansen, and S. Ringberg, "Elektrooptisk minspaning 1994-1998," FOA, Linköping, Användarrapport, FOA-R--99-01076-310--SE, ISSN 1104 9154 1999, pp. 27.

[3] I. Kürsat and B. A. B. Baertlein, "Numerical Simulation of Thermal Signatures of Buried Mines over a Diurnal Cycle," in *Proc. Detection and Remediation Technologies for Mines and Minelike Targets V*, Orlando, USA: SPIE, 2000, vol. 4038.

[4] P. L. Martínez, "Detection of Landmines from Measured Infrared Images using Thermal Modeling of the Soil," Ph.D. Thesis, Department of Electronics and Computer Science, University of Santiago de Compostella, Santiago de Compostella, 2003.

[5] H. Brunzell and A. Ericsson, "Dual-antenna impulse radar for improved detection of buried land mines," in *Proc. Detection and Remediation Technologies for Mines and Minelike targets III*, Orlando, USA: SPIE, 1998, vol. 3392, pp. 725-734.

[6] A. Ericsson and A. Gustafsson, "Detection and classification results for an impulse radar mine detection system," in *Proc. Detection and Remediation Technologies for Mines and Minelike targets II*, Orlando, USA: SPIE, 1997, vol. 3079, pp. 636-642.

[7] A. Kjellström and L. Sarholm, "Analysis of TNT and related compounds in vapor and solid phase in different types of soil," in *Proc. Detection and Remediation Technologies for Mines and Minelike targets V*, Orlando, USA, 2000, vol. 4038, pp. 496-503.

[8] S. Sjökvist, "Heat Transfer Modelling and Simulation in Order to Predict Thermal Signatures -The Case of Buried Land Mine," Licentiate of Engineering Thesis, Applied Thermodynamics and Fluid Mechanics, Linköping University, Institute of Technology, Linköping, 1999.

[9] M. Uppsäll, L. M. Pettersson, M. Georgson, and S. Sjökvist, "Temporal IR contrast variation of buried land mines," in *Proc. Detection and Remediation Technologies for Mines and Minelike targets V*, Orlando USA: SPIE, 2000, vol. 4038, pp. 146-155.

[10] S. Sjökvist, M. Uppsäll, S. Nyberg, A. Linderhed, and M. Lundberg, "Optical detection of land mines at FOI," in *Proc. Subsurface and Surface Sensing Technologies and Applications III*, San Diego, USA: SPIE, 2001, vol. 4491, pp. 20-30.

[11] A. Linderhed, M. Lundberg, S. Nyberg, S. Sjökvist, and M. Uppsäll, "Optical measurements of real minefields," in *Proc. Detection and Remediation Technologies for Mines and Minelike Targets VII*, Orlando, USA: SPIE, 2002, vol. 4742, pp. 160-171.

[12] C. Nelsson and P. Nilsson, “Measurement Equipment at the Department of IR Systems,” IR System, Linköping Sweden, FOA-R--99-01111-615--SE, April 1999 1999, pp. 85.

[13] M. Khalili and M. Eisl, “ARC Final Public Report,” FOI, Reprint, FOI-S--1282--SE 2004, pp. 97.

[14] “TNO Physics and Electronics Laboratory,” TNO Observation Systems Research Programs, Mine Detection, Sept, 2004, available from: http://www.tno.nl/instit/fel/os/prg/the_mine_detection.html.

[15] P. Skoglar, “Modelling and control of EO/IR-gimbal for UAV survaillance applications,” Swedish Defence Research Agency, Division of Sensor Technology, Linköping, Scientific report, FOI-R--0893--SE, ISSN 1650-1942, June 2003, pp. 120.

[16] M. Ulvklo, J. Nygårds, J. Karlholm, and P. Skoglar, “Image processing and sensor management for autonomous UAV surveillance,” in *Proc. Airborne Intelligence, Surveillance, Reconnaissance (ISR) Systems and Applications*, Orlando USA: SPIE, 2004, vol. 5409, pp. 50-65.

[17] B. Zitova and J. Flusser, “Image registration methods: a survey,” *Image and Vision Computing*, vol. 21, pp. 977-1000, 2003.

[18] B. S. Reddy and B. N. Chatterji, “An FFT-based technique for translation, rotation, and scale-invariant image registration,” *IEEE Transactions on Image Processing*, vol. 5, pp. 1266-1271, 1996.

[19] D. Loyd and G. Andersson, “THAFEM - a finite element program for heat transfer analysis,” in *Finite Element Systems - A Handbook*, C. A. Brebbia, Ed., 3 ed: Springer - Verlag, 1985, pp. 721-732.

[20] S. V. Patankar, *Numerical Heat Transfer and Fluid Flow*, Hemisphere Publishing Corporation, 1980, ISBN 0-89116-522-3, pp. 197.

[21] O. C. Zienkiewicz, *The Finite Element Method*. London, McGraw-Hill, 1977.

[22] Comsol AB, *Femlab Users Guide*, 2004.

[23] H. S. Carslaw and J. C. Jaeger, *Conduction of Heat in Solids*, 2 ed. Oxford, Clarendon Press, 1959.

[24] J. W. Deardorff, “Efficient prediction of ground surface temperature and moisture, with inclusion of a layer of vegetation,” *Journal of Geophysical Research*, vol. 83, pp. 1889 - 1904, 1978.

[25] T. Miller, “Mathematical Model of Heat Conduction in Soil for Land Mine Detection,” CSIRO, Division of Mathematics and Statistics, /Australia, DMS-C95/95, 1996-01-23 1996, pp. 30+9+10.

[26] D. Clement and W. Jessen, “A Background Model in the Thermal Infrared: Status, Validation, and Applications,” ForschungsgeseIIschaft für Angewandte Naturwissenschaften Forschungsinstitut für Optik (FGAN-FfO), Schloss Kressbach Tübingen Germany, BETA-Tgb. -Nr. 1993/38 1993, pp. 10.

[27] J. S. Accetta and D. L.Shumaker, *The Infrared and Electro-Optical Systems Handbook*, SPIE Optical Engineering Press, 1993, ISBN 0-8194-1072-1.

[28] J. G. Hartley, *Coupled Heat and Moisture Transfer in Soils -A Review*, vol. 4, Hemisphere Publishing Corporation, 1987.

[29] M. Kaviany, *Principles of Heat Transfer in Porous Media*, 2 ed. Ann Arbour, Michigan, Springer Verlag, 1999, 0-387-94550-4, pp. 709.

[30] S. Sjökvist, M. Georgson, S. Ringberg, and D. Loyd, “Simulation of thermal contrast on solar radiated sand surfaces containing buried minelike

objects," in *Proc. Second International Conference on The Detection of Abandoned Land Mines*, Edinburgh, UK: The Institution of Electrical Engineers, IEE, Oct 12-14, 1998, pp. 115-119.

[31] S. Sjökvist, R. Garcia-Padron, and D. Loyd, "Heat Transfer Modelling Of Solar Radiated Soil, Including Moisture Transfer," in *Proc. Third Baltic Heat Transfer Conference*, Gdansk, Poland: IFFM Publishers, ISBN 8-3907-5269-7, 22-24 Sept, 1999, pp. 707-714.

[32] P. Jacobs, *Infrared Characterization of Targets and Background*, vol. TT26, Spie Optical Engineering Press, 1996, 0-8194-2180-4.

[33] D. A. de Vries, "Thermal Properties of Soil," in *Physics of Plant Environment*, W. R. van Wijk, Ed. New York: John Wiley & Sons, 1963, pp. 210-235.

[34] D. A. de Vries, "Simultaneous Transfer of Heat and Moisture in Porous Media," *Transactions American Geophysical Union*, vol. 39, pp. 909-916, 1958.

[35] J. R. Philip and D.A. De Vries, "Moisture Movement in Porous Materials under Temperature Gradients," *Transactions Am. Geophysical Union*, vol. 38, pp. 222-232, 1957.

[36] P.-E. Jansson, "Simulation Model for Soil Water and Heat Conditions," Swedish University of Agricultural Sciences, Department of Soil Sciences, Uppsala, Technical Report, March 1996 1996, pp. 79.

[37] M. V. Centeno, "New Formulae for the Equivalent Night Sky Emissivity," *Solar Energy*, vol. 28, pp. 489-498, 1982.

[38] S. B. Idso and R. D. Jackson, "Thermal Radiation From the Atmosphere," *Journal of Geophysical Research*, vol. 5397, 1969.

[39] F. G. Wollenweber, "Thermal background modeling and its use in Science and Technology," in *Proc. Characterization, Propagation, and Simulation of Sources and Backgrounds II*, Orlando, USA: SPIE, 1992, vol. 1687, pp. 84-106.

[40] W. R. Reynolds, "Survey and analysis: the measurements and modelling of terrestrial thermal backgrounds," in *Proc. Characterization and Propagation of Sources and Backgrounds*, Orlando, USA: SPIE, 1994, vol. 2223, pp. 404-423.

[41] L. K. Balick, R. K. Scoggins, and L. E. Link, "Inclusion of a Simple Vegetation Layer in Terrain Temperature Models for Thermal IR Signature Prediction," *Transactions on Geoscience and Remote Sensing*, vol. GE-19, pp. 143-152, 1981.

[42] S. Sjökvist, A. Linderhed, S. Nyberg, and M. Uppsäll, "Temporal method for IR minefield feature detection," in *Proc. Detection and Remediation Technologies for Mines and Minelike Targets IX*, Orlando, USA: SPIE, 2004, vol. 5415, pp. 175-186.

[43] J. Karlholm, M. Ulvklo, S. Nyberg, A. Lauberts, and A. Linderhed, "A survey of methods for detection of extended ground targets in EO/IR imagery," FOI, Linköping, Scientific report, FOI-R--0892--SE 2003.

[44] J. Karlholm, M. Ulvklo, J. Nygårds, M. Karlsson, S. Nyberg, M. Bengtsson, L. Klasen, A. Linderhed, and M. Elmqvist, "Target detection and tracking processing chain: a survey of methods with special reference to EO/IR sequences," FOA, Linköping, FOA-R--00-01767-408,616--SE 2000.

[45] G. H. Granlund, *Signal Processing for Computer Vision*, Kluwer Academic Press, 1995, 0-7923-9530-1.

[46] R. C. Gonzales and R. E. Woods, *Digital Image Processing*, Second ed. Upper Saddle River, NJ, ., 2002.

[47] A. Rosenfeld and A. C. Kak, *Digital Picture Processing*. London, Academic press, 1976.

[48] S. Sjökvist, A. Linderhed, S. Nyberg, M. Uppsäll, and D. Loyd, "Minefield temporal feature extraction supported by heat transfer modelling," in *Proc. International Conference on Requirements and Technologies for the Detection, Removal and Neutralization of Landmines and UXO*, Brussels, Belgium: EUDEM2-SCOT 2003, 15-18 Sept, 2003.

[49] J. M. Wozencraft and I. M. Jacobs, *Principles of Communication Engineering*. Illinois, Waveland Press, 1990.

[50] C. Bruschini and B. Gros, "A Survey of Current Sensor Technology Research for the Detection of Landmines," DeTeC - Demining Technology Center at the EPFL, Sept, 2004, available from: http://diwww.epfl.ch/lami/detec/susdemsurvey.html.

[51] H. Schleijpen, "Landmine detection technology research in the Netherlands," in *Proc. Detection and Remediation Technologies for Mines and Minelike Targets VIII*, Orlando: SPIE, April 2003, 2003, vol. 5089, pp. 755-766.

[52] J. McFee, Y. Das, and A. Faust, "Canadian landmine detection research program," in *Proc. Detection and Remediation Technologies for Mines and Minelike Targets VIII*, Orlando, USA: SPIE, 2003, vol. 5089, pp. 767-782.

[53] J. Habersat, C. Marshall, and G. Maksymonko, "NVESD mine lane facility," in *Proc. Detection and Remediation Technologies for Mines and Minelike Targets VIII*, Orlando, USA: SPIE, 2003, vol. 5089, pp. 1137-1145.

[54] A. Kenton, D. Geci, J. McDonald, K. Ray, C. Thomas, J. Holloway, D. Petee, and N. Witherspoon, "Littoral assessment of mine burial signatures (LAMBS): buried-landmine hyperspectral data collections," in *Proc. Detection and Remediation Technologies for Mines and Minelike Targets VIII*, Orlando, USA: SPIE, 2003, vol. 5089, pp. 150-160.

[55] M. Strand, N. Witherspoon, J. Holloway, K. Tinsley, D. Petee, J. Taylor, E. Branham, and J. Thomas, "Environmental factors impacting the performance of airborne lidar sensors in the surf zone," in *Proc. Detection and Remediation Technologies for Mines and Minelike Targets VIII*, Orlando, USA: SPIE, 2003, vol. 5089, pp. 274-283.

[56] V. Holmes, J. Wright, K. McCarley, A. Gelbart, N. Witherspoon, and J. Holloway, "Lidar signatures of very shallow water (VSW) and surf zone (SZ) mines," in *Proc. Detection and Remediation Technologies for Mines and Minelike Targets VIII*, Orlando, USA: SPIE, 2003, vol. 5089, pp. 284-295.

[57] Y. Das, J. McFee, K. Russell, G. Cross, and T. Katsube, "Soil information requirements for humanitarian demining: the case for a soil properties database," in *Proc. Detection and Remediation Technologies for Mines and Minelike Targets VIII*, Orlando, USA: SPIE, 2003, vol. 5089, pp. 1146-1157.

[58] J. Hendrickx, R. v. Dam, B. Borchers, J. Curtis, H. Lensen, and R. Harmon, "Worldwide distribution of soil dielectric and thermal properties," in *Proc. Detection and Remediation Technologies for Mines and Minelike Targets VIII*, Orlando, USA: SPIE, 2003, vol. 5089, pp. 1158-1168.

[59] R. v. Dam, B. Borchers, J. Hendrickx, and S. Hong, “Soil effects on thermal signatures of buried nonmetallic landmines,” in *Proc. Detection and Remediation Technologies for Mines and Minelike Targets VIII*, Orlando, USA: SPIE, 2003, vol. 5089, pp. 1210-1218.

[60] A. Hocaoglu and P. Gader, “Detection of tripwires using diffusion,” in *Proc. Detection and Remediation Technologies for Mines and Minelike Targets VIII*, Orlando, USA: SPIE, 2003, vol. 5089, pp. 527-535.

[61] F. Cremer, J. Schavemaker, W. d. Jong, and K. Schutte, “Comparison of vehicle-mounted forward-looking polarimetric infrared and downward-looking infrared sensors for landmine detection,” in *Proc. Detection and Remediation Technologies for Mines and Minelike Targets VIII*, Orlando, USA: SPIE, 2003, vol. 5089, pp. 517-526.

[62] G. Forssell, “Passive IR polarization measurements applied to covered surface landmines,” in *Proc. Detection and Remediation Technologies for Mines and Minelike Targets VIII*, Orlando, USA: SPIE, 2003, vol. 5089, pp. 547-557.

[63] J. Samson, L. Witter, A. Kenton, and J. Holloway, “Real-time implementation of a multispectral mine target detection algorithm,” in *Proc. Detection and Remediation Technologies for Mines and Minelike Targets VIII*, Orlando, USA: SPIE, 2003, vol. 5089, pp. 130-139.

[64] S. Moran, W. Austin, J. Murray, N. Roddier, R. Bridges, R. Vercillo, R. Stettner, D. Phillips, A. Bisbee, and N. Witherspoon, “Rapid overt airborne reconnaissance (ROAR) for mines and obstacles in very shallow water, surf zone, and beach,” in *Proc. Detection and Remediation Technologies for Mines and Minelike Targets VIII*, Orlando, USA: SPIE, 2003, vol. 5089, pp. 214-224.

[65] A. Nevis, R. Hilton, J. Taylor, B. Cordes, and J. McLean, “Advantages of three-dimensional electro-optic imaging sensors,” in *Proc. Detection and Remediation Technologies for Mines and Minelike Targets VIII*, Orlando, USA: SPIE, 2003, vol. 5089, pp. 225-237.

[66] J. Holloway, F. Crosby, D. Petee, H. Suiter, and N. Witherspoon, “Laser diode arrays for naval reconnaissance,” in *Proc. Detection and Remediation Technologies for Mines and Minelike Targets VIII*, Orlando, USA: SPIE, 2003, vol. 5089, pp. 238-249.

[67] J. Taylor, P. Davis, and L. Wolff, “Underwater partial polarization signatures from the shallow water real-time imaging polarimeter (SHRIMP),” in *Proc. Detection and Remediation Technologies for Mines and Minelike Targets VIII*, Orlando, USA: SPIE, 2003, vol. 5089.

[68] J. Schoonmaker, J. Dirbas, and G. Gilbert, “Multispectral observations of the surf zone,” in *Proc. Detection and Remediation Technologies for Mines and Minelike Targets VIII*, Orlando, USA: SPIE, 2003, vol. 5089, pp. 312-321.

[69] F. Cremer, W. d. Jong, K. Schutte, W. Liao, and B. Baertlein, “Detectability of surface-laid landmines with a polarimetric IR sensor,” in *Proc. Detection and Remediation Technologies for Mines and Minelike Targets VIII*, Orlando, USA: SPIE, 2003, vol. 5089, pp. 505-516.

[70] E. Winter, “Detection of mines using hyperspectral remote sensors and detection algorithms,” in *Proc. Detection and Remediation Technologies for Mines and Minelike Targets VIII*, Orlando, USA: SPIE, 2003, vol. 5089, pp. 625-630.

[71] J. Keller, M. Skubic, P. Gader, T. Wang, and R. Luke, "Real-time tripwire detection on a robotic testbed," in *Proc. Detection and Remediation Technologies for Mines and Minelike Targets VIII*, Orlando, USA, 2003, vol. 5089, pp. 1287-1297.

[72] L. Wolff, D. Socolinsky, C. Eveland, J. Yalcin, and J. Holloway, "Image fusion of shortwave infrared (SWIR) and visible for detection of mines, obstacles, and camouflage," in *Proc. Detection and Remediation Technologies for Mines and Minelike Targets VIII*, Orlando, USA: SPIE, 2003, vol. 5089, pp. 1298-1306.

[73] M. G. Bello and G. J. Dobeck, "Comparison of support vector machines and multilayer perceptron networks in building mine classification models," in *Proc. Detection and Remediation Technologies for Mines and Minelike Targets VIII*, Orlando, USA: SPIE, 2003, vol. 5089, pp. 77-94.

[74] S. Stetson and F. Crosby, "Automated threshold selection for a constant false alarm rate," in *Proc. Detection and Remediation Technologies for Mines and Minelike Targets VIII*, Orlando, USA: SPIE, 2003, vol. 5089, pp. 1383-1394.

[75] T. Meitzler, D. Bryk, E. Sohn, K. Lane, J. Raj, and H. Singh, "Fuzzy-logic-based sensor fusion for mine and concealed weapon detection," in *Proc. Detection and Remediation Technologies for Mines and Minelike Targets VIII*, Orlando, USA: SPIE, 2003, vol. 5089, pp. 1353-1362.

[76] S. Kempinger and I. Chant, "A systems description of a functioning broad band electro-optical mine detection sensor," in *Proc. Detection and Remediation Technologies for Mines and Minelike Targets VIII*, Orlando, USA, 2003, vol. 5089, pp. 1345-1352.

[77] J. Schavemaker, E. d. Breejen, K. Benoist, K. Schutte, P. Tettelaar, M. d. Bijl, P. Fritz, L. Cohen, W. v. d. Mark, and R. Chignell, "LOTUS field demonstration of integrated multisensor mine detection system in Bosnia," in *Proc. Detection and Remediation Technologies for Mines and Minelike Targets VIII*, Orlando, USA: SPIE, 2003, vol. 5089, pp. 1324-1335.

[78] J. Pressley, L. Page, B. Green, T. Schweitzer, and P. Howard, "Ground standoff mine detection system (GSTAMIDS) block 0 contractor test results," in *Proc. Detection and Remediation Technologies for Mines and Minelike Targets VIII*, Orlando, USA: SPIE, 2003, vol. 5089, pp. 1336-1344.

[79] J. Kostrzewa, W. Meyer, S. Laband, W. Terre, P. Petrovich, K. Swanson, C. Sundra, W. Sener, and J. Wilmott, "Infrared microsensor payload for miniature unmanned aerial vehicles," in *Proc. Unattended Ground Sensor Technologies and Applications*, Orlando, USA, 2003, vol. 5090, pp. 265-274.

[80] "Canadian Forces Landmine Database," National Defence Mine/countermine Information Centre, Canada, Sept, 2004, available from: http://ndmic-cidnm.forces.gc.ca.

[81] J. Johnson, *Analysis of Imaging Forming Systems*, vol. 513, SPIE Milestone Series, 1985.

[82] C. Larsson, S. Abrahamsson, S. Ringberg, and S. Ödman, "Radar, multispectral and biosensor techniques for mine detection," in *Proc. Symp. on Anti-personnel mines*, Montreux: Intern. Committee of the Red Cross, April 21-23, 1993.

[83] S. Sjökvist, M. Georgson, S. Ringberg, M. Uppsäll, A.-L. Christiansen, and D. Loyd, "Modelling of thermal heat-transfer of landmines - a heat transfer analysis," in *Proc. 1st international disposal conference*, Lund: ISSN 1404-0220, Nov 12-13, 1997, pp. 137-148.

[84] S. Sjökvist, M. Georgson, S. Ringberg, M. Uppsäll, and D. Loyd, "Thermal Effects on Solar Radiated Sand Surfaces Containing Land Mines, -A Heat Transfer Analysis," in *Proc. Fifth International Conference on Advanced Computational Methods in Heat Transfer*, Cracow, Poland: Computational Mechanics Publications, ISBN 1-8531-2591-1, ISSN 1462-6063, June 17-19, 1998, pp. 177-187.

[85] M. Georgson, S. Ringberg, S. Sjökvist, M. Uppsäll, and D. Loyd, "Detection of buried objects with infrared imaging technique - analysis of outdoor measurements," in *Proc. 2nd international conference on the detection of abandoned land mines*, Edinburgh, UK: IEE, Oct 12-14, 1998, vol. 458, pp. 120-123.

[86] M. Georgson, L. Pettersson, S. Sjökvist, and M. Uppsäll, "Mine detection using infrared imaging technique," in *Proc. Mine identification novelties Euro-Conference "Mine-1999". "Sensor systems and signal processing techniques applied to the detection of mines and unexploded ordnance"*, Firenze, Italy: FOA reprint, Oct. 1-3, 1999, vol. FOA-B--99-00502-310-SE, pp. 66-71.

[87] S. Sjökvist, M. Lundberg, I. Gu, and M. Ulvklo, "Aspects of an airborne system for detection of landmines using multispectral imaging," in *Proc. SSAB symp. on image analysis*, Gothenburg, Sweden, March 9-10, 1999, pp. 9-12.

[88] M. Georgson, "FOA Activities on Optical Methods," in *Proc. Nordic Demining Research Forum*, Göteborg, Mars 10, 2000.

[89] M. Lundberg, "Analysis of Multispectral Imaging Data," in *Proc. Nordic Demining Research Forum*, Gothenburg, 2000.

[90] S. Sjökvist, "Forskning som räddar liv," in *Marinnytt*, 2000, pp. 38-39.

[91] M. Lundberg and I. Y. H. Gu., "3-D Matched Filter for Detection of Landmines using Spatio-Temporal Thermal Modeling," in *Proc. Proceedings: Detection and Remediation Technologies for Mines and Minelike Targets V*, Orlando, USA: SPIE, 2000, vol. 4038, pp. 179-188.

[92] M. Georgson, M. Uppsäll, and S. Sjökvist, "Elektrooptisk minspaning 1999-2000. Electrooptical mine detection 1999-2000," FOI, Linköping, FOI-R--0066--SE 2001, pp. 11.

[93] L. Svensson and M. Lundberg, "Land Mine Detection in Rotationally Invariant Noise Fields," in *Proc. of the 2001 IEEE Workshop on Statistical Signal Processing*, Singapore, Aug, 2001, pp. 170-173.

[94] M. Lundberg, "Infrared Land Mine Detection by Parametric Modeling," in *Proc. IEEE, International Conference on Acoustics Speech and Signal Processing*: ICASSP '01, May, 2001.

[95] M. Lundberg, L. Svensson, and I. Y. H. Gu, "Infrared Detection of Buried Land Mines Based on Texture Modeling," in *Proc. Detection and Remediation Technologies for Mines and Minelike Targets VI*, Orlando, USA: SPIE, 2001, vol. 4394, pp. 199-206.

[96] M. Lundberg, "Electro-Optical Land Mine Detection and Contributions to Iterative Decoding and Power Estimation," Licentiate Thesis, Department

of Signals and Systems, Chalmers University of Technology, Gothenburg, Sweden, 2001.

[97] K. Schutte, H. Sahli, D. Schrottmayer, F. J. Varas, M. Uppsäll, and E. d. Brejen, "ARC: A camcopter based mine field detection system," in *Proc. Fifth International Airborne Remote Sensing Conference*, San Francisco, Californa, 17-20 September, 2001.

[98] R. Garcia-Padron, D. Loyd, and S. Sjökvist, "Heat and moisture transfer in wet sand exposed to solar radiation - models and experiments concerning buried objects," *Subsurface sensing technologies and applications*, vol. 3, pp. 125-150, 2002.

[99] A. Linderhed, "2-D empirical mode decompositions - in the spirit of image compression," in *Proc. Wavelet and independent component analysis applications IX*, Orlando, USA: SPIE, April 3-5, 2002, vol. 4738, pp. 1-8.

[100] A. Linderhed, "Wavelet packet decompositions of texture images: analysis of cost functions, filter influences, and image models," in *Proc. Wavelet and independent component analysis applications IX*, Orlando, USA: SPIE, April 3-5, 2002, vol. 4738, pp. 9-20.

[101] M. Uppsäll, S. Sjökvist, A. Linderhed, and S. Nyberg, "Sammanställning av vetenskaplig verksamhet inom ARC," FOI, Linköping, FOI-S--1077--SE 2003.

[102] M. Lundberg, "Land Mine Detection using Dual-Band Electro-Optical Sensing," Ph.D. Thesis, Department of Signals and Systems, Chalmers University of Technology, Gothenburg, Sweden, 2003.

[103] M. Eisl, "ARC Public Annual Report 1," FOI, Linköping, Reprint, FOI-S--1283--SE 2004, pp. 44.

[104] M. Eisl, "ARC Public Annual Report 2," FOI, Linköping, Reprint, FOI-S--1284--SE 2004, pp. 49.

[105] M. Uppsäll, "The EU-project ARC -results and experiences," in *Proc. Nordic Demining Research Forum*, Fredrikshamn Denmark, 2004.